

Alma Mater Studiorum – Università di Bologna

DOTTORATO DI RICERCA IN

*Ingegneria elettronica, telecomunicazioni e tecnologie dell'informazione*

Ciclo 32

Settore Concorsuale: *09/F2 - Telecomunicazioni*

Settore Scientifico Disciplinare: *ING-INF/03 - Telecomunicazioni*

TITOLO TESI

# **Centralized and Decentralized Self-x features in Heterogeneous 5G Networks**

**Presentata da:** *Babak Mafakheri*

**Coordinatore Dottorato:**  
*Dr. Alessandra Costanzo*

**Supervisore:**  
*Dr. Roberto Riggio*

**Co-Supervisor:**  
*Dr. Leonardo Goratti*  
*Dr. Elio Salvadori*  
*Dr. Chiara Buratti*

**Esame finale anno 2020**



# Declaration of Authorship

I, Babak MAFAKHERI, declare that this thesis titled, “Centralized and Distributed Self-x Features in Heterogeneous 5G Networks” and the work presented in it are my own. I confirm that:

- This work was done wholly or mainly while in candidature for a research degree at this University.
- Where any part of this thesis has previously been submitted for a degree or any other qualification at this University or any other institution, this has been clearly stated.
- Where I have consulted the published work of others, this is always clearly attributed.
- Where I have quoted from the work of others, the source is always given. With the exception of such quotations, this thesis is entirely my own work.
- I have acknowledged all main sources of help.

Signed:



Date:

11/Feb/2020



*Dedicated to*

*My beloved parents who have been always  
a source of encouragement, inspiration  
and motivation.*



# *Acknowledgements*

First of all, I would like to thank my main Ph.D. advisor, **Dr. Leonardo Goratti** for supporting me during these past four years. Leonardo is someone you will instantly love and never forget once you meet him. He has been super supportive and has given me the freedom to pursue various projects. He has also provided insightful discussions about the research. I am very grateful to Leonardo for his scientific advice and knowledge and many insightful discussions and suggestions. He is the best advisor and one of the smartest people I know. I hope that I could be as lively, enthusiastic, and energetic as Leonardo. I also have to thank the other advisors of my Ph.D. **Dr. Elio Salvadori, Dr. Roberto Riggio, and Dr. Chiara Buratti** for their helpful advice and suggestions in general.

I greatly appreciate the support received through the collaborative work undertaken with the **University of Bologna** and **Fondazione Bruno Kessler (FBK)**, Italy for the funding received towards my Ph.D. as well as **Safran Group**, Germany during my apprenticeship. Special thanks to **Prof. Roberto Verdone**, my master thesis supervisor, to motivate me to choose the program and **Dr. Tinku Rasheed** to allow me spending 6 months of my mobility abroad in Safran Group.

My thanks also go out to the support I received from **Dr. Sam Reisenfeld** and **Dr. Robert Abbas** from Macquarie University, Australia for the collaborative work I undertook with them and for all their advice and believing in my research.

Finally, I especially thank my father **Naser**, mother **Jamileh**, and sister **Sara**. My hard-working parents have sacrificed their lives for my sister and myself and provided unconditional love and care. I love them so much, and I would not have made it this far without them. My sister has been my best friend all my life and I love her and miss her so much. I hope we can see each other very soon and be able to live close together with all my family as we use to. I know I always have my family to count on when times are rough.



# Abstract

The continuous evolution of mobile network technology is leading to the 5th Generation (5G) of cellular networks, a level of development that exhibits unprecedented network features, capability, and intelligence. New technological cost-efficient solutions are, therefore, required to boost the network capacity and advance its capabilities in order to support the Quality of Service (QoS) requirements. Network densification is known to be as one of the promising approaches aiming to increase the network capacity and reduce latency. For example Heterogeneous Wireless Networks (HWN) can provide flexible and diverse network access to the users by integration of different wireless technologies. By introducing dense and diverse networks, the importance of network coordination and automated controllability has never been higher. Despite the advantages of network densifications, there are challenges that have to be addressed properly in order to use the best performance of heterogeneous networks. An example of HWN is the 5 GHz unlicensed band which is open to different wireless systems such as WiFi or Unlicensed LTE. The presence of the two mentioned OFDM-based systems in the same band rise the importance of studying their performance when sharing the same band with the other technologies and introduce new models and methods to reach the friendly coexistence. Another example of dense networks is roaming, especially in the 5G systems, with ever-increasing heterogeneous users. In the small cells and densified networks, Mobile Network Operators (MNOs) need to share their mobile networks with other operators more often to reduce the operator investment costs on infrastructure. Thus, the mobile networks are transferring from uniquely own single authorities to complex interactions among heterogeneous participants which rise the need for a new level of controllability. Since the Distributed Ledger Technologies (DLT) recently emerged as a revolutionary approach to decentralization with distributed controlling system, we noticed the roaming scenario has many potentials of taking advantage of these distributed coordinations for better performance while being cost-efficient.

In this doctoral dissertation, we first lay down a tractable semi-analytical method that allows to evaluate and quantify the impact of LTE transmissions on WiFi. Specifically, resorting to stochastic geometry and the characteristic function approach, we model the crucial mechanism of Clear Channel Assessment (CCA) in the WiFi network under the assumption of Rayleigh distributed channel fading. We then model the packet error probability for the reception of un-coded WiFi data packets affected by LTE transmissions, Rayleigh fading, and shadowing. In the next step in our analysis, resorting to a tractable one-dimensional Markov chain model, we obtain closed-form expression of the average WiFi network throughput in saturation condition

using selected values of the CCA energy detection threshold, while varying the LTE transmission parameters. We also extend the work by remodeling our one-dimensional Markov chain for non-saturation conditions while generalizing the interference to any possible OFDM-based systems. We finally discuss that the method we develop is very general and can aid steering future designs of the heterogeneous LTE/WiFi network management.

After evaluating the affected WiFi performance with semi-analytical approaches, in the next phase of this dissertation we experimentally measure the throughput performance of a WiFi, 802.11n, network when the WiFi client reception is affected by LTE downlink transmissions. Our practical approach is based on a modular experimental test-bed. Specifically, the test-bed is composed of the open source platform srsLTE for the LTE part and the OpenWRT operating system for the WiFi part. The measurements are done by modifying various physical layer parameters in the LTE-eNB for downlink communication that operates in the same 5 GHz band of WiFi. We initially compare our measurement results with the case without LTE interference and we experimentally demonstrate that coexistence between WiFi and LTE is hard to achieve. We further discuss that even the 3GPP features cannot guarantee coexistence in all cases and this might hamper the practicality of mobile technology in the unlicensed radio spectrum. For this reason, we enhance our test-bed introducing the Software-Defined Radio Access Network (SD-RAN) controller 5G-EmPOWER, thus borrowing from the higher agility of software-defined networking. By using the SD-RAN control to adaptively tune LTE-eNB downlink transmission parameters, we experimentally prove the validity of this approach to improve WiFi network throughput, as well as we shed light onto the new potentials that the SD-RAN controller can bring to automated network optimization in a centralized approach.

The last part of this dissertation is allocated to the distributed nature which imposes novel challenges on controllability of various networks in a decentralized manner. Blockchains and the fifth generation of the mobile network (5G) are currently under the spotlight and are expected to create new market opportunities for small and large enterprises alike. To this extent, we present a new network architecture for national and international roaming in mobile networks based on a single permissioned blockchain (Hyperledger Fabric) with smart contracts. The proposed solution improves the Mobile Network Operator (MNO) visibility on their subscribers' activities in the visited network, enables quick payment reconciliation, and reduces fraudulent transactions. The work also reports on a proof-of-concept implementation of the proposed blockchain-based roaming solution and on its validation.

**Key words:** 4G, 5G, 5 GHz band, Aggregate Interference, Blockchain, Distributed Ledger, Energy Detection, Heterogeneous Networks, Hyperledger, LAA, Poisson Process, SD-RAN, Smart Contracts, Stochastic Geometry, Unlicensed LTE, (Un)Saturated Throughput, Wireless LAN.

# Contents

<b>Declaration of Authorship</b>	<b>iii</b>
<b>Acknowledgements</b>	<b>v</b>
<b>List of Figures</b>	<b>xiii</b>
<b>List of Tables</b>	<b>xv</b>
<b>List of Abbreviations</b>	<b>xvii</b>
<b>1 Introduction</b>	<b>1</b>
1.1 Motivations and Objectives . . . . .	1
1.2 Problem Statement . . . . .	2
1.2.1 LTE/WiFi Coexistence in Unlicensed 5GHz Band . . . . .	2
LTE-U . . . . .	3
LTE-LAA . . . . .	4
1.2.2 Challenges in Roaming . . . . .	4
Billing settlement . . . . .	5
Security and Trust . . . . .	5
1.3 Main Contributions . . . . .	6
1.3.1 Analysis of WiFi Throughput affected by Unlicensed LTE . . . . .	6
1.3.2 Centralized Control of Unlicensed LTE and WiFi . . . . .	6
1.3.3 Blockchain-based Roaming . . . . .	7
1.4 Outline of the Dissertation . . . . .	7
<b>2 Backgrounds and State of the Art</b>	<b>9</b>
2.1 Heterogeneous Wireless Networks . . . . .	9
2.2 Unlicensed LTE . . . . .	9
2.2.1 LTE/WiFi Coexistence . . . . .	10
2.2.2 Interference Modeling . . . . .	11
2.3 Blockchain and Distributed Ledgers . . . . .	11
2.3.1 Blockchain in Telecom . . . . .	13
2.3.2 Blockchain for 5G Networks . . . . .	13
<b>3 On Performance of Wi-Fi Networks Interfered by Unlicensed LTE</b>	<b>15</b>
3.1 System Model . . . . .	15
3.2 Effects of Unlicensed LTE on PHY Layer of 802.11 . . . . .	17
3.2.1 Energy-Detection Analysis . . . . .	17
3.2.2 Bit Error Probability analysis . . . . .	22
3.3 Effects of Unlicensed LTE on MAC layer of 802.11 . . . . .	25

3.3.1	Saturated 802.11 Throughput Analysis . . . . .	25
3.3.2	Saturated Throughput Numerical Results . . . . .	29
3.4	Unsaturated WiFi Analysis in a Poisson Field of Interference . . . . .	37
3.4.1	Clear Channel Assessment . . . . .	37
3.4.2	Unsaturated CSMA/CA Analysis . . . . .	39
3.4.3	Unsaturated 802.11 Throughput Computation . . . . .	41
3.4.4	Model Validation and Numerical Results . . . . .	42
3.5	Conclusion of the Chapter . . . . .	44
<b>4</b>	<b>Centralized Coordination of Unlicensed-LTE/WiFi</b> . . . . .	<b>45</b>
4.1	LTE/WiFi Test-bed Implementation . . . . .	45
4.1.1	Test-Bed Components . . . . .	46
4.1.2	Measurement Environment . . . . .	48
4.2	Coexistence Experiments of Unlicensed LTE and WiFi . . . . .	50
4.2.1	Evaluation Methodology . . . . .	50
4.2.2	Impacts of the LTE Transmitted Power . . . . .	50
4.2.3	Impacts of MCS-index . . . . .	52
4.2.4	Impacts of Number of LTE Resource Blocks . . . . .	52
4.3	Dynamic Interference Coordination Through SD-RAN Control . . . . .	53
4.3.1	5G-EmPOWER Controller . . . . .	54
4.3.2	SD-RAN Enabled Test-Bed Architecture . . . . .	55
4.3.3	Measurement Results . . . . .	57
4.4	Conclusion of the Chapter . . . . .	59
<b>5</b>	<b>Decentralized Coordination of Small Cells in Roaming</b> . . . . .	<b>61</b>
5.1	Roaming in 5G Networks . . . . .	61
5.1.1	Roaming Architecture . . . . .	62
5.1.2	Challenges and Requirements . . . . .	63
5.2	Blockchain-based Roaming in 5G Networks . . . . .	63
5.2.1	Blockchain Topology . . . . .	64
5.2.2	Role of Blockchain in Roaming . . . . .	64
5.2.3	Roaming Charging with Blockchain . . . . .	65
5.3	Proof of Concept . . . . .	66
5.3.1	Components . . . . .	67
5.3.2	Transactions and Consensus . . . . .	68
5.3.3	Evaluation . . . . .	68
5.4	Conclusion of the Chapter . . . . .	69
<b>6</b>	<b>Conclusions and Future Works</b> . . . . .	<b>71</b>
<b>A</b>	<b>Proofs</b> . . . . .	<b>75</b>
A.1	Derivation of Theorem 2 . . . . .	75
A.2	Derivation of Lemma 2 . . . . .	76
A.3	Derivation of Theorem 3 . . . . .	76
A.4	Derivation of equation (3.22) . . . . .	78
A.5	Derivation of equation (3.27) . . . . .	78
	<b>Bibliography</b> . . . . .	<b>79</b>

# List of Figures

1.1	Mechanisms of transmission of LTE in unlicensed bands . . . .	4
3.1	General scenarios for (a) studying CCA affected by interference and, (b) bit error probability analysis. . . . .	16
3.2	Presence of LTE transmission for studying of WiFi CCA performance under Case Study "B". . . . .	17
3.3	One-dimensional Markov Chain modeling BEB. . . . .	25
3.4	Case study A, threshold -62 dBm . . . . .	30
3.5	Case study B varying the threshold . . . . .	31
3.6	Bit Error Rate, having LTE-TX=18dBm . . . . .	32
3.7	Wi-Fi throughput; LTE-TX=10 dBm; Wi-Fi Modulation 16-QAM . . . . .	32
3.8	Wi-Fi throughput; LTE-TX=18 dBm; Wi-Fi Modulation 16-QAM . . . . .	33
3.9	Wi-Fi throughput; LTE-TX=24 dBm; Wi-Fi Modulation 16-QAM . . . . .	35
3.10	WiFi throughput vs. Distance vs. LTE-TX. Targeting $P_{fa}$ and WiFi modulation of 64-QAM . . . . .	36
3.11	WiFi Modulation Effects, Targeting $P_{fa}$ , LTE-TX=18 dBm . . . . .	36
3.12	One-dimensional Markov Chain modeling BEB. . . . .	40
3.13	Normalized WiFi throughput, SNR $\approx$ 30 dB, $\Lambda = -62$ dBm . . . . .	43
4.1	Conceptual representation of hidden node problem in u-LTE/WiFi coexistence . . . . .	46
4.2	srsLTE test-bed configuration . . . . .	49
4.3	u-LTE/WiFi test-bed implementation . . . . .	49
4.4	Impact of LTE transmitted power on WiFi throughput . . . . .	51
4.5	Impact of LTE transmitted power on WiFi packet loss . . . . .	51
4.6	Impact of LTE MSC on WiFi throughput . . . . .	52
4.7	Impact of LTE Bandwidth on WiFi throughput . . . . .	53
4.8	5G-EmPOWER Operating System Architecture . . . . .	55
4.9	5G-EmPOWER messaging structure . . . . .	55
4.10	Centralized coordination of WiFi/LTE . . . . .	56
4.11	Sequence diagram showing the proposed approach to control eNB physical layer parameters . . . . .	57
4.12	5G-EmPOWER controller measurements environment . . . . .	58
4.13	WiFi client moves away from LTE-eNB . . . . .	59
4.14	WiFi client moves towards LTE-eNB . . . . .	60
5.1	Roaming in 5G Network . . . . .	62
5.2	Roaming with a third party clearing house. . . . .	64
5.3	Blockchain-based Roaming. . . . .	65
5.4	Blockchain enabled billing settlement for roaming in NSA core . . . . .	66

5.5	Configuration of Roaming Blockchain . . . . .	67
5.6	Roaming Blockchain Scalability . . . . .	69
6.1	Conceptual representation of SD-RAN based Multi-tire network control . . . . .	74

# List of Tables

3.1	Parameters to evaluate Saturated numerical results . . . . .	28
3.2	Parameters to evaluate Unsaturated numerical results . . . . .	44
4.1	Transmitted block sizes with respect to MCS-index . . . . .	52
4.2	Parameters to evaluate effects of LTE-BW . . . . .	53



# List of Abbreviations

<b>3GPP</b>	<b>3<sup>rd</sup> Generation Partnership Project</b>
<b>4G</b>	<b>4<sup>th</sup> Generation</b>
<b>5G</b>	<b>5<sup>th</sup> Generation</b>
<b>AP</b>	<b>Access Point</b>
<b>AWGN</b>	<b>Additive White Gaussian Noise</b>
<b>BEP</b>	<b>Bit Error Probability</b>
<b>BSS</b>	<b>Basic Service Set</b>
<b>CCA</b>	<b>Clear Channel Assessment</b>
<b>CF</b>	<b>Characteristic Function</b>
<b>CSAT</b>	<b>Carrier Sense Adaptive Transmission</b>
<b>CSMA/CA</b>	<b>Carrier Sense Multiple Access with Collision Avoidance</b>
<b>CW</b>	<b>Contention Window</b>
<b>DCF</b>	<b>Distributed Coordination Function</b>
<b>DIFS</b>	<b>DCF InterFrame Space</b>
<b>DLT</b>	<b>Distributed Ledger Technology</b>
<b>DRS</b>	<b>Discovery Reference Signal</b>
<b>ED</b>	<b>Energy Detection</b>
<b>eNB</b>	<b>evolved Node B</b>
<b>EPC</b>	<b>Evolved Packet Core</b>
<b>HSS</b>	<b>Home Subscriber Server</b>
<b>HWN</b>	<b>Heterogeneous Wireless Network</b>
<b>IoT</b>	<b>Internet of Things</b>
<b>LAA</b>	<b>Licensed Assisted Access</b>
<b>LAN</b>	<b>Local Area Network</b>
<b>LBO</b>	<b>Local BreakOut</b>
<b>LBT</b>	<b>Listen Before Talk</b>
<b>LTE</b>	<b>Long Term Evolution</b>
<b>LWA</b>	<b>LTE WLAN Aggregation</b>
<b>LWIP</b>	<b>LTE WLAN with IPsec</b>
<b>MAC</b>	<b>Medium Access Control</b>
<b>MC</b>	<b>Markov Chain</b>
<b>MCOT</b>	<b>Maximum Channel Occupancy Time</b>
<b>MCS</b>	<b>Modulation and Coding Scheme</b>
<b>MME</b>	<b>Mobility Management Entity</b>
<b>MNO</b>	<b>Mobile Network Operator</b>
<b>NSA</b>	<b>Non Stand Alone</b>
<b>OFDM</b>	<b>Orthogonal Frequency Division Multiplexing</b>
<b>PDSCH</b>	<b>Physical Downlink Shared Channel</b>
<b>PEP</b>	<b>Packet Error Probability</b>
<b>PoET</b>	<b>Proof of Elapsed Time</b>

<b>PoW</b>	<b>Proof of Work</b>
<b>PoS</b>	<b>Proof of Stack</b>
<b>PPP</b>	<b>Poisson Point Process</b>
<b>QoS</b>	<b>Quality of Service</b>
<b>RSSI</b>	<b>Received Signal Strength Indicator</b>
<b>r.v</b>	<b>random variable</b>
<b>SD-RAN</b>	<b>Software Defined Radio Access Network</b>
<b>SINR</b>	<b>Signal to Noise and Interference Ratio</b>
<b>SIFS</b>	<b>Short InterFrame Space</b>
<b>SISO</b>	<b>Single Input Single Output</b>
<b>TB</b>	<b>Transport Block</b>
<b>TDM</b>	<b>Time Division Multiplexing</b>
<b>TTI</b>	<b>Transmission Time Interval</b>
<b>UE</b>	<b>User Equipment</b>
<b>UHD</b>	<b>Universal Hardware Driver</b>
<b>UDP</b>	<b>User Datagram Protocol</b>
<b>VoLTE</b>	<b>Voice over LTE</b>
<b>WLAN</b>	<b>Wireless Local Area Networking</b>

# Chapter 1

## Introduction

### 1.1 Motivations and Objectives

The introduction of Heterogeneous Wireless Networks (HWNs) technology brings new aspects of network densification. It provides higher network capacity, higher Quality of Service (QoS) for users, wider coverage, etc. With the evolution of cellular technology toward 5G and the possibility to use different frequency bands, network scenarios become even more complex and heterogeneous. One such example of HWNs is the coexistence of different technologies in unlicensed bands (e.g. Unlicensed LTE and WiFi). Despite all the benefits, the diversity of various technologies create challenges in terms of control and management of the network. Being heterogeneous is not only limited to the networks, but also among participants and users. For example, with the rapid evolution of 5G networks in terms of network densifications, the cellular networks are shifting from uniquely owned single authority systems to complex systems among heterogeneous participants; with roaming as a clear example.

An outstanding example of a heterogeneous network is the 5 GHz unlicensed band, which can be used not only by WiFi capable devices but also by LTE networks. Notably, in releases 12, 13, and 14, the Third Generation Partnership Project (3GPP) standardized LTE access in unlicensed spectrum as a supplement to costly and scarce licensed carriers. For instance in Release 13, 3GPP focused on spectrum aggregation over licensed and unlicensed frequency bands for downlink communications [1]. Both systems are based on Orthogonal Frequency-Division Multiplexing (OFDM) but with radically different numerology and framing structure. The general approach consists of enabling the coexistence by means of some form of mutual exclusivity in such a way that they do not hamper each other. Motivated by the general idea to use unlicensed frequency bands for a heterogeneous wireless system composed of two uncoordinated technologies that rely on different versions of OFDM (i.e. WiFi and LTE), **our first motivation was to deliver a complete yet simple mathematical model that enable studying the performance of WiFi when sharing the same band with the other OFDM-based system.** The performance study is meant to constitute the basis for the development of new coexistence methods. The main reason to focus on WiFi lays in the extreme popularity of this wireless technology.

Introducing an accurate model to analyze the performance of WiFi in a

heterogeneous network can help to adjust some parameters in both LTE and WiFi to increase the fairness of coexistence of the two technologies with a distributed approach. However, to the best of our knowledge, there is still lack of studies that introduce the new dimension of a centralized intelligent entity such as a Software Defined-Radio Access Network (SD-RAN) controller that can monitor and tune transmissions parameters in both WiFi and unlicensed LTE at runtime in order to reach fair coexistence. Therefore, **our second motivation was to (i) carry out measurements in a realistic environment when the reception of WiFi station is affected by unlicensed LTE as a proof of concept to our semi-analytical works and (ii) use the results of the analysis and measurements to leverage the functionality of a centralized SD-RAN controller to reach the fair coexistence.**

Regarding heterogeneous participants and customers of cellular networks we noticed the increasing number of roaming users (e.g. cross-domain operating connected-vehicles) require seamless connectivity not only within a single geographical area (e.g. a country), but also across the globe. Hence, it constitutes a key challenge in the context of available radio access and core network technologies. Mobile Network Operators (MNOs) are implementing national and international roaming as one of the technological solutions which allow sharing of network resources among themselves. Technically, roaming refers to the ability for a cellular customer to automatically send and receive data or access other services, including home data services, when traveling outside the geographical coverage area of the home network, using the coverage of a visited network. The seamless expansion of coverage is facilitated by integrating high-cost systems and providing complicated access/authentication settings together with a wholesale roaming agreement between a mobile users home MNO and the visited MNO. As technology evolves and globalization and network densification continues, the need for reasonably priced roaming services has never been higher. The distributed nature imposes new degrees of autonomous network controllability in a cost-efficient approach. We believe a smart contract-based Blockchain can have the capabilities to handle in a decentralized and shared way the roaming subscriber identification as well as roaming billing settlements. Thus, **our last motivation was to propose and design a decentralized and transparent approach to manage and accomplish billing settlements among non-trusted MNOs by using Blockchain technology.**

## 1.2 Problem Statement

### 1.2.1 LTE/WiFi Coexistence in Unlicensed 5GHz Band

In heterogeneous network scenarios that include both LTE small cells and WiFi, LTE transmissions cause the medium to be reported busy after the crucial Clear Channel Assessment (CCA) mechanism that is carried out by WiFi devices prior to transmitting packets. The CCA operation can be based on

non-coherent energy detection (ED-CCA) that lasts for  $4 \mu\text{s}$  so that the physical layer is found busy for any signal that is at least 20 dB above the minimum receiver sensitivity ( $-82 + 20 = -62 \text{ dBm}$ ) in the 20 MHz channel. Depending on the threshold used in the detection, the ED-CCA mechanism affects differently the WiFi throughput. The effect on throughput depends also on the location of LTE and WiFi transmitters in space since simultaneous transmissions (e.g. hidden nodes problem or undetected transmissions) of the two wireless systems over the same frequency band may occur and this resulting effect ought to be evaluated. Although some methods were already introduced by 3GPP for friendly coexistence of unlicensed LTE and WiFi (the most important are reviewed below), many studies have shown that improvements are still required to solve the coexistence problem [2]. Considering the fact that traditionally WiFi is the dominant technology in the 2.4 GHz and 5 GHz unlicensed bands and it has been using widely in the indoor environments, **thus, (i) a tractable model that allows to quantify completely the impact of LTE transmissions on the WiFi throughput is needed to steer future designs for the coexistence; and (ii) a centralized intelligence entity with ability to coordinate the two technologies at runtime is require to increase the whole network efficiency while satisfying the fair coexistence.** In follow, we briefly explain the two main mechanisms of unlicensed LTE, introduced by 3GPP, while focusing on some of their problems and challenges.

### LTE-U

It is based on an adaptive *ON/OFF* period (i.e. duty cycle) to avoid continuous transmission of LTE in the unlicensed band in order to give opportunity to WiFi transmission. The duty-cycle duration can vary depending on the WiFi activity and channel conditions, where it is set based on WiFi transmissions using carrier sensing. For example, in a dense environment when there is no channel available, the LTE-U eNB uses the Carrier-Sensing Adaptive Transmission (CSAT) algorithm to apply Time-Division Multiplexing (TDM) as shown in Figure 1.1(a). If the channel is sensed idle, the duty cycle can be set to the maximum value of 95%. In other words, the *ON* period will be set to 20 msec while the *OFF* period is 1 msec. The long *ON* period, as concluded in [3], can cause a serious problem to WiFi since the beacon transmission/reception will be disrupted. Further, as indicated in [4], despite CSAT algorithm can be a relief to LTE-U/WiFi coexistence, the overall throughput of the WiFi network is anyway degraded during the LTE-U *ON* period. Moreover, the problem of undetected LTE signals by the WiFi Access Point (AP) can still remain as the received energy level of LTE during WiFi CSMA/CA mechanism could be lower than -62 dBm (Energy Detection threshold in 802.11). There is evidence that even a low level of energy can be harmful to WiFi [5] especially when LTE uses lower bandwidth values (e.g. 3 or 5 MHz) [5]–[7].

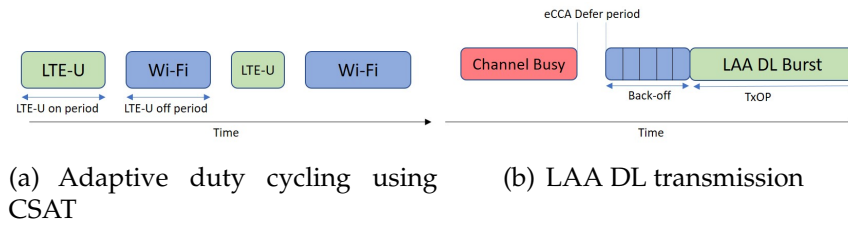


FIGURE 1.1: Mechanisms of transmission of LTE in unlicensed bands

## LTE-LAA

Unlike some countries such as the USA and South Korea where LTE-U can be used, other markets such as Europe and Japan require continuous examination of the presence of other signals occupying the channel by the unlicensed LTE eNB before any transmission. This mechanism is referred to as Listen Before Talk (LBT), which measures the energy level over the channel within a period of time and compares it with a pre-defined threshold. If the measured energy level is higher than the threshold, the node is not allowed to transmit [8], [9]. The first issue that arose between LAA and WiFi is the energy detection threshold values to use in the two technologies. The IEEE 802 community explicitly announced in several liaison statements to 3GPP RAN1 that the an ED threshold of -72 dBm for LAA will not result in fair coexistence [10]. In addition, as shown in Figure 1.1(b), when the LBT mechanism of LAA detects the channel busy the backoff counter is frozen and the LTE-LAA continues to sense the channel until finds it idle. Once the backoff counter reaches to zero the LTE-LAA occupies the channel for the duration of  $T_{xOP}$  which cannot be longer than Maximum Channel Occupancy Time (MCOT), e.g., 10 ms for some priority classes [11] and [12]. The short duration of the WiFi ED-CCA (i.e. 4  $\mu$ s) compared to  $T_{xOP}$  can cause WiFi to refrain from transmitting. Moreover, there has been additional concerns about the use of LAA's Discovery Reference Signal (DRS), which can also block WiFi [13]. Besides, as highlighted in [14], as a result of using different ED thresholds (e.g. -62 dBm and -72 dBm) in different technologies the hidden nodes problem appears more often in LTE/WiFi coexistence.

### 1.2.2 Challenges in Roaming

Roaming is a service that allows a mobile user of one MNO to use the services of another MNO when inside the latter's coverage area. The 3GPP standards support two roaming models: (i) Local BreakOut roaming, where the data traffic of the roaming user is served directly by the visited MNO allowing for more efficient routing in terms of latency and bandwidth and (ii) Home-routed roaming where the data traffic of the roaming user is always served by the home MNO giving more control over the user's traffic.

Currently, among almost all MNOs the Home-routed approach is mostly applied. This is mainly due to the fact that although the Local BreakOut (LBO) shows good performance in theory, MNOs prefer to keep the control over their user identities, subscriptions, security, billing etc which is not easily achieved in this architecture. Apart from this, neither the 4G nor 5G standard incorporates shared, distributed database approaches, which could in turn highly facilitate, optimize and harmonize the data management and various functionalities. Since it has been realized that from a technical point of view it makes no sense to tunnel back all IP data packets of roamers (i.e. using home-routed), **it might be worth to investigate new possible decentralized models for the billing settlements while roaming in 5G networks.** To this extent, we first mention below two of the challenges in LBO roaming:

### Billing settlement

In the LBO roaming for charging, roaming information must be associated with charging accounts. The problem with this configuration is that the visited network does not have the subscriber charging information whereas the home network also does not have the subscriber roaming information. This means that the MNOs need to manage multiple relationships, interconnect globally, and handle complicated financial relationships [15]. To this extent, two possible relationship scenarios between operators are establishing either direct relationship or indirect through intermediaries. In the former scenario, although MNOs do have a choice to connect directly to all the other MNOs, it is obvious that a point-to-point relationship with each roaming partner is not feasible and is cost-prohibitive because each MNO needs to maintain hundreds of such agreements to share resources efficiently for having universal roaming service. Whereas in the latter scenario, a 3<sup>rd</sup> operator or a clearing-house is used to connect the two operators. Although this kind of roaming is working in current LTE network by establishing settlement relationships with all relevant operators, it still has many drawbacks. First of all, the presence of an intermediate entity applies many extra expenses to the network; more importantly, it raises the concept of security and trust by introducing a 3<sup>rd</sup> party.

### Security and Trust

Before gaining access to the visited MNO, the roamer identity must be authenticated through the home MNO. There exists a number of user authentications and key exchange protocols that are proposed in the literature for roaming. However, each of them concentrates solely on the mutual authentication between the user and the visited MNO. Moreover, The roaming user may have accepted to different policies in the home MNO regarding the access to user information (user protection act) than that in the visited MNO. Therefore, it requires re-accepting the roaming privacy terms before providing any services.

## 1.3 Main Contributions

Following by the motivations and challenges mentioned in sections 1.1 and 1.2, the contributions provided by this dissertation can be divided to three parts:

### 1.3.1 Analysis of WiFi Throughput affected by Unlicensed LTE

The first contribution of this work consists of obtaining a tractable and accurate analytical model of the WiFi throughput which is affected by LTE transmissions over the unlicensed 5 GHz frequency band. To this end, we model the LTE transmitters as interferer to WiFi nodes. We are conscious that in the unlicensed band, LTE and WiFi are peers, nevertheless, LTE can rely also on licensed chunks of spectrum that are not permitted to WiFi. Guided by this mindset, we first model the impact of LTE transmissions over the ED-CCA mechanism carried out by WiFi nodes in their Physical Layer (PHY). Second we focus on modeling the CSMA/CA mechanism of MAC layer affected by transmissions of unlicensed LTE in both saturation and unsaturated conditions. Finally, we introduce the average of both saturated and unsaturated throughput performance of the WiFi network in a cross-layer analysis approach. The method proves to be very powerful and lend itself to generalizations since we manage to study the effect of single LTE interferer and aggregate LTE interference. The numerical results at the end allow to adjust LTE's parameters in order to preserve WiFi performance in a decentralized way.

Further, we discuss the opportunities that network softwarization can offer to control the behavior of the heterogeneous network to pave the way for the next contribution.

### 1.3.2 Centralized Control of Unlicensed LTE and WiFi

In light of the discussion undertaken above, to the best of our knowledge, there is still lack of studies that introduce the new dimension of a centralized intelligent entity such as an SD-RAN controller that can monitor and tune transmissions parameters in both WiFi and unlicensed LTE at runtime in order to reach fair coexistence. Therefore, the research contribution of this part of the dissertation is twofold: (i) we carry out measurements in a realistic office environment when the reception of WiFi station is affected by unlicensed LTE and (ii) we use the results of the measurements to leverage the functionality of the SD-RAN controller to self-optimize the interference based on the network priorities in a centralized manner.

### 1.3.3 Blockchain-based Roaming

The last contribution of the dissertation is assigned to the decentralized billing settlements approach by introducing a Blockchain-based architecture for roaming in 5G network. We first introduce some challenges of roaming and show how the Blockchain and distributed ledger technologies are able to solve them. To this extend, we propose a permissioned Blockchain framework that allows non-trusting operators to perform peer-to-peer self-transactions for the roaming users, relying on the capabilities of the smart contracts. The method can be used to remove the intermediaries (e.g., clearinghouses) which are currently handling transactions among operators for the roaming; as a result, it eliminates the risks of trust and extra expenses appeared due to existence of these intermediaries.

## 1.4 Outline of the Dissertation

This dissertation consists of six chapters, which are briefly summarized as follows. In the current chapter, we first motivate our work and present its objectives. We then state the problems and discuss the approaches undertaken to solve the problems. Lastly, we highlight the main contributions of our work.

Chapter 2 starts with background of heterogeneous wireless networks. It also describes the unlicensed LTE which has been progressed by the 3GPP as a continuous evolution of mobile network technology which is leading to 5th Generation of cellular networks. Since the ultimate goal of the dissertation is to introduce both centralized and decentralized network coordination in HWNs, the chapter also discusses the two enabling technologies of Software Defined Radio Access Control (SD-RAN) and Blockchain to enable self-x features in heterogeneous networks. Further, it walks through the state-of-the-art studies on both direction of the work. On one side, the co-existence of LTE/WiFi in unlicensed 5 GHz band is introduced presenting the key findings of the most promising works and research. The literature review starts looking at analytical works and continues by presenting experimental studies as well as sheds light on some softwarization works. On the other side, the focal point of research by industry and academia for the use of Blockchain in telecoms industry with the focus on cellular networks is presented.

In Chapter 3, we first study the performance of physical layer of WiFi interfered by unlicensed LTE. We consider energy detector receiver modeling the probabilities of false alarm and detection resorting to the characteristic function approach. This allows us to obtain a new set of ED-CCA thresholds to use. Moreover, we model the bit error probability that characterizes the reception of a WiFi data packet under LTE interference, fading, and path-loss. We continue by studying MAC layer performance quantifying the average WiFi network throughput relying on a one-dimensional Markov Chain model in both saturated and unsaturated conditions. The analysis in

this chapter allows us to evaluate the combined effect of different energy detection thresholds, different values of the LTE transmitted power, WiFi data packet size and modulation order. Finally, numerical results are shown and discussed among the sections.

Chapter 4 starts with presenting measurements results that quantify the effects of LTE transmissions in the unlicensed 5 GHz band on the WiFi throughput performance in an actual open office environment. It continues by representing the methodology based on adopting a new degree of controllability added by an SD-RAN controller to coordinate the transmissions of both technologies, thus leveraging on the network programmability paradigm. We present a centralized approach to improve coexistence, which we illustrate it through a sequence diagram, in order to enable modification of the LTE-eNB parameters based on network conditions to preserve the WiFi downlink throughput. Finally, measurement results demonstrate the viability of our approach and the improvement that can arise from controlling the LTE transmission parameters at runtime.

Chapter 5 is assigned to decentralized coordination of heterogeneous network through Distributed Ledger Technologies (DLT) for the roaming use-case. In this chapter, we propose a permissioned Blockchain framework that allows non-trusting MNOs to perform peer to peer, self-transactions adopting smart contract agreements to accomplish charging and billing settlements for roaming. The chapter starts with a brief description and challenges of the roaming architecture in 5G networks, continuing with some background on Blockchain technology, the role of Blockchain in roaming, and architecture of Blockchain-based roaming. Finally, the proof of concept based on hyperledger fabric is described.

Finally, in Chapter 6 we recap the contributions of this dissertation and summarize the obtained results. After the conclusions, we also highlight several promising research directions for future work.

## Chapter 2

# Backgrounds and State of the Art

### 2.1 Heterogeneous Wireless Networks

By integration of different wireless technologies such as cellular networks (4G and 5G), wireless Local Area Networks (LANs) and ad hoc networks, Heterogeneous Wireless Networks (HWNs) can provide flexible and diverse network access to the users. The promises of HWNs is to improve network throughput and reduce latency. They offer a variety of exciting application anytime and anywhere based on availability of radio networks even in roaming areas [16]. Despite the advantages, backhauling, handover, roaming, and interference are identified as some of the key technical challenges facing HWNs that have to be coordinated properly. Since some cells such as picocells and femtocells will be user-deployed without operator supervision, their proper operation highly depends on their self-organizing features [17], [18]. One such example of HWNs which attracts many attention in both academia and industry is the coexistence of LTE and WiFi in unlicensed 5GHz band. To reach to the fair and friendly coexistence many investigations have been done in recent years with both centralized and decentralized approaches. Moreover, with rapid uptake of 5G network densification, the interaction among heterogeneous participants (e.g. roaming) are increasing dramatically. In the rest of this chapter we introduce some of the challenges in (i) coexistence of unlicensed-LTE/WiFi and (ii) decentralized network coordinations in roaming. We also briefly review the state-of-the art and some of the proposed approaches to combat the existing challenges in each of the directions.

### 2.2 Unlicensed LTE

The continuous evolution of mobile network technology is leading to 5th Generation (5G) of cellular networks, a level of development that exhibits unprecedented network features, capability, and intelligence. To reach this goal, the Third Generation Partnership Project (3GPP) is progressing through intermediate stages in which new important features are being added. Notably, in releases 12, 13, and 14, 3GPP standardized LTE access in unlicensed spectrum as a supplement to costly and scarce licensed carriers. For instance in Release 13, 3GPP focused on spectrum aggregation over licensed and unlicensed frequency bands for downlink communications [1]. In Release 14

this feature was extended also to specific uplink channels [19]. As a result of increasing interests in using unlicensed band by cellular networks, academia and industries have investigated a lot on sharing mechanisms for unlicensed LTE and 5G technologies [20]–[23].

On the 5 GHz band although there are some technologies on integration of LTE and WiFi radio links and using WiFi to access the unlicensed spectrum, there is high attention of using LTE Radio Access Network (RAN) in unlicensed spectrum. Some examples of the former technologies are LTE-WLAN Aggregation (LWA) and LTE-WLAN radio level integration with IPsec tunnel (LWIP) [24]–[26]. For the use of LTE RAN in unlicensed spectrum as summarized in [27], two different types of LTE networks were developed by 3GPP: LTE-Unlicensed (LTE-U) and Licensed Assisted Access (LTE-LAA) [11]. Both systems are designed to operate in the 5 GHz band. The work in [27] explains in detail LAA, highlighting both advantages and disadvantages of this approach. On the other hand, LTE-U and MultiFire (which is another type of unlicensed LTE) are described in [28]. For using LTE RAN to access to the unlicensed spectrum, the main challenge is the fair coexistence with other wireless technologies operating in the same band. Generally, the existing technologies in the unlicensed band operate in decentralized and asynchronous manner whereas LTE is designed to have an exclusive access to the channel. Thus, it is very critical to provide an exact analytical model to evaluate the WiFi performance in presence of unlicensed LTE as well as design an unlicensed LTE system which is able to coexist with other pre-existing technologies in a fair and friendly manner. Some of the challenges of such coexistence are described in [29] and [30].

### 2.2.1 LTE/WiFi Coexistence

With LTE small cells transmitting in the 5 GHz unlicensed spectrum an interesting problem to study consists of evaluating the impact over other unlicensed wireless technologies has arisen. Depending on the type of unlicensed LTE, better coexistence can be achieved. Among the systems that could be affected by unlicensed LTE transmissions, this work focuses on studying the impact on WiFi as, probably, the most popular unlicensed technology. It is worth reminding that, despite both systems make use of Orthogonal Frequency Division Multiplexing (OFDM) modulation, the physical layer numerology is radically different between the two systems, as well as the networking aspects. To address this pressing problem, amidst many initiatives, also 3GPP started investigating how to improve LTE and WiFi coexistence. The two surveys in [31] and [20] provide a thorough overview of co-existence issues between WiFi and LTE, as well as they present various methods to preserve the throughput of both systems. Throughput and fairness analysis of LTE-U and WiFi over the unlicensed band was provided in [32]. In [33], the authors proposed a fair downlink traffic management scheme in hybrid LTE-LAA and WiFi network to improve coexistence of both systems. A study on improving coexistence between WiFi and LTE-LAA with adaptive energy detection (ED) threshold was presented in [34].

Although most of these systems are endowed with collision avoidance mechanisms, it is still possible to collide with WiFi either during active periods of LTE Unlicensed [3] or due to hidden node problems. Such a situation gives rise to inter-network interference between heterogeneous uncoordinated Orthogonal Frequency-Division Multiplexing (OFDM)-based transmitters. Moreover, they can cause WiFi to detect the channel busy more often during Clear Channel Assessment (CCA) and less possibility to transmit as a result.

In addition, experimental studies in which different test-beds were set-up to measure the impact of LTE on the WiFi throughput can be found in [35] and [7]. As evident also in [10], the debate between 3GPP RAN 1/RAN 4 and IEEE 802 committee started around the ED threshold that is required for the coexistence with LTE-LAA and IEEE 802.11 stresses the importance of adjusting the ED threshold of both technologies. The authors of [28] concluded that LAA can have better coexistence with WiFi whereas MulteFire [36] is the most flexible one in terms of deployment. The works in [3] discussed the duty cycle of LTE-U, both theoretically and experimentally, to show that a maximum duty cycle of 95% cannot preserve WiFi performance.

## 2.2.2 Interference Modeling

The spatial distribution of interfering transmitters plays a major role, as well as their modulation and coding schemes and transmitted powers. In this regard, analytically tractable PPPs can model the spatial distribution of interference [37], [38]. Advanced analytical models of interference in wireless ad hoc networks and cellular networks were developed in past years under various assumptions on the position of interfering transmitters over the space. In this regard, stochastic geometry has found a prime role as shown in [39]–[42]. The most used assumption is the spatial Poisson distribution of the interfering devices, which has proved to be both mathematically tractable and accurate for performance evaluation. For example, accurate symbol error probability expressions were obtained in closed form for M-QAM and M-PSK modulations under the assumption of a Poisson distribution of interfering transmitters in [43] and [44]. These inspiring analytical models will be reused also in this work.

## 2.3 Blockchain and Distributed Ledgers

A Blockchain is a distributed database of records, i.e., an immutable public ledger of all digital transactions that have ever been executed and shared among the network participants. Every single transaction in the public ledger is verified employing a consensus mechanism among the participants in the system, whereas the transaction is validated once a consensus is reached among the majority. [45]. It is considered as a permanent database shared by all nodes participating in the network. The database is a collection of blocks which holds the record of every transaction ever executed. Each block includes collections of signatures transactions. A block can be appended to

the chain of blocks after reaching to the consensus. For example, in bitcoin which uses proof of work, the new block is added after solving a puzzle which is to find a number that hash value is less than the current target. Upon joining the network, each node receives this database and stands as a proof of every transaction. Furthermore, these nodes can jointly validate new transactions without requiring any intermediate or central entity. This particular characteristic of Blockchain makes the network completely trusted and secure and eliminates the need for any trusted third party. Bitcoin, the decentralized peer-to-peer digital currency [46], is one of the most successful examples that uses Blockchain technology to execute peer-to-peer transactions between users without the need for any intermediaries. Within the Blockchain, cryptology supplants intermediaries as the trusting entity, with all network participants running complex mathematical algorithms to certify the integrity of the system [47].

Some of the main elements of Blockchain are:

*Transaction.* Transactions are the critical data structure of a Blockchain. Normally, a transaction is made by the participant nodes or autonomous objects such as smart contracts. These transactions indicate transfer of tokens or crypto-currencies from a sender to the specific receiver. To protect the authentication of a transaction, the hash function and asymmetric encryption are activated. With a proper hash function (e.g. SHA-256) it is impossible to recover the input from the output of the function. Further, the asymmetric encryption allows each node in the Blockchain network generates a pair of public and private keys. The former is a digital signature function while the latter is associated with a verification function.

*Block.* Each set of arbitrary transactions are stored in a block which is created by participating nodes in a consensus process. They are the storage units for transactions that record details such as date, time, currency amount, and transaction participants. Each block on the Blockchain has a limited storage size (e.g., 30KB in Ethereum). Therefore, depending on the size of the transactions, a single block can hold a few hundred of transactions. Also, each block stores a unique 'hash' that distinguishes itself from other blocks.

*Chain.* Blocks are organized into a linear sequence overtime referred to as the Blockchain. As the number of blocks in the Blockchain increases, they become more challenging to change or remove the block data, thus increasing the cost of attack.

Moreover, the consensus mechanism in the Blockchain presents a vital role to eliminate the trust concern by identifying the authorized parties that can append the next block into the chain. Two of the most popular consensus approaches adopted by different Blockchains are Proof of Work (PoW) [48] and Proof of Stake (PoS) [49]. In PoW, miners compete to solve mathematical puzzles by consuming CPU/GPU, energy, and time. The miner has to solve the puzzle first and to append the block is rewarded for the work done. Alternatively, PoS works differently with no miners doing work for a reward. Instead, block creator is chosen in a deterministic way by the network based on the amount of cryptocurrency one is holding [49]. These

block creators receive network fees as a reward for validating the transactions that could protect the system from Sybil attack and double-spending. The two mentioned consensus algorithms are mostly used in a permissionless Blockchains where everyone can join to the distributed ledger and be as participants. However, there is another type of Blockchain, permissioned, where the participant nodes are selected by a consortium of organizations who are responsible for controlling and administration of participants [50]. One such a consensus used in permissioned Blockchain (e.g., hyperledger Sawtooth) is Proof of Elapsed Time (PoET). Each of the network participants generates a random time and goes to sleep for that specified duration. The first node who wakes up commits a new block to the Blockchain, broadcasting the necessary information to the whole peer network. The same process then repeats for the discovery of the next block. There are some other consensus mechanism such as KAFKA or RAFT [51]. Generally, Since the number of predefined participants are limited in a permissioned Blockchain, the consensus algorithms are normally less complex and more efficient.

Although these kind of systems may introduce some computational costs, they can provide decentrality, security, transparency, and robustness. That is why the Blockchain and Distributed Ledger Technologies are widely used in many different areas as a hot topic for academia and industries [52]–[57].

### 2.3.1 Blockchain in Telecom

Blockchain and its practicality for various scenarios have seen a great interest in recent years in Telecom industries. There have already been many talks and researches focused on the performance of Blockchain in IoT, cloud computing, spectrum sharing and so on. The Ankr project is a Blockchain-based decentralized cloud solution which offers the clients to run application in cheaper prices [58]. Authors in [59] remark spectrum sharing from primary users (licensed holders) to secondary users through a public Blockchain. In [60] authors investigate on challenges and opportunities of decentralized solutions in cloud and fog computing. A practical case can be found in the white paper of QLINK startup [61] which discusses the implementation of decentralized WiFi sharing. In this white paper, it is shown how an owner of a WiFi access point can share its Hotspots in return off some awards without any need of trusted third party. Moreover, in [62] authors address different aspects of Blockchain in mobile networks such as in IoT, Smart Cities, and 5G service enablers. The authors propose a seamless provisioning between heterogeneous access nodes and devices with a smart contract-enabled Blockchain. There are many other examples of research about the usage of Blockchain in telecommunications word such as as [63], [64].

### 2.3.2 Blockchain for 5G Networks

The fusion of 5G and Blockchain has many potential to unleash surge of financial values. This relationship is multifold and can be used in many different areas. One such an example is in Internet of Things. The 5G system with

capabilities of low latency, high speed and capacity allows the IoT devices to become widely used. These devices can leverage the security, decentralization, immutability and consensus arbitration of Blockchains as foundational layers [65]–[67]. Blockchain can also enable a new generation of access technology selection mechanisms required for the realization of 5G networks. One more important potential of Blockchain for the cellular networks (e.g. 4G and 5G) is in roaming scenario [68]. It has the potential to reduce losses due to fraud detection applications. To this extent, Blockchain can not only ease the billing settlements between home operator and visited operator, but also it can increase the identity management of roaming users. The benefits of using Blockchain in roaming is multifolded. First, it can save expenses by eliminating the intermediaries (e.g. clearinghouses). Second, It reduces the subscriber fraud. Third, It provides faster and easier device identification, etc [69]. The concepts also revealed by recent applications of DLT permit further applications beyond roaming: the network services rendered by MNOs can be aligned and synchronized, an approach already in discussion in the area of Network Slicing. Different MNOs must guarantee a distinct network quality and service level agreement [70] which again are of crucial importance for autonomous vehicles crossing national borders. DLT can be used as slice broker, for cross-charging, as service management tool and is thus the currently missing trust link between MNOs [71]–[73].

## Chapter 3

# On Performance of Wi-Fi Networks Interfered by Unlicensed LTE

In this chapter we analyze the performance of a WiFi device when interfered by presence of unlicensed LTE in 5 GHz band. We first evaluate in details the CCA mechanism of 802.11 affected by LTE looking at Energy Detection (ED) procedure and compare the results with the case of absence of LTE interference. We then analyze the bit error rate when the two systems are transmitting simultaneously. Finally, we present the performance of CSMA/CA in both saturated and unsaturated conditions. While discussing about unsaturated conditions, we generalize the performance of WiFi throughput when it is affected by transmission of an OFDM-based system rather targeting specific unlicensed LTE.

### 3.1 System Model

Figure 3.1(a) illustrates the scenario that we use to model ED-CCA, whereas Figure 3.1(b) the one we use to conduct the bit error probability analysis. In both figures, the WiFi terminal under test is assumed to be located in the center of a two-dimensional reference system. In the first figure, this is the terminal that does the ED-CCA operation, whereas in the other one (Figure 3.1(b)) it is the recipient of an intended data transmission. In both scenarios, in the 2-dimensional space, the region of interest for this study is a circular region of area  $A$  and radius  $R$ . In Figure 3.1(a),  $r_s$  denotes the ED-CCA sensing range of a WiFi node that ensures a target probability of detecting an ongoing communication. Different values of  $r_s$  correspond to different energy detection thresholds. On the other hand,  $r_u$  in Figure 3.1(b) denotes the WiFi link distance during a data session.

We assume that only one WiFi link is active during ED-CCA (situation with minimum amount of energy to detect), whilst for conducting the bit error probability analysis, WiFi transmitters are assumed distributed over the space according to a homogeneous Poisson Point Process (PPP) of constant intensity  $\lambda_w$ . For LTE transmissions, we are interested in studying both the of single LTE interferer and generalizing it to the case of aggregate LTE interference. This allows us to study two extreme conditions of low and high interference energy that may affect both the CCA operation of WiFi and data

packet reception due to the increased bit error probability. To model the aggregate interference, we assume that LTE transmitters are displaced over the space according to a PPP of constant intensity  $\lambda_l$ . We denote by  $\Omega$  the set of active LTE transmitters, i.e., an LTE interferer located at point  $X$  of the spatial point process contributes to the interference *iff* it belongs to  $\Omega$ .

The generic expression of the Poisson distribution with intensity  $\lambda_x$  for the number of points in a measurable set  $\mathcal{A}$  of area  $A$  is

$$P_r\{\kappa = K\} = \frac{(\lambda_x A)^K}{K!} \exp(-\lambda_x A). \quad (3.1)$$

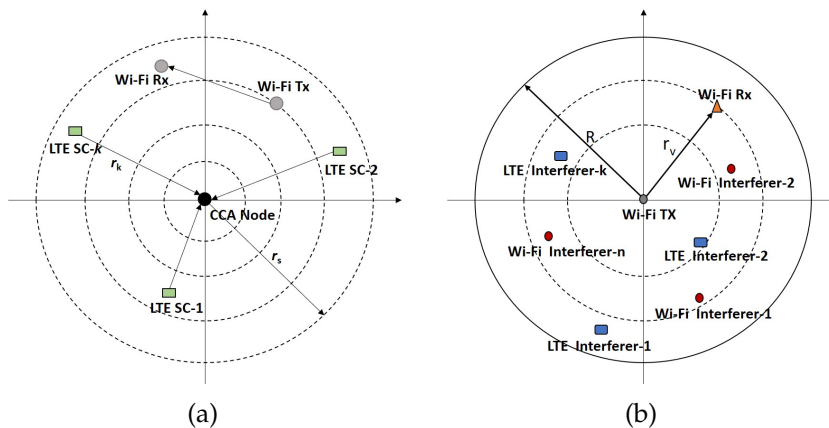


FIGURE 3.1: General scenarios for (a) studying CCA affected by interference and, (b) bit error probability analysis.

The additional assumptions that we use to develop the analysis are the following. The location of interfering WiFi and LTE nodes are assumed random and independent over the space and all links are affected by a path-dependent loss with exponent  $\alpha$ . The path-loss model assumed in this work is such that  $l(x, y) = \|x - y\|^\alpha$  with one point that coincides with the origin of the reference system. Further, we assume that the distance  $r$  separating an LTE interfering transmitter and the test WiFi receiver is a random variable (r.v.) that follows the 2-dimensional uniform distribution with probability  $\frac{2r}{R^2} dr$  in the interval  $[r, r + dr)$ . Communication links (useful and interfering) are assumed mutually independent and corrupted by Additive White Gaussian Noise (AWGN) that is assumed to be a circularly symmetric complex ( $\mathcal{CN}$ ) random process ( $n(t)$ ) with zero mean and variance  $\sigma^2$ . All links are affected by Rayleigh distributed amplitude channel fading. Power fading coefficients (generically denoted by  $g$ ) are assumed i.i.d. r.v.s. with unitary mean energy.

Referring to Figure 3.1(a), the test WiFi node that carries out ED-CCA during the downlink transmission of LTE small cells in the same unlicensed frequency band shall detect the channel busy even if no other WiFi node is active. Although it follows from CSMA/CA, this has a negative effect on the WiFi network throughput since the probability to access the channel is

lower depending also on the type of unlicensed LTE system. The resulting heterogeneous network can be studied modeling the ED-CCA behavior affected by LTE transmissions whereby probabilities of false alarm ( $P_{fa}$ ) and detection ( $P_d$ ). Moreover, at the receiver side, the WiFi sampling frequency is different from the one used in LTE. Thus, we can introduce a re-sampling factor to model the effect. To completely model it, we should consider the frequency selective behavior of the phenomena but for the sake of simplicity we introduce a constant re-sampling as shown in the numerical results of Section 3.3.1

The general approach that will be pursued consists of deriving closed form expression of the characteristic function (CF) of the ED decision variable (d.v.)  $Y$ , with  $\Psi(v) := \mathbb{E}\{e^{jvx}\}$  that denotes the CF of a r.v.  $x$ . Subsequently, we will resort to the Gil-Pelaez inversion theorem [74] to compute the complementary probability

$$P_r\{X > x\} = \frac{1}{2} + \frac{1}{\pi} \int_0^\infty \text{Im} \left( \frac{\Psi(v)e^{-jvx}}{v} \right) dv, \quad (3.2)$$

with  $\text{Im}(\cdot)$  that denotes the imaginary operator. Through the CF, we can remove the statistical dependence upon the position of the LTE interfering devices and channel fading.

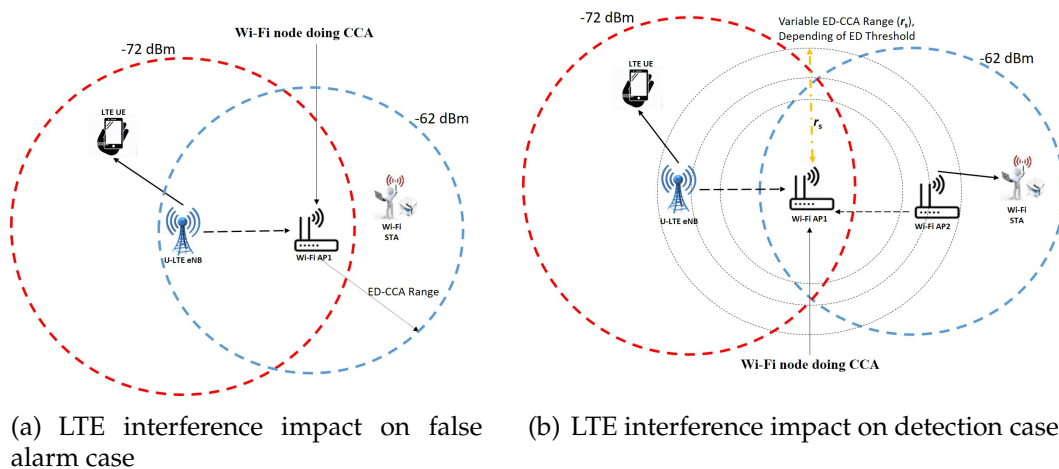


FIGURE 3.2: Presence of LTE transmission for studying of WiFi CCA performance under Case Study "B".

## 3.2 Effects of Unlicensed LTE on PHY Layer of 802.11

### 3.2.1 Energy-Detection Analysis

We study the ED receiver when LTE transmissions affect the ED-CCA operation of WiFi (e.g. IEEE 802.11n). Introducing the false alarm event, we are able to evaluate the effect of different energy detection thresholds. The initial

results of this chapter is published in [75]. As mentioned, LTE transmissions are modeled as an interfering random process. The typical definition of false alarm and detection is

$$P_{fa}(\lambda) := P_r\{Y > \lambda | \mathcal{H}_0\}, \quad P_d(\lambda) := P_r\{Y > \lambda | \mathcal{H}_1\}, \quad (3.3)$$

where  $\mathcal{H}_0$  and  $\mathcal{H}_1$  are the two statistical hypotheses of the absence and presence of signals, respectively, and  $\lambda$  is the energy detection threshold. Conditioning upon the distribution of the interference, channel fading and distance, the ED decision variable  $Y$  follows either a central or a non-central Chi-Square distribution. We observe that the latter distribution has a non-centrality parameter ( $\mu$ ) that can be distinguished depending on the active signals. The CF of the non-central Chi-Square distributed r.v. is  $\Psi(v) = (1 - j2v)^{-Q} \exp\left(\frac{jv}{1-j2v}\mu\right)$ , with  $2Q$  defined as the number of degrees of freedom. We analyze two different case studies of interest that will be evaluated to a great extent in the remainder of the paper and that will be compared in terms of network throughput.

**Case study A: Fixed threshold** The energy detection threshold remains fixed to -62 dBm. False alarm can happen only due to noise and in the presence of a sufficiently strong signal (LTE or WiFi) the medium will be detected busy, thus implying that a WiFi node will refrain from transmitting. In this situation, the WiFi node doing ED-CCA is able to detect any signal that occupies the communication channel. In the subsequent analysis, we develop hypotheses  $\mathcal{H}_0^{(A)}$  and  $\mathcal{H}_1^{(A)}$ .

**Case study B: Modified threshold** Referring to Figure 3.2(a) and 3.2(b), the ED threshold is increased in the presence of LTE transmissions to compensate the higher level of energy over the channel that may otherwise exceed the ED threshold. Increasing the threshold, a WiFi node can ignore weak LTE signals, while a strong aggregate LTE power will still cause the channel to be detected busy.

In Figure 3.2(a), WiFi AP1 is carrying out the ED-CCA operation when no other WiFi transmission is ongoing (hypothesis  $\mathcal{H}_0^{(B)}$ ). In this Case study, we try to ignore presence of LTE transmission by increasing ED-CCA threshold and compare the final throughput to the one in Case study A. Figure 3.2(b) illustrates instead the ED-CCA with different threshold values when another WiFi transmitter is active (hypothesis  $\mathcal{H}_1^{(B)}$ ). Relying on [75], we provide the expression of the pre-enveloped OFDM signal for WiFi as follows

$$S(t) = \sum_{k=-\infty}^{\infty} \sum_{n=0}^{N-1} a_n^{(k)} p(t - kt_s) e^{j2\pi f_n t} = \sum_{k=1}^{2Q} x_k(t - kt_s),$$

where  $2Q = WT$  is equal to the number of samples acquired during  $T = 4\mu\text{s}$  ED-CCA time.  $W$  is the signal bandwidth,  $|a_n^{(k)}| = \sqrt{\frac{\varepsilon_s}{N}}$  is the signal amplitude of the  $k$ th OFDM symbol on the  $n$ th sub-carrier,  $\varepsilon_s$  is the transmitted symbol energy,  $p(t)$  is the waveform with unitary energy,  $N$  is the number of OFDM sub-carriers with  $f_n = f_c + \Delta f(n - \frac{N-1}{2})$ , centered at frequency  $f_c$ ,

and  $\Delta f$  is the sub-carrier spacing (312.5 kHz in 802.11n).

Similarly to the case of a useful signal, the OFDM signal for LTE can be written as

$$\tilde{\zeta}(t) = \sum_{m=0}^{N'-1} a_m b(t-v) e^{j2\pi f_m(t-v)+\varphi} = \sum_{m=0}^{N'-1} x_m(t-v, \varphi), \quad (3.4)$$

where  $|a_m| = \sqrt{\frac{\varepsilon_I}{N'}}$  is the per sub-carrier energy with  $\varepsilon_I$  the transmitted LTE symbol energy,  $N' \neq N$  denotes the number of OFDM sub-carriers,  $f_m = f_c + \Delta F(m - \frac{N'-1}{2})$  and  $\Delta F$  is the sub-carrier spacing (15 kHz for LTE),  $b(t)$  is the transmitted waveform with unitary energy,  $v$  is a random delay time that takes into account that the LTE transmission is asynchronous with respect to the useful WiFi signal, and  $\varphi$  is a uniformly distributed r.v. in the interval  $[0, 2\pi)$ .

The aggregate LTE interfering signal can be obtained from equation (3.4) straightforwardly as  $I(t) = \sum_{X \in \Omega} \zeta_X(t)$ , where  $\zeta_X$  stands for the interfering LTE signal located at point  $X$  in the spatial point process. The general expression of the received signal with interference, corrupted by additive noise and fading is:

$$r(t) = h_s S(t) + \sum_{k=1}^K h_{I_k} \mathbb{1}_k \zeta_k(t) + n(t), \quad (3.5)$$

where  $\mathbb{1}_k$  is an indicator r.v. that is one when the  $k$ -th interfering signal  $\zeta_k(t)$  is present and zero otherwise. The expression can also be used to evaluate the benchmarking performance for the ED-CCA affected only by path-loss and fading setting  $\Omega = \emptyset$ . On the other hand,  $I(t)$  reduces to  $\tilde{\zeta}(t)$  in case exactly one LTE interferer is active.

Terms  $h_s$  and  $h_{I_k}$  respectively denote the effect introduced by the channel fading for the WiFi signal and the  $k$ -th LTE signal with  $h := \theta e^{j\phi(t)}$ , which is such that  $|h|^2 = g$  after the squaring operation of the ED receiver. Complying with the two statistical hypotheses for false alarm and detection, we denote by  $r_0$  the received signal when no WiFi transmission is on the air (i.e. hypothesis  $\mathcal{H}_0$ ), and with  $r_1$  the received signal when the WiFi transmission is present (i.e. hypothesis  $\mathcal{H}_1$ ). The received signal under the case study A when exactly one LTE interfering signal affects the ED-CCA operation can be written as

$$\begin{aligned} r_0^{(A)}(t) &= n(t), \text{ under } \mathcal{H}_0^{(A)} \\ r_1^{(A)}(t) &= h_s S(t) + h_I \mathbb{1}_{\tilde{\zeta}} \tilde{\zeta}(t) + n(t), \text{ under } \mathcal{H}_1^{(A)}. \end{aligned} \quad (3.6)$$

where  $\mathbb{1}_{\tilde{\zeta}}$  is the indicator variable in Case study A for the combination of useful and interfering signal with  $h_s S(t) + h_I \mathbb{1}_{\tilde{\zeta}} \tilde{\zeta}(t) = X_S(t) + \mathbb{1}_{\tilde{\zeta}} X_I(t)$ . In

Case study B, we can write

$$\begin{aligned} r_0^{(B)}(t) &= h_I \zeta(t) + n(t) = X_I(t) + n(t), \text{ under } \mathcal{H}_0^{(B)} \\ r_1^{(B)}(t) &= h_s S(t) + h_I \zeta(t) + n(t) \\ &= X_S(t) + X_I(t) + n(t), \text{ under } \mathcal{H}_1^{(B)}. \end{aligned} \quad (3.7)$$

In the rest of the chapter, we assume  $r_1^{(A)}(t) = r_1^{(B)}(t)$ , or in other words that in  $\mathcal{H}_1$  both WiFi and interfering signals are present. Since  $r(t)$  is the complex envelope of the received signal after carrier frequency down-conversion,  $r(t) = r_R(t) + jr_I(t)$  and  $r_R(t)$  (respectively  $r_I(t)$ ) denotes the real (respectively imaginary) part. Relying on [76], the analog d.v.  $Z$  (in the continuous time domain) can be found by applying the following operation to the received signal:  $Z = \frac{1}{2\sigma^2} \int_0^T |r(t)|^2 dt$ , where  $T$  is the integration time and  $\sigma^2 = \frac{N_0}{2}$  is the power spectral density of the additive noise in the real band-pass signal. After sampling the continuous time problem, we obtain d.v.  $Y$  for the discrete time version of the variable  $Z$  as follows

$$Y = \frac{1}{2\sigma^2} \sum_{q=1}^{2Q} \frac{r_q^2}{2W}, \quad (3.8)$$

Due to the assumption that all links are independent, the cross-terms are neglected and we distinguish the d.v. based on the case studies:  $\mathcal{H}_0^{(A)}$ ,  $\mathcal{H}_0^{(B)}$  and  $\mathcal{H}_1$ , respectively as:

$$\begin{aligned} Y_0^{(A)} &= \frac{1}{2\sigma^2} \sum_{q=1}^{2Q} \left( \frac{n_q^2}{2W} \right), \\ Y_0^{(B)} &= \frac{1}{2\sigma^2} \sum_{q=1}^{2Q} \left( \frac{X_{Iq}^2 + n_q^2}{2W} \right), \\ Y_1 &\simeq \frac{1}{2\sigma^2} \sum_{q=1}^{2Q} \left( \frac{X_{sq}^2 + X_{Iq}^2 + n_q^2}{2W} \right), \end{aligned} \quad (3.9)$$

where the approximation in  $Y_0^{(B)}$  holds since the interfering signal and the noise term are uncorrelated, whereas the approximation in  $Y_1$  holds since the cross-term between WiFi and LTE signal can be neglected due to the different spacing and sub-carriers' number. While  $Y_0^{(A)}$  is central Chi-Square distributed,  $Y_0^{(B)}$  and  $Y_1$  follow a non-central Chi-Square distribution [75] with non-centrality parameters as

$$\begin{aligned} \mu_0^{(B)} &= \frac{1}{2\sigma^2} \sum_{q=1}^{2Q} X_{Iq}^2 = g_I \frac{2Q \cdot \varepsilon_{rI}}{2\sigma^2} \times c \\ \mu_1 &= \frac{1}{2\sigma^2} \sum_{q=1}^{2Q} (X_{sq}^2 + X_{Iq}^2) = g_s 2Q \frac{\varepsilon_{rs}}{2\sigma^2} + c \times g_I 2Q \frac{\varepsilon_{rI}}{2\sigma^2}, \end{aligned} \quad (3.10)$$

where  $\varepsilon_{rs}$  and  $\varepsilon_{rl}$  denote the received WiFi energy and LTE energy per sample. The factor  $c$  is the re-sampling factor that takes into account different sampling rate in WiFi and LTE.

In the remainder of this section, we will introduce three theorems that evaluate the two main parameters of ED-CCA mechanism, probability of false alarm and probability of detection, under different network interference scenarios. To this end, we first derive the close form expression of the characteristic functions considering Rayleigh amplitude fading and path-loss. Then, the two probabilities can be obtained numerically using the Gil-Pelaez inversion theorem.

**Theorem 1** (No Interference Case). *In the no interference case, under statistical hypothesis  $\mathcal{H}_0^{(A)}$ , the false alarm probability is simply computed as  $P_{fa} = \Gamma(Q, \lambda/\sigma^2)/\Gamma(Q)$ . When the signal is affected by Rayleigh amplitude fading and path-loss, the detection probability  $P_d$  can be computed through the CF of the non-central Chi-Square distribution and equation (3.2) by numerical inversion.*

*Proof.* The proof of the false alarm probability follows from [77] under statistical hypothesis  $\mathcal{H}_{0(B)}$ . For detection, we begin with the expression of the CF,  $\Psi(v|g)$ , of the d.v.  $Y$  conditioned on the power fading  $g$ . Since  $g$  is exponentially distributed, we can remove the conditioning whereby the expectation operation  $\Psi(v) = \mathbb{E}_g(\Psi(v|g))$  as follows

$$\Psi(v) = \frac{1}{(1 - j2v)^Q} \times \frac{1}{1 - \frac{jv}{1-2jv}\mu}. \quad (3.11)$$

Without interference, the non-centrality parameter of the Chi-Square can be written as:  $\mu = 2Q \frac{\varepsilon_s^2}{2\sigma^2} = 2Q \frac{\varepsilon_s}{N_0} r_s^{-\alpha}$ . We finally apply the Gil-Pelaez inversion theorem to  $\Psi(v)$ . □

**Theorem 2** (Single interference Case). *In case exactly one LTE interferer is active, the false alarm probability  $P_{fa}$  can be obtained through numerical inversion (by means of equation (3.2)) of the CF  $\Psi_0^{(B)}$  of the d.v.  $Y_0^{(B)}$  with non-centrality  $\mu_0^{(B)}$  given in the first of equation (3.10) in statistical hypothesis  $\mathcal{H}_{0(B)}$ . The detection probability  $P_d$  is obtained numerically inverting the CF  $\Psi_1$  of the d.v.  $Y_1$  under the statistical hypothesis  $\mathcal{H}_1$  with non-centrality  $\mu_1$  in the second of (3.10).*

$$\begin{aligned} \Psi_0^{(B)}(v) = & \frac{1}{(1 - j2v)^Q} \times \frac{2R^\alpha}{c \times 2Q \frac{\varepsilon_I}{N_0} \frac{jv}{j2v - 1} (2 + \alpha)} \times \\ & {}_2F_1 \left( 1, \frac{2 + \alpha}{\alpha}, 2 + \frac{2}{\alpha}, \frac{R^\alpha}{2Q \frac{\varepsilon_I}{N_0} \left( \frac{jv}{1-2jv} \right)} \right), \end{aligned} \quad (3.12)$$

$$\Psi_1(v) = \frac{1}{(1-j2v)^Q} \times \frac{1}{1-2Q \frac{jv\epsilon_s}{(1-j2v)N_0} r_s^{-\alpha}} \times \frac{2R^\alpha}{c \times 2Q \frac{\epsilon_1}{N_0} \frac{jv}{j2v-1}} \times \frac{{}_2F_1\left(1, \frac{2+\alpha}{\alpha}, 2 + \frac{2}{\alpha}, \frac{R^\alpha}{2Q \frac{\epsilon_1}{N_0} \left(\frac{jv}{1-2jv}\right)}\right)}{2+\alpha}, \quad (3.13)$$

where  ${}_2F_1(\cdot)$  the hypergeometric function and  $r_s$  is the ED-CCA range that is varied for results that is shown in the numerical results of Section 3.3.1.

The proof of this theorem is provided in Appendix A.1.

**Lemma 2:** For any  $s \in \mathbb{C}$ , with path-loss exponent  $\alpha > 2$  and  $R > 0$  the following integral holds:

$$\int_0^\infty \frac{1}{1+s^{-1}r^\alpha} \frac{2r}{R^2} dr = \frac{2\pi s^{2/\alpha} \csc\left(\frac{2\pi}{\alpha}\right)}{\alpha R^2}, \quad (3.14)$$

where we have used the 2-dimensional uniform distribution. Equation (3.14) is proved in Appendix A.2.

**Theorem 3** (Aggregate interference Case). *Reusing the assumptions of Theorem 2, the probabilities of false alarm and detection affected by aggregate LTE interference can be derived by numerical inversion of the corresponding characteristic functions  $\Psi_0^{(B)}$  and  $\Psi_1$  obtained respectively under statistical hypotheses  $\mathcal{H}_0^{(B)}$  and  $\mathcal{H}_1$ .*

$$\Psi_0^{(B)}(v) = \frac{1}{(1-2jv)^Q} \times \exp\left(-\lambda_1\left(\frac{jv}{-1+j2v} \frac{2Qc\epsilon_1}{N_0}\right)^{2/\alpha} \frac{2\pi^2}{\alpha} \csc\left(\frac{2\pi}{\alpha}\right)\right), \quad (3.15)$$

$$\Psi_1(v) = \frac{1}{(1-j2v)^Q} \times \frac{1}{1-2Q \frac{jv\epsilon_s}{(1-j2v)N_0}} \times \exp\left(-\lambda_1\left(\frac{jv}{(-1+j2v)} c \times 2Q \times \frac{\epsilon_1}{N_0}\right)^{2/\alpha} \frac{2\pi^2}{\alpha} \csc\left(\frac{2\pi}{\alpha}\right)\right), \quad (3.16)$$

The proof of this theorem is provided in Appendix A.3.

### 3.2.2 Bit Error Probability analysis

To conduct the BEP analysis, we rely on the work developed in [43] for M-QAM. We will develop the BEP with aggregate LTE interference, single LTE interferer as well as without. We assume that the signal from a test WiFi transmitter is sent to the intended recipient at distance  $r_u$  as in Figure 3.1(b). The test transmission is affected by WiFi intra-network interference (interference of other WiFi transmitters caused by missed detection or simultaneous

transmissions). Such process is modeled with a PPP of intensity  $\lambda_w$ . The aggregate LTE interfering process is also a PPP of intensity  $\lambda_l$ . The WiFi transmitters use M-QAM while LTE transmitters  $M'$ -QAM. The derivations shown hereinafter are done under the assumption of Rayleigh distributed amplitude channel fading and log-normal distributed shadowing, further conditioned upon the WiFi link distance  $r_u$ . As in [43], we consider the case in which the position of the interferer devices slowly varies in time (reasonable in indoors).

Let us write the aggregate interference as  $U = \sum_{i=1}^{\infty} \frac{e^{2\sigma_1 G_i}}{r_i^\alpha} X_i$ , where  $\sigma_1$  denotes the shadowing factor,  $G_i \sim \mathcal{N}(0, 1)$  and  $X_i$  is approximated by a zero-mean circularly symmetric (CS) complex Gaussian r.v. with variance that depends upon the energy of the interference:  $X_i \sim \mathcal{N}_c(0, 2E)$ . For any location in space of the interfering transmitters, we denote  $A = \sum_{i=1}^{\infty} \frac{e^{2\sigma_1 G_i}}{r_i^\alpha}$ , which is modeled with a skewed Stable distributed r.v.:  $A \sim \mathcal{S}\left(2/\alpha, 1, \pi\lambda_l \mathcal{C}_{2/\alpha}^{-1} e^{2\sigma_1^2/(\alpha/2)^2}\right)$ , with  $\mathcal{C}_x := (1-x)/(\Gamma(2-x)\cos(\pi x/2))$  for  $x \neq 1$ ,  $\mathcal{C}_x = 2/\pi$  if  $x = 1$  and  $\Gamma(\cdot)$  the Gamma function. Resorting to [43] the r.v.  $U$  is modeled as the sum of independent CS Gaussian r.v.s. and  $U \sim \mathcal{N}_c(0, V)$ .

We continue the BEP analysis assuming that both useful and interfering symbols in their respective constellations are equiprobable and that the constellation is symmetric with respect to the complex plane, as in the case of M-QAM or  $M'$ -QAM modulation. In this way, it holds that  $V = 2A\varepsilon_{I,\text{sym}}/3$ , in which the energy of an LTE interfering symbol can be written as  $\varepsilon_{I,\text{sym}} = \log_2(M')\varepsilon_{\text{bl}}$  and for a WiFi transmission the symbol energy is as  $\varepsilon_{s,\text{sym}} = \log_2(M)\varepsilon_{\text{bs}}$ . We compute  $\varepsilon_{\text{bs}} = \frac{P_{\text{ts}}}{R_{\text{bs}}}$ , with  $P_{\text{ts}}$  the transmitted power of WiFi and  $R_{\text{bs}}$  the transmission rate; similarly,  $\varepsilon_{\text{bl}} = \frac{P_{\text{tl}}}{R_{\text{bl}}}$  is the energy per bit measured 1 m away from the interfering transmitter.

The BEP can be found from the average symbol error probability obtained in [43] using the approximation that is shown below (this typically holds for high SNR values).

$$P_b(\eta) \simeq \left( \frac{4}{\log_2 M} \times \left(1 - \frac{1}{\sqrt{M}}\right) \times \ell_{\frac{\pi}{2}} \right) - \left( \frac{4}{\log_2 M} \times \left(1 - \frac{1}{\sqrt{M}}\right)^2 \times \ell_{\frac{\pi}{4}} \right), \quad (3.17)$$

where

$$\ell_y = \frac{1}{\pi} \int_0^y \left(1 + \frac{g_b}{\sin^2 x} \eta\right)^{-1} dx, \quad (3.18)$$

$g_b = \frac{3\log_2 M}{2(M-1)}$  and  $\eta$  is the average received SINR. The general expression that was obtained in [43] is given below:

$$\eta := \frac{e^{2\sigma_s G_s}}{r_u^\alpha (V+1)} \times \frac{\varepsilon_{\text{bs}}}{N_0}. \quad (3.19)$$

with  $\sigma_s$  the shadowing factor for the useful link.

For the aggregate LTE interference case, the expression above can be rewritten as:

$$\eta_{\text{agg}} = \frac{e^{2\sigma_s} \times \log_2 M \times \frac{\epsilon_{\text{bs}}}{N_0}}{r_u^\alpha (V_{\text{agg}} + 1)}, \quad (3.20)$$

where

$$V_{\text{agg}} = \frac{2\epsilon_{\text{bl}}/3}{N_0} \times \mathbb{E}\{\Delta^{\alpha/2}\} \times \log_2 M' \\ \times \lambda_1 \pi \left[ \frac{\Gamma(2 - \frac{2}{\alpha}) \cos(\frac{\pi}{\alpha})}{1 - \frac{2}{\alpha}} \right] \times \Gamma\left(1 + \frac{2}{\alpha}\right) e^{\frac{2\sigma_s^2}{(\alpha/2)^2}}. \quad (3.21)$$

Where  $\Delta$  is the factor to denote the number of active LTE and is distributed uniformly over interval  $[0,1]$ . Relying on [78], we can show that  $\mathbb{E}\{\Delta^{\alpha/2}\} = n_{\text{Lte}}^2 + \frac{2n_{\text{Lte}}(1-n_{\text{Lte}})\alpha}{\alpha+2}$ , with  $n_{\text{Lte}}$  the probability of having LTE transmission when Wi-Fi is active in downlink. It is worth noting the presence of  $\mathbb{E}\{\Delta^{\alpha/2}\}$  in equation (3.21) is due to asynchronously of Wi-Fi and LTE stations. To find the BEP with exactly one LTE interferer within the Wi-Fi range, we can reuse (3.17) but with the SINR computed as follows

$$\eta_{\text{one}} = \frac{2b}{a} \times \frac{R^\alpha}{2 + \alpha} \times \frac{{}_2F_1\left(1, \frac{2+\alpha}{\alpha}, 2 + \frac{2}{\alpha}, -\frac{R^\alpha}{a}\right)}{\Gamma(1 + 2/\alpha)}. \quad (3.22)$$

where  $a$  and  $b$  have the following expressions:

$$a = \frac{2}{3} e^{2\sigma_s} \log_2 M' \times \frac{\epsilon_{\text{bl}}}{N_0}, \quad b = e^{2\sigma_s} \log_2 M \times \frac{\epsilon_{\text{bs}}}{N_0} r_u^{-\alpha}$$

The proof of equation (3.22) is given in Appendix A.4. We can compute the average BEP in an AWGN channel for M-QAM modulation using (3.20) for the case of  $V \rightarrow 0$  (negligible aggregate interference power) to obtain  $\eta_{\text{awgn}}$ .

From the BEP, we can also compute the packet error probability (PEP) of an uncoded data packet transmission:  $P_e(\eta) = 1 - (1 - P_b(\eta))^{\ell_f}$ , where  $\ell_f$  is the frame size in bits and  $\eta$  is computed as  $\eta_{\text{agg}}$ ,  $\eta_{\text{one}}$  or  $\eta_{\text{awgn}}$ .

We notice that the BEP due to other WiFi signals ( $P_b^{(\text{WiFi})}$ ) is computed by substituting the intensity  $\lambda_w$  as well as transmitted power and modulation order of WiFi signals ( $\epsilon_{\text{bs}}, M$ ) in equation (3.21).

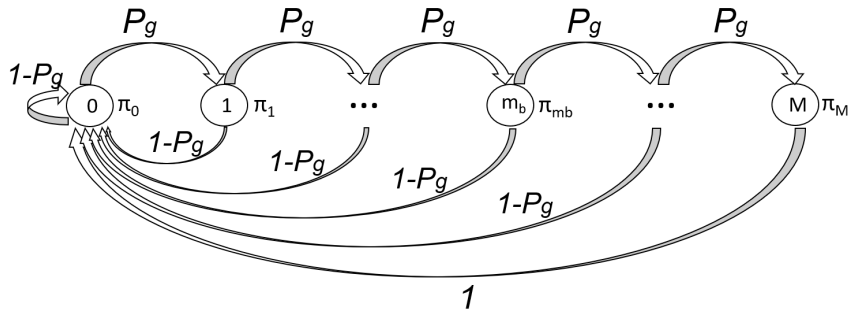


FIGURE 3.3: One-dimensional Markov Chain modeling BEB.

### 3.3 Effects of Unlicensed LTE on MAC layer of 802.11

#### 3.3.1 Saturated 802.11 Throughput Analysis

The average throughput of the 802.11 network under saturation conditions, including modified ED-CCA and PEP in the model, is obtained whereby the one-dimensional Markov Chain (MC) model of the Binary Exponential Back-off (BEB) shown in Figure 3.3. We can reuse the model in [79] and rely on [80] provided that the constant transition probability in the MC model is modified appropriately. Referring to Figure 3.3, the  $i$ th state of the Markov model denotes the  $i$ th backoff state of a WiFi node, being  $\Pi_i$  the respective steady state probability. As per the 802.11 CSMA/CA, the contention window can be doubled only until the maximum backoff exponent  $m_b$  is met, and a data packet can be transmitted only up to  $M_b$  times before this is discarded and removed from the queue of the device. The main result that we will demonstrate is provided in equation (3.31). The general expression of the average WiFi throughput is

$$S := \frac{[Expected\ No.\ of\ bits\ in\ Successful\ Transmission]}{[Average\ slot\ duration]}. \quad (3.23)$$

In the numerator of equation (3.23), the following two terms contribute to the throughput on average:

- I : Probability of WiFi packet to successfully survive collisions with LTE transmissions when the medium is assessed idle after ED-CCA.
- II : Probability of WiFi packet to survive collisions while an ongoing transmission (WiFi, LTE or both signals) is miss-detected after ED-CCA.

Let us denote with  $\tau$  the probability that a randomly selected test WiFi node will transmit over the wireless channel and with  $n_w$  the exact number of WiFi competing stations. Since the spatial process of WiFi stations is assumed PPP distributed with intensity  $\lambda_w$ , this will be taken in account whereby  $\bar{n}_w = \lambda_w |A|$ . Reusing the approach in [79], we can define  $\tau := \frac{2}{1+\overline{CW}}$ , where  $\overline{CW}$  denotes the WiFi contention window (CW) size averaged with respect to

the backoff state in Figure 3.3. From the figure, the constant transition probability,  $P_g$ , can be found in terms of the conditional collision probability  $P$ ,  $P_d$ ,  $P_{fa}$  and the packet error probability  $P_e(\eta)$ . Conditioning on  $n_w$ , it is easy to establish that  $P_{tr} = 1 - (1 - \tau)^{n_w}$  is the probability that at least one WiFi node transmits over the wireless medium. Moreover, the conditional collision probability of the WiFi channel can be expressed as  $P = 1 - (1 - \tau)^{(n_w - 1)}$ , whereas  $P_s$  and  $P_c$  respectively denote the probabilities of packet success and collision:

$$\begin{aligned} P_s &= n_w \tau (1 - \tau)^{n_w - 1}, \\ P_c &= 1 - (1 - \tau)^{n_w} - n_w \tau (1 - \tau)^{n_w - 1}. \end{aligned} \quad (3.24)$$

The hurdle in the analysis is due to the non-linear relation between  $\tau$  and  $P$ . The probability  $P_g$  describes the possible events that cause the transition from the  $i$ -th to the  $(i + 1)$ -th state in the MC model. Below, we describe those events:

- I : Test WiFi packet does not survive the collision with other WiFi transmissions when the same contention window is selected by more than one node after DIFS.
- II : Test WiFi packet does not survive the collision due to miss-detection of other transmissions (WiFi only or both LTE and WiFi).
- III : Test WiFi packet does not survive collision with LTE transmission after sensing the channel idle.
- IV : Loss of packets due to channel fading, path-loss and noise when only the test packet has been transmitted.

In the throughput analysis, we distinguish the PEP between the case of packet collisions due to other WiFi signals ( $P_e^{(WiFi)}$ ) and LTE signals ( $P_e(\eta)$ ). Both probabilities are computed based on the analysis derived in Section 3.2.2. We denote with  $P_e^{(sys)}$  the PEP in the presence of both LTE and other WiFi transmissions which instead computed as:  $P_e^{(sys)} = P_e^{(WiFi)} + P_e(\eta) - P_e^{(WiFi)} \times P_e(\eta)$ . We are now able to write explicitly  $P_g$  as follows

$$\begin{aligned} P_g(n_w, P_{fa}(\lambda), P_d(\lambda, r), P_{ts}, P_{tl}, P_b(r_s), \ell_f) = \\ P \times P_e^{(WiFi)} + P \times \omega(n_w) + (1 - P) \times \varrho(n_w), \end{aligned} \quad (3.25)$$

where  $\omega(n_w)$  and  $\varrho(n_w)$  are written as

$$\begin{aligned} \omega &= P_e^{(sys)} \times (1 - P_d^{n_w - 1}), \\ \varrho &= P_e(\eta) \times (1 - P_{fa}). \end{aligned} \quad (3.26)$$

Since the spatial deployment of WiFi nodes is PPP, we can remove the dependence upon  $n_w$  in equations (3.25) and (3.26). Therefore, to find the transition probability  $\bar{P}_g$  independent on specif values of  $n_w$ , we rewrite equation

(3.26) as:

$$\begin{aligned}\bar{\omega} &= P_e^{(\text{sys})} \left( 1 - P_d^{-1} \times e^{-\bar{n}_w(1-P_d)} \right), \\ \bar{\varrho} &= P_e(\eta) \times (1 - P_{\text{fa}}).\end{aligned}\quad (3.27)$$

The proof of equation (3.27) is provided in Appendix A.5.

Relying on the method in [79], the average CW has the following expression:

$$\overline{\text{CW}} = W_0 \left( \frac{1 - \bar{P}_g}{1 - (\bar{P}_g)^{M_b+1}} \right) \times \left( \frac{1 - (2\bar{P}_g)^{m_b}}{1 - 2\bar{P}_g} \right) + W_0 2^{m_b} \bar{P}_g^{m_b} \times \left( \frac{1 - (\bar{P}_g)^{M_b+1-m_b}}{1 - (\bar{P}_g)^{M_b+1}} \right). \quad (3.28)$$

Using the inequality in [79, eq. 10], we are able to obtain a simple polynomial equation of degree  $M_b + 2$ .

$$\begin{aligned}2(1 - \bar{P}_g^{M_b+1})(\bar{n}_w - 1)(\varrho - \omega - P_e^{(\text{sys})}) = \\ (\varrho - \bar{P}_g) \left( 1 + W_0 + \bar{P}_g W_0 \sum_{i=1}^{m_b-1} (2\bar{P}_g)^i - \bar{P}_g^{M_b+1} (1 - W_M) \right)\end{aligned}\quad (3.29)$$

Since the MC is ergodic, the polynomial equation admits only one valid solution that is the positive real root other than the obvious case when the root is one. After solving the polynomial equation above with respect to  $\bar{P}_g$ , we can insert it in equation (3.28) to obtain the average contention window size and hence  $\tau$ . Based on the knowledge of this latter probability, we are able to compute the probabilities  $P_{\text{tr}}$ ,  $P_s$  and  $P_c$ . Considering the PPP deployment of WiFi nodes and considering the fact that  $n_w(1 - \tau)^{n_w-1} = -\frac{\partial}{\partial \tau}(1 - \tau)^{n_w}$ , we can obtain the average probabilities of success and collision with the same approach used in equation (3.27):

$$\begin{aligned}\bar{P}_s &= \tau \bar{n}_w e^{-\tau \bar{n}_w} \\ \bar{P}_c &= 1 - e^{-\tau \bar{n}_w} - \tau \bar{n}_w e^{-\tau \bar{n}_w}\end{aligned}\quad (3.30)$$

$$S = \frac{(\bar{P}_s(1 - P_e(\eta))(1 - P_{\text{fa}}) + \bar{P}_c(1 - P_d)(1 - P_e^{(\text{sys})})) \times \ell_f}{(T_{\text{slot}} + T_{\text{OP}}P_{\text{fa}})(1 - \bar{P}_{\text{tr}}) + \bar{P}_s T_c P_e(\eta) + \bar{P}_s T_s (1 - P_e(\eta)) + \bar{P}_c T_c P_e^{(\text{sys})} + \bar{P}_c T_s (1 - P_e^{(\text{sys})})}. \quad (3.31)$$

For the sake of computing the average throughput, we also denote with  $T_s$  and  $T_c$  the success and collision times, respectively, as follows:

$$\begin{aligned}T_s &= T_{\text{mac}} + T_{\text{phy}} + DIFS + SIFS + T_{\text{Payload}} + T_{\text{Ack}} + 2 \times T_{\text{Delay}}, \\ T_c &= T_{\text{mac}} + T_{\text{phy}} + DIFS + T_{\text{Payload}} + T_{\text{Delay}},\end{aligned}$$

where  $T_{\text{Payload}} = \frac{\ell_f}{R_{\text{bs}}}$  and  $R_{\text{bs}}$  is the Wi-Fi bit rate. We shall denote with  $T_{\text{slot}}$  the duration of an idle time slot that coincides with that of a backoff. Moreover, we take into account that the medium can be occupied by LTE transmissions and during that time Wi-Fi nodes refrain from transmitting since the channel can be detected busy based on the energy detection. To model this in simple manner, we take into account an additional idle time interval in equation (3.31) denoted by  $T_{\text{OP}}$ , which is equivalent to either  $T_{\text{xOP}}$  used in LTE-LAA or the *ON* period of LTE-u.

TABLE 3.1: Parameters to evaluate Saturated numerical results

Param.	Description	Value
$P_{\text{tI}}$	LTE transmit power	{10, 18, 24} dBm
$P_{\text{ts}}$	WiFi transmit power	20 dBm
$R$	Radius of the area $A$	30 m
$r_{\text{u}}$	WiFi transmission range	$0 \leq r_{\text{u}} \leq R$
$\alpha$	Path-loss exponent	4 (indoors)
$\lambda_{\text{l}}$	Density of LTE aggregate interference	0.0014 nodes/ $m^2$
$\lambda_{\text{w}}$	Density of WiFi nodes	0.0018 nodes/ $m^2$
$R_{\text{bI}}$	LTE bit rate (16 QAM & 20MHz )	67 Mbps
$R_{\text{bs}}$	WiFi bit rate (QPSK, 16 QAM, 64 QAM)	19.5, 39, 58.5 Mbps [81]
$f_{\text{s}}^{(\text{lte})}$	LTE sampling frequency	30.72 MHz
$f_{\text{s}}^{(\text{wifi})}$	WiFi sampling frequency	20 MHz
$n_{\text{bI}}$	Number of bits per LTE symbol	4 in case of 16-QAM
$n_{\text{sI}}$	Number of samples per LTE symbol	2208 [82]
$T_{\text{mac}}$	MAC header	224 bits
$T_{\text{phy}}$	PHY header time	20 $\mu\text{s}$
$DIFS$	DCF Inter-frame spacing	34 $\mu\text{s}$
$SIFS$	Shortest Inter-frame spacing	16 $\mu\text{s}$
$W_0$	Initial CW size	16 back-off slots
$T_{\text{Ack}}$	Ack Delay	300 $\mu\text{s}$
$T_{\text{Delay}}$	Propagation delay	1 $\mu\text{s}$
$\ell_f$	Frame Size (Bytes)	256-4256
$M_{\text{b}}$	Max. packet retries	7
$m_{\text{b}}$	Max. backoff stages	6
$\sigma_{\text{s}}$	Channel shadowing factor	10 dB
$T_{\text{OP}}$	Channel Occupancy Time	4 ms
$n_{\text{Lte}}$	Probability of Active LTE	0.025

### 3.3.2 Saturated Throughput Numerical Results

Table 3.1 shows the numerical parameters that we plug in the analytical work done in previous sections. As mentioned, the study focuses on the 5 GHz unlicensed band. Moreover, we rely on a WiFi system with 20 MHz channel bandwidth, 20 dBm transmit power and  $N = 52$  OFDM data sub-carriers (e.g. IEEE 802.11n that operates in mixed mode [83]). To evaluate ED-CCA performance, both received WiFi energy and interference energy are collected over  $4 \mu\text{s}$ . The LTE system bandwidth is assumed to be also  $W = 20$  MHz with  $N' = 12$  sub-carriers in one resource block. While different modulations were evaluated, we show and plot the effects of one of the (i.e. 16-QAM modulated LTE downlink data transmissions) to reduce the number of figures in this dissertation. The path-loss exponent is assumed to be  $\alpha = 4$  for both LTE and WiFi signals (indoor scenarios). In equations (3.12) to (3.15) the energy of the interfering signal is calculated with the near field hypothesis (i.e. energy computed  $1m$  away from the transmitter) for different values of the LTE transmitted power, since the dependency on interferer's location was removed within the area of radius  $R$ . As discussed in Section 3.2.2,  $n_{\text{Lte}}$  represents the probability of LTE transmission when WiFi is active. It can refer to either *ON* period of LTE-u or the probability of hidden node problem in LAA. The selected value of 0.025 is the minimum portion of *ON* duration based on duty cycle pattern [11].

Relying on [84], in equation (3.32) we perform a simplified link budget analysis to compute the received SNR per bit, i.e.  $\varepsilon/N_0$ , for both WiFi and LTE transmissions with a transmitted energy per bit generally computed as  $\varepsilon = P_t/R_b$ , at a rate of  $R_b$  bits/s. Further, a constant re-sampling factor due to the different sampling frequencies in LTE and WiFi is introduced as  $c := f_s^{(\text{lte})}/f_s^{(\text{wifi})}$ . During the ED-CCA operation, the received WiFi energy  $\varepsilon_{\text{rs}}^{(\text{CCA})}$  and the interference energy  $\varepsilon_{\text{rl}}^{(\text{CCA})}$ , respectively, can be expressed as:

$$\begin{aligned}\varepsilon_{\text{rs}}^{(\text{CCA})} &= \left( \frac{P_{\text{ts}}}{L(r)} \right) \times \frac{1}{f_s^{(\text{wifi})}} \times 2Q \\ \varepsilon_{\text{rl}}^{(\text{CCA})} &= \left( n_{\text{bI}} \times \frac{P_{\text{tI}}/R_{\text{bI}}}{L_0} \right) \times \frac{c \times 2Q}{n_{\text{sI}}},\end{aligned}\quad (3.32)$$

where  $L$  is the path-loss at distance  $r$ ,  $L_0 = L(1)$  the path-loss at one meter and  $2Q = 80$  is the numbers of samples during detection. To compute  $L$  we assume a noise figure equal to 15 dB.

We show the results for the ED-CCA analysis in Figure 3.4 and 3.5 for the case study A and B, respectively, as described in Section 3.2.1. The yellow curve describing  $P_{\text{fa}}$  for noise only as in Case study A is shown in Figure 3.5(a). From Figure 3.4, we notice that the presence of interference yields a slight increase in the detection probability due to higher energy collected during sensing when the threshold is fixed to -62 dBm. Figure 3.5(a) illustrates  $P_{\text{fa}}$  in Case study B varying the energy detection threshold  $\lambda$  and we notice that interference yields always higher false alarm (i.e.  $\mathcal{H}_0^{(\text{B})}$ ) compared to noise only (i.e.  $\mathcal{H}_0^{(\text{A})}$ ). The probability  $P_{\text{d}}$  in Case study B is shown instead

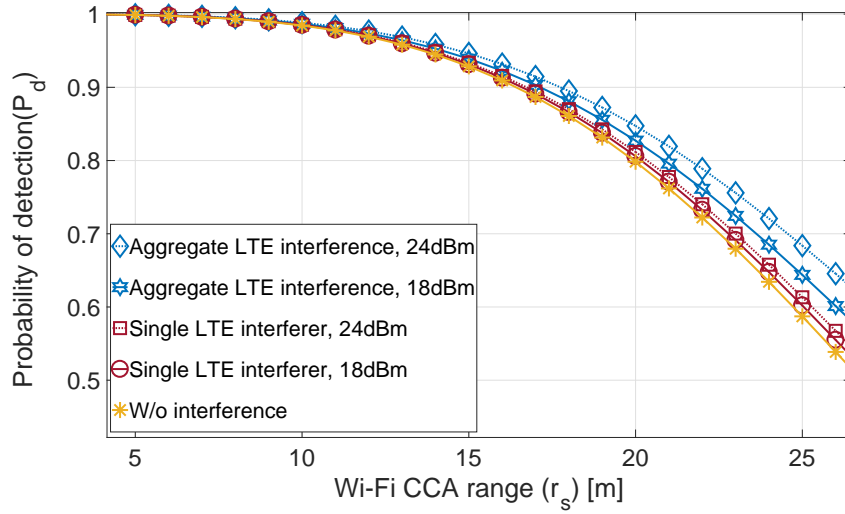
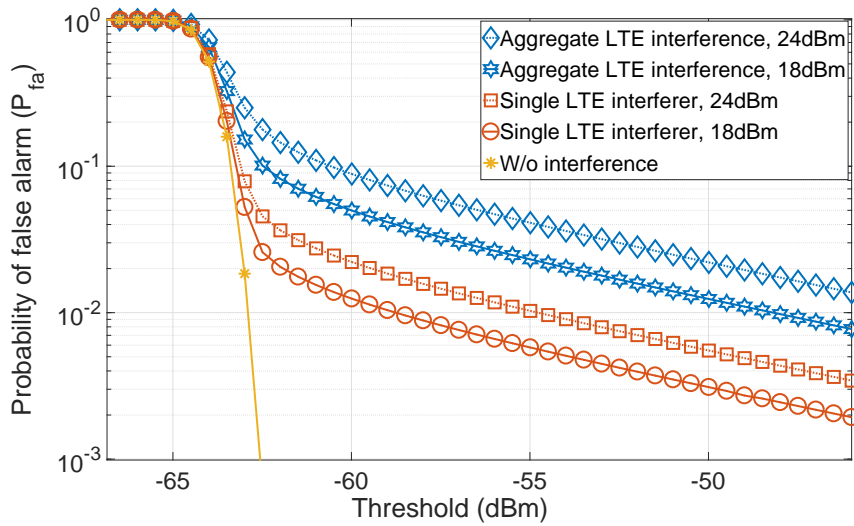


FIGURE 3.4: Case study A, threshold -62 dBm

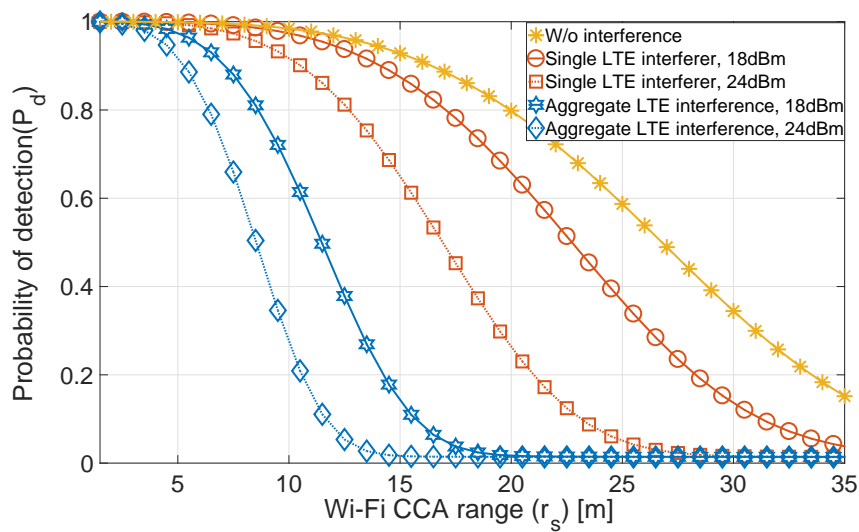
in Figure 3.5(b) varying the sensing range  $r_s$  for 18 dBm and 24 dBm of the LTE transmitted power and using both analyses of single and aggregate LTE interference. Unlike Case study A, the detection can be reduced changing the threshold for detection depending on the value of  $P_{fa}^*$  that is targeted to remain constant. For aggregate LTE interference and 24 dBm of transmitted power (referred to as severe condition), in Case study B with threshold equal to -62 dBm, the false alarm probability increases to 0.1 as shown in Figure 3.5(a). Thus, the ED threshold has to be increased to nearly -46 dBm when we fix the target  $P_{fa}^* \leq 0.01$ . With single LTE interfering transmitter and 18 dBm of transmitted power, the threshold has to be increased to 60.5 dBm. Figure 3.5(b) allows to conclude also that, in severe interference condition, targeting  $P_d^* = 0.9$  corresponds to 65% loss in the WiFi ED-CCA range  $r_s$ : from 15 m without interference to 5 meters.

Figure 3.6 shows the BEP results obtained through the analysis in Section 3.2.2 respectively for WiFi modulations 64-QAM, 16-QAM, and QAM with and without interference while varying the WiFi link distance. All curves are obtained setting the LTE transmitted power to 18 dBm. As expected, LTE transmissions in the same band of WiFi cause the BEP to increase, which degrades the WiFi throughput.

To compute the WiFi throughput in Case study A we insert in equation (3.31) the values of  $P_{fa} \ll 0.01$  and  $P_d > 0.9$  that are obtained when assuming the threshold -62 dBm. Furthermore, we fix  $r_s = 15$  m based on the ED-CCA performance that are achieved without LTE. For Case study B, we pick the minimum threshold that guarantees  $P_{fa}^* \leq 0.01$ . Based on that we can find the corresponding  $P_d$  when fixing  $r_s = 15$  m. Throughput results are shown in Figure 3.7 to 3.9 for different values of the LTE transmitted power. The first sub-plot in each figure shows the throughput versus the WiFi link distance  $r_u$  for frame size  $\ell_f = 4096$  bytes. The second sub-plot in each figure shows instead throughput versus the frame size while  $r_u = 3.5$  m.



(a) False alarms probabilities under  $\mathcal{H}_0^{(B)}$



(b) Detection probabilities under  $\mathcal{H}_1^{(B)}$

FIGURE 3.5: Case study B varying the threshold

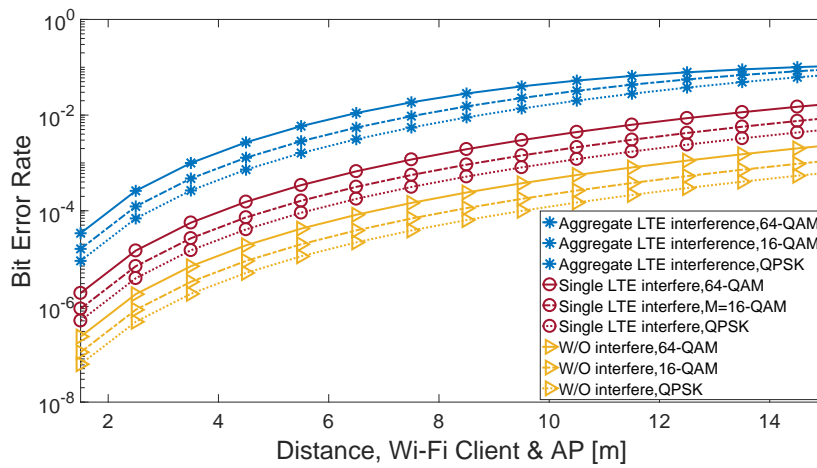
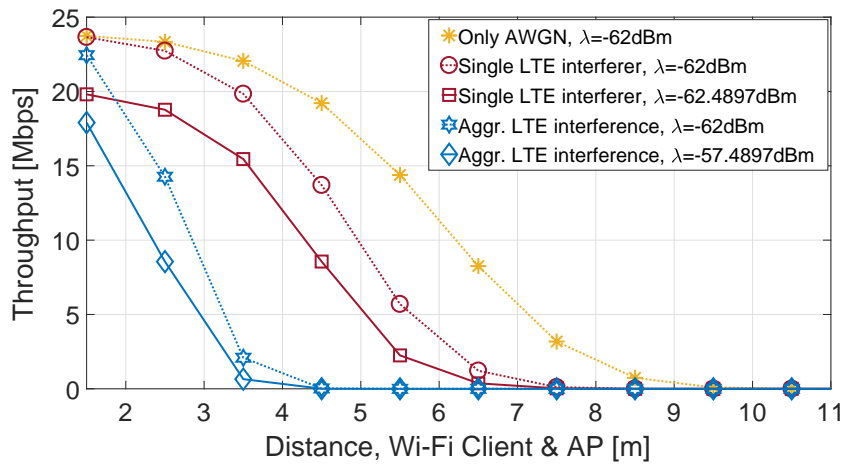
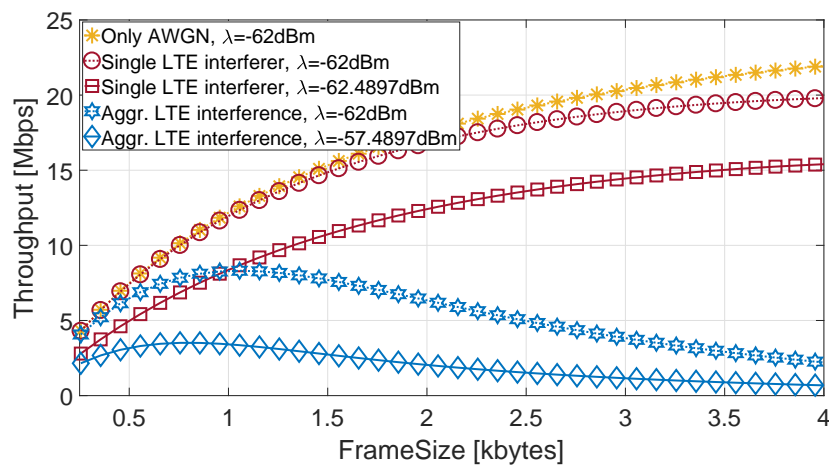


FIGURE 3.6: Bit Error Rate, having LTE-TX=18dBm

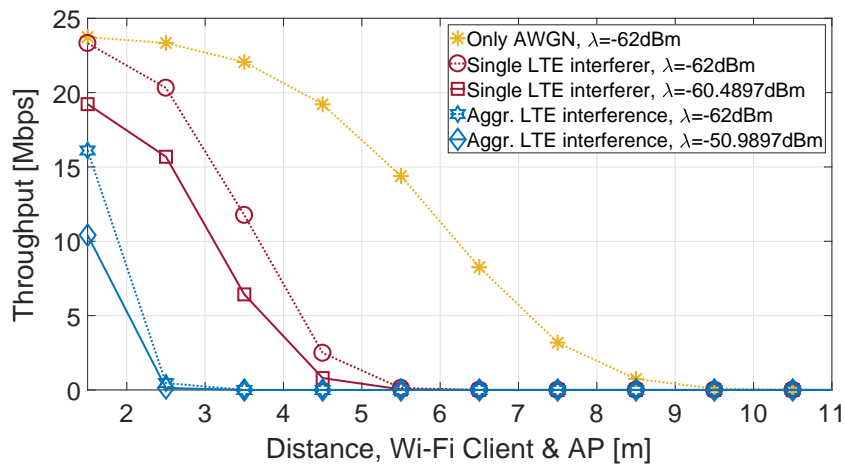


(a) With respect to useful link distance

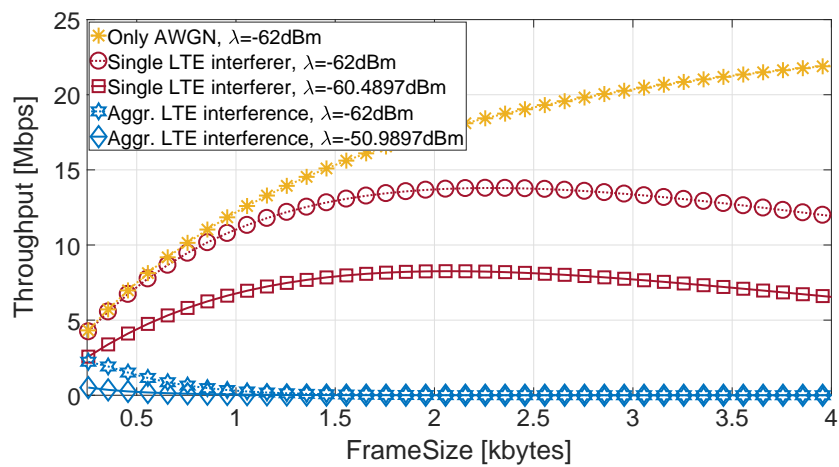


(b) With respect to frame size

FIGURE 3.7: Wi-Fi throughput; LTE-TX=10 dBm; Wi-Fi Modulation 16-QAM



(a) With respect to useful link distance



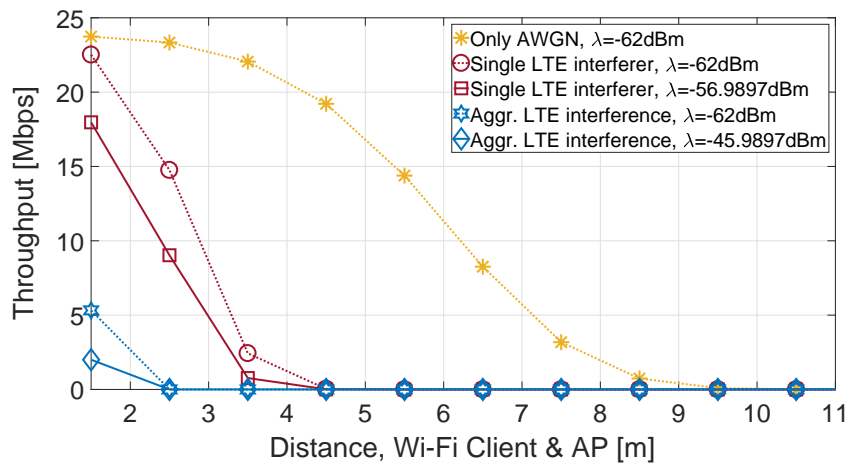
(b) With respect to frame size

FIGURE 3.8: Wi-Fi throughput; LTE-TX=18 dBm; Wi-Fi Modulation 16-QAM

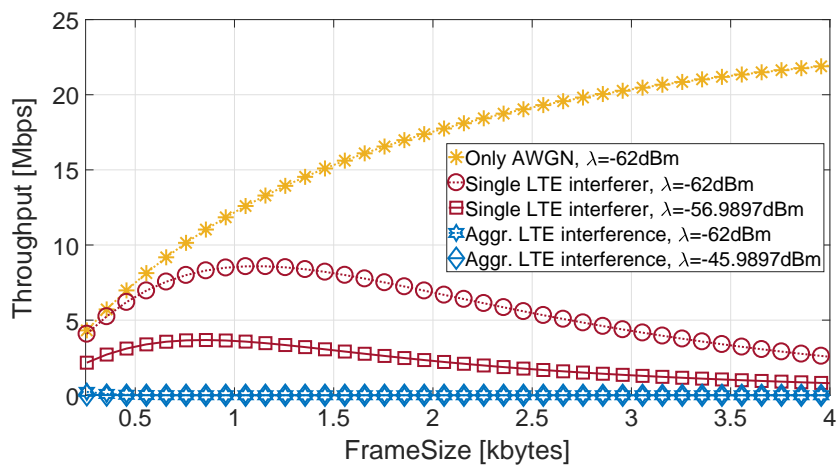
The results in Figure 3.7 to 3.9 show the sensitivity of the WiFi throughput with respect to both the ED threshold and LTE transmitted power. We notice that also the number of active LTE transmitters plays a major role. For instance, aggregate interference causes the collapse of the WiFi network throughput due to increased BEP values. Based on the results, to achieve simple coordination between WiFi and LTE the LTE transmitted power can be tuned to 10 dBm or lower and enable a single LTE small cell active in downlink to avoid the disruption of WiFi. On the other hand, increase the energy detection has always negative effect since it favors the heterogeneous network to become an Aloha system.

Figure 3.10 shows the combined effect of the LTE transmitted power and the WiFi link distance  $r_u$  on the WiFi throughput for Case study A. No active LTE transmitter, single active LTE transmitter and aggregate LTE transmissions are analyzed for a 64-QAM modulation used in the WiFi link. From the figure, we notice that single LTE transmitter causes the achievable range  $r_u$  to shrink (e.g. 4 m for 10 dBm of LTE transmitted power) but with LTE power values lower than 10 dBm, the WiFi throughput can be preserved.

In Figure 3.11, we show the spectral efficiency of the WiFi network versus  $r_u$ , comparing the cases with LTE transmissions to the case without. The spectral efficiency was computed by numerically finding the maximum WiFi throughput over the three modulations 64-QAM, 16-QAM and QAM for each value of  $r_u$  and dividing by the WiFi system bandwidth. We notice that, with a LTE transmitted power of 18 dBm, the distance at which WiFi will start using 16-QAM reduces from 4.5 m without LTE to 3.5 m with single active LTE transmitter. With aggregate LTE transmissions no sustainable modulation format can be used after 2.5 m.



(a) With respect to useful link distance



(b) With respect to frame size

FIGURE 3.9: Wi-Fi throughput; LTE-TX=24 dBm; Wi-Fi Modulation 16-QAM

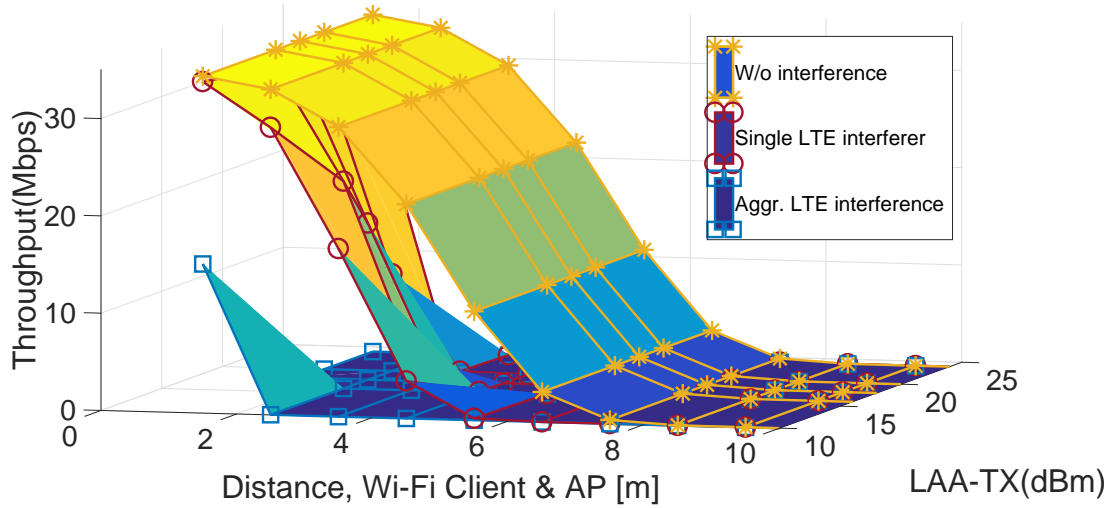


FIGURE 3.10: WiFi throughput vs. Distance vs. LTE-TX. Targeting  $P_{fa}$  and WiFi modulation of 64-QAM

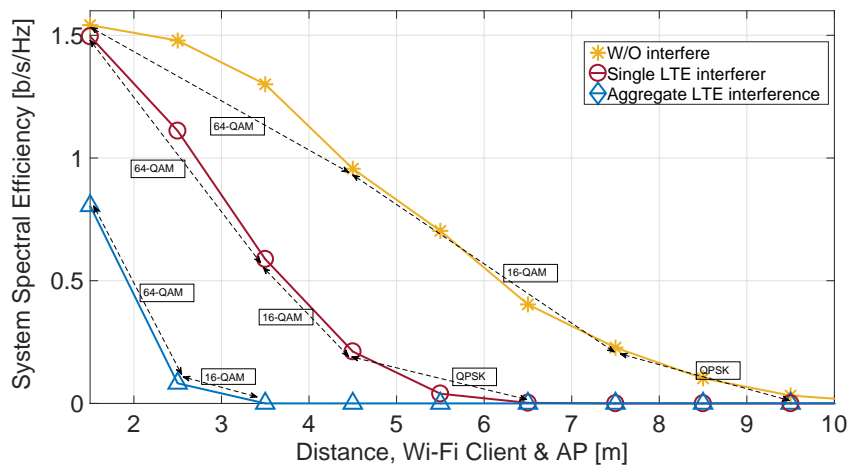


FIGURE 3.11: WiFi Modulation Effects, Targeting  $P_{fa}$ , LTE-TX=18 dBm

## 3.4 Unsaturated WiFi Analysis in a Poisson Field of Interference

This section aims to develop an analytical method to compute the average throughput of an unsaturated WiFi network in the 5 GHz band generalizing the cases of interference. Compared to the works done in sections 3.2.1 and 3.3.1, here we do not consider two different use cases for energy detection mechanism but we define new hypothesis to evaluate the performance of CCA affected by general OFDM-based signals other than WiFi (i.e. inter-network interference). We then expand the one dimensional Markov-chain to the unsaturated conditions. As the presence of interference in this section is generalized to any OFDM-based systems, we do not consider specific LTE signals. Thus, we need to briefly evaluate the CCA mechanism again and then use it for the unsaturated analysis of CSMA/CA. As a result, some computation in CCA mechanism are similar to the ones in section 3.2.1, but with different approach.

### 3.4.1 Clear Channel Assessment

Since the goal of this section is to find a tractable WiFi unsaturated throughput when affected by any OFDM-based system, we do not consider the two use cases introduced in Section 3.2.1. Thus, we reformulate the d.vs. in equation (3.9) based on the new hypothesis as follows.

We define three statistical hypotheses to evaluate presence/absence of interference:

- When  $\mathbb{1}_S = \mathbb{1}_k = 0$ , which defines hypothesis  $\mathcal{H}_0$  to evaluate the false alarm probability ( $P_{fa}$ ).
- When  $\mathbb{1}_S = \mathbb{1}_k = 1$ , which defines hypothesis  $\mathcal{H}_1$  to evaluate the detection probability in the presence of both intra- and inter-network interferer signals ( $P_{d1}$ ).
- When  $\mathbb{1}_k = 1$  but  $\mathbb{1}_S = 0$ ; which defines hypothesis  $\mathcal{H}_2$  to evaluate the detection probability in presence of inter-network interferer signals but absence of intra-network signals ( $P_{d2}$ ).

We also mention that the hypothesis of presence of WiFi signal and noise (i.e.  $\mathbb{1}_k = 0, \mathbb{1}_S = 1$ ) is used only for performance comparison in the numerical results by assuming  $\zeta_k(t) \rightarrow 0 \forall k \in K$  in equation (3.5). Based on these

hypothesis the different d.v.'s are expressed as:

$$\begin{aligned}
 Y_0 &= \frac{1}{2\sigma^2} \sum_{q=1}^{N_s} \left( \frac{n_q^2}{2W} \right), \text{hyp. } \mathcal{H}_0 \\
 Y_1 &\simeq \frac{1}{2\sigma^2} \sum_{q=1}^{N_s} \left( \frac{X_{S_q}^2 + X_{I_q}^2 + n_q^2}{2W} \right), \text{hyp. } \mathcal{H}_1 \\
 Y_2 &= \frac{1}{2\sigma^2} \sum_{q=1}^{N_s} \left( \frac{X_{I_q}^2 + n_q^2}{2W} \right), \text{hyp. } \mathcal{H}_2
 \end{aligned} \tag{3.33}$$

with  $N_s$  degrees of freedom and non-centrality parameter:

$$\mu_1 = \frac{1}{2\sigma^2} \sum_{q=1}^{N_s} (X_{S_q}^2 + X_{I_q}^2) = g_S N_s \frac{\varepsilon_{rS}}{2\sigma^2} + g_I N_s \frac{\varepsilon_{rI}}{2\sigma^2},$$

where  $\varepsilon_{rS}$  and  $\varepsilon_{rI}$  denote respectively the received intra- and inter-network interference energy per sample during CCA.  $g_S$  and  $g_I$  are the i.i.d. exponentially distributed power fading coefficients of 802.11 and interference signals. Similarly,  $Y_2$  also follows a non-central Chi-square distribution with the same degrees of freedom but non-centrality  $\mu_2 = \frac{1}{2\sigma^2} \sum_{q=1}^{N_s} X_{I_q}^2 = g_I N_s \frac{\varepsilon_{rI}}{2\sigma^2}$ . We remark that under  $\mathcal{H}_0$  the d.v. follows a central Chi-Square distribution, which is the condition to evaluate the false alarm probability in absence of any signal.

Under hypotheses  $\mathcal{H}_1$  and  $\mathcal{H}_2$ , two distinct detection events with respective probabilities  $P_{d1}$  and  $P_{d2}$  are computed in case of Rayleigh fading and path-loss that affect the signal propagation. We use the Gil-Pelaez inversion integral [74] and the Characteristic Function (CF) approach  $\Psi(v) := \mathbb{E}\{e^{jvx}\}$ , where  $\mathbb{E}\{\cdot\}$  represents the expected value. Thus, we need to find the CFs of the non-central Chi-square r.v.'s. with non-centralities  $\mu_1$  and  $\mu_2$ , respectively. Relying on [75], and with the same methods already mentioned in Section 3.2.1, the CF of the d.v.'s. under statistical hypothesis  $\mathcal{H}_1$  and  $\mathcal{H}_2$  are

$$\begin{aligned}
 \Psi_1(v) &= \frac{1}{(1-j2v)^{N_s}} \times \frac{1}{1 - \frac{jv\varepsilon_{rS}N_s r_v^{-\alpha}}{(1-j2v)N_0}} \times \\
 &\exp\left(-\lambda_1 \left( \frac{jv}{(-1+j2v)} \times \frac{\varepsilon_{rI}N_s}{N_0} \right)^{2/\alpha} \frac{2\pi^2}{\alpha} \csc\left(\frac{2\pi}{\alpha}\right)\right),
 \end{aligned} \tag{3.34}$$

$$\begin{aligned}
 \Psi_2(v) &= \frac{1}{(1-j2v)^{N_s}} \times \\
 &\exp\left(-\lambda_1 \left( \frac{jv}{(-1+j2v)} \times \frac{\varepsilon_{rI}N_s}{N_0} \right)^{2/\alpha} \frac{2\pi^2}{\alpha} \csc\left(\frac{2\pi}{\alpha}\right)\right),
 \end{aligned} \tag{3.35}$$

where  $\lambda_1$  is the density of the PPP distributed interfering nodes (i.e.  $K \rightarrow \infty$ ) within the area  $A = \pi R^2$  and  $\alpha$  is the path-loss exponent. Finally,  $P_{d1}$  and

$P_{d2}$  can be obtained through numerical inversion of their CFs, using the Gil-Pelaez inversion integral:  $\left( P_r\{X > \Lambda\} = \frac{1}{2} + \frac{1}{\pi} \int_0^\infty \text{Im}\left(\frac{\Psi(v)e^{-jv\Lambda}}{v}\right) dv \right)$ .

### 3.4.2 Unsaturated CSMA/CA Analysis

After deriving the effect of both inter- and intra-network interference on ED-CCA and PEP (the same as in Section 3.2.2), in this section we evaluate the performance of CSMA/CA to model the Binary Exponential Back-off (BEB). We will obtain the general unsaturated 802.11 throughput expression that is simple to evaluate and allows to model accurately both Layer-1 and Layer-2 for evaluating network performance, which yields a cross-layer analysis approach.

Figure 3.12 shows the one-dimension MC model of the BEB. In unsaturated conditions, WiFi nodes contend for channel access *iff* there are packets in the queue awaiting for transmission. All states of the ergodic MC are characterized by a steady state probability  $\Pi_i$ , with  $\Pi_{-1}$  that denotes the thinking state. A WiFi node can leave this state with probability  $P_b$  or remain with  $1 - P_b$ . The MC is analyzed at the embedded time instants of back-off counter zero.

To derive the transition probability ( $P_g$ ), we rely on the analysis developed in Section 3.4.1 for the target node. CCA is done in all back-off slots, as well as during the Distributed Inter Frame Space (DIFS). In the last back-off slot, if the channel is sensed idle, the packet will be transmitted and the MAC will wait a Short Inter Frame Space (SIFS) to receive the ACK frame. If the ACK is not received, the contention window (CW) size is doubled and a new back-off counter uniformly distributed in the range  $[0, 2^i CW]$  is selected in the  $i$ -th back-off stage. The process returns to state 0 with probability  $P_b(1 - P_g)$  if at least one packet is waiting for transmission or, otherwise, to the thinking state with probability  $(1 - P_b)(1 - P_g)$ . The only exception is the final steady state ( $M_b$ ) where the process returns to state 0 and  $-1$  with probabilities  $P_b$  and  $(1 - P_b)$ , respectively. We are now able to develop the transition probability as:

$$P_g = P(n_w) \cdot P_e^{(\text{sys})} + P(n_w) \cdot \omega + (1 - P(n_w)) \cdot \varrho, \quad (3.36)$$

where  $P(n_w) = 1 - (1 - \tau)^{n_w - 1}$  is the conditional collision probability,  $\tau = \frac{2}{1 + \overline{CW}}$  the average transmission probability,  $\overline{CW}$  the average contention window size and  $n_w$  the number of WiFi nodes competing for the channel access [85]. On the other hand,  $\omega$  and  $\varrho$  are as follows:

$$\omega(n_w) = P_e^{(\text{sys})} \cdot (1 - P_{d1}^{n_w - 1}), \quad \varrho = P_e^{(\text{int})} \cdot (1 - P_{d2}), \quad (3.37)$$

where we write  $P_e^{(\text{sys})} = P_e^{(\text{WiFi})} + P_e^{(\text{int})} - P_e^{(\text{WiFi})} \cdot P_e^{(\text{int})}$ . Also,  $P_e^{(\text{WiFi})}$  and  $P_e^{(\text{int})}$  are found with the same methods in Section 3.2.2. The right hand side of equation (3.36) is composed of three probabilities with each describing the

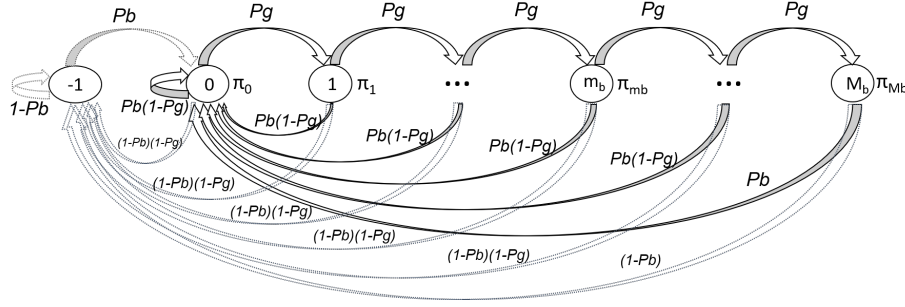


FIGURE 3.12: One-dimensional Markov Chain modeling BEB.

event of moving from state  $i$  to state  $i + 1$  in Figure 3.12 ( $i \in [0, M_b]$ ). We explain the terms below:

- Event of packets collision due to simultaneous transmission of at least two WiFi nodes in case they chose the same number of back-off slots after DIFS and in the presence of inter-network interference ( $P \cdot P_e^{(\text{sys})}$ ).
- Event of packets collision between the target node transmission and at least another WiFi node that misses the detection in presence of inter-network interference ( $P \cdot \omega$ ).
- Event of packets collision when the target node misses the detection of other signals in absence of intra-network interference ( $(1 - P) \cdot \rho$ ).

Since also WiFi nodes are PPP distributed, we can average  $\omega$  in equation (3.26) with respect to  $n_w$  as shown below:

$$\bar{\omega} = P_e^{(\text{sys})} \times \left( 1 - P_{d1}^{-1} \times e^{-\bar{n}_w(1-P_{d1})} \right), \quad (3.38)$$

Solving the MC model, the steady state probabilities,  $\pi_{-1}$  and  $\pi_0$  are:

$$\begin{aligned} \pi_{-1} &= \frac{\pi_0}{P_b} (1 - P_b)(1 - P_g) \sum_{i=0}^{M_b-1} P_g^i + P_g^M (1 - P_b), \\ \pi_0 &= \frac{1}{\frac{1-P_b}{P_b} + \sum_{i=0}^{M_b} P_g^i}. \end{aligned} \quad (3.39)$$

Moreover, relying on [79], we can find the average CW size:

$$\begin{aligned} \overline{CW} &= W_0 \pi_0 \times \left( \sum_{i=0}^{m_b-1} (2P_g)^i + \sum_{i=m_b}^{M_b} 2^{m_b} P_g^i \right) = \\ &= \frac{W_0 P_b (1 - P_g) \sum_{i=0}^{m_b-1} (2P_g)^i + P_b W_M P_g^{m_b} (1 - P_g^{M_b+1-m_b})}{(1 - P_b)(1 - P_g) + P_b (1 - P_g^{M_b+1})}, \end{aligned} \quad (3.40)$$

where  $W_0 2^{m_b} = W_M$  is the maximum CW value. We exploit that  $P \leq \tau(1 - \pi_{-1})(\bar{n}_w - 1)$  in which we plug the expressions of  $\tau$  based on equation (3.40)

and  $P$  from equation (3.25) to obtain a polynomial of degree  $M_b + 2$ .

$$(P_g - \varrho)(1 + \overline{CW}) - 2(P_e^{(\text{sys})} + \varrho - \overline{\omega})(\overline{n}_w - 1)(1 - \pi_{-1}) \leq 0$$

Solving the polynomial for  $P_g$ , we can easily compute  $\overline{CW}$  and  $\tau$ . The structure of the polynomial ensures the existence of only one positive real solution other than one.

### 3.4.3 Unsaturated 802.11 Throughput Computation

To introduce a model as realistic as possible to quantify IEEE 802.11 unsaturated throughput, we rely on the analysis done in section 3.4.2 to find out probabilities of success and collision as well as comprising affected ED-CCA and PEP shown in sections 3.4.1 and 3.2.2, respectively.

The average WiFi network throughput ( $S$ ) is defined as the fraction of the channel access time that is needed to successfully transmit packets (i.e. reception of the acknowledgment frame) [85]. Referring to equation (3.41), successful transmission corresponds to two events: 1) only the target node transmits but missing the detection of inter-network transmitters (i.e. Hypothesis  $H_2$ ); 2) the target node transmission collides with other WiFi packets due to miss-detection (i.e. Hypothesis  $H_1$ ) but surviving the collision. Based on the probabilities corresponding to these two events, we compute the average system throughput while in the denominator of (3.41) we include the probabilities of all possible events, including the probability  $P_{\text{idle}}$  of an idle time slot ( $T_{\text{slot}}$ ). The unconditional probabilities of success ( $P_s$ ) and collision ( $P_c$ ) are:

$$S = \frac{P_s(1 - P_e^{(\text{int})})(1 - P_{\text{d2}}) + P_c(1 - P_e^{(\text{sys})})(1 - P_{\text{d1}})}{T_{\text{slot}}(P_{\text{idle}}) + P_s T_c P_e^{(\text{int})} + P_s T_s (1 - P_e^{(\text{int})}) + P_c T_c P_e^{(\text{sys})} + P_c T_s (1 - P_e^{(\text{sys})})} \times \ell_f. \quad (3.41)$$

$$P_s(n_w) = n_w \tau (1 - \tau)^{n_w - 1}, \quad P_c(n_w) = 1 - P_{\text{idle}} - P_s. \quad (3.42)$$

The idle probability is computed as  $P_{\text{idle}}(n_w) = (1 - \tau(1 - \pi_{-1}))^{n_w}$  with  $1 - \pi_{-1}$  the probability of at least one packet in the buffer of a node. We average  $P_{\text{idle}}$ ,  $P_s$  and  $P_c$ , with respect to  $n_w$ , through the same method in appendix A.5, using that  $n_w(1 - \tau)^{n_w - 1} = -\frac{\partial}{\partial \tau}(1 - \tau)^{n_w}$ :

$$\begin{aligned} \overline{P_s} &= \tau \overline{n}_w e^{-\tau \overline{n}_w}, \quad \overline{P_{\text{idle}}} = e^{-(1 - \pi_{-1}) \overline{n}_w} \\ \overline{P_c} &= 1 - \overline{P_{\text{idle}}} - \overline{P_s}. \end{aligned} \quad (3.43)$$

For computing the average throughput, we write the success time as  $T_s = T_{\text{mac}} + T_{\text{phy}} + DIFS + SIFS + T_{\text{Payload}} + T_{\text{Ack}} + 2 \times T_{\text{Delay}}$  and collision time as  $T_c = T_{\text{mac}} + T_{\text{phy}} + DIFS + T_{\text{Payload}} + T_{\text{Delay}}$  with  $T_{\text{Payload}} = \ell_f / R_{\text{bs}}$ . Finally, the probability  $P_b$  is modeled based on the assumption that inter-arrival

times of new packets are exponentially distributed within the  $T_{\text{slot}}$  time interval:  $P_b = 1 - e^{-\delta T_{\text{slot}}}$  and  $\delta$  denotes the constant arrival process intensity.

### 3.4.4 Model Validation and Numerical Results

Let us first consider the case without inter-network interference: when  $P_{\text{fl}} \rightarrow 0$  mW, from equation (3.33),  $\mathcal{H}_2 \simeq \mathcal{H}_0$ , which leads to the fact that  $P_{\text{d2}} \rightarrow P_{\text{fa}}$ . Under this condition and setting the energy detection threshold ( $\Lambda$ ) to  $-62$  dBm the false alarm probability tends to be very small ( $P_{\text{d2}} \rightarrow P_{\text{fa}} \simeq 0$ ). Moreover, we can see from equations (3.17) and (3.20) that  $P_e^{(\text{int})} \rightarrow P_e^{(\text{noise})}$ , where  $P_e^{(\text{noise})}$  is the packet error probability due to noise only. In the ideal case in which  $P_e^{(\text{noise})} = 0$ ,  $P_e^{(\text{WiFi})} = 1$  (i.e.  $P_e^{(\text{sys})} = 1$ ),  $P_{\text{d2}} = 0$ ,  $P_{\text{d1}} = 1$  and  $\pi_{-1} = 0$  (saturation condition), we can find results in [85] from equations (3.25), (3.42), and (3.41).

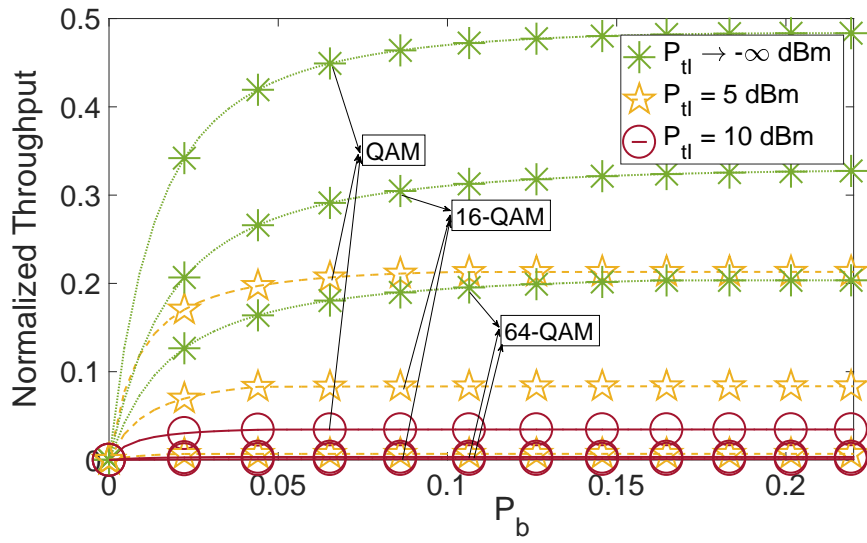
From numerical evaluation using the values in Table 3.2, we found  $P_e^{(\text{sys})} \approx 1$ , so that the second term in the numerator of (3.41) has negligible contribution.

All devices operate for center frequency  $f_c = 5$  GHz and bandwidth 20 MHz. WiFi nodes transmitted power ( $P_{\text{ts}} = P_{\text{tu}}$ ) is fixed to 20 dBm, whereas that of inter-network interfering nodes ( $P_{\text{fl}}$ ) is varied. We assume path-loss exponent  $\alpha = 4$  to model an indoor environment.  $\lambda_1 = 3.5 \times 10^{-3}$  nodes/m<sup>2</sup> to have, on average, one inter-network interfering node within the range  $R$ . The density of competing intra-network WiFi nodes  $\lambda_w$  may vary. The received interference energy per sample used in equations (3.34) and (3.35) for the two types of interference are

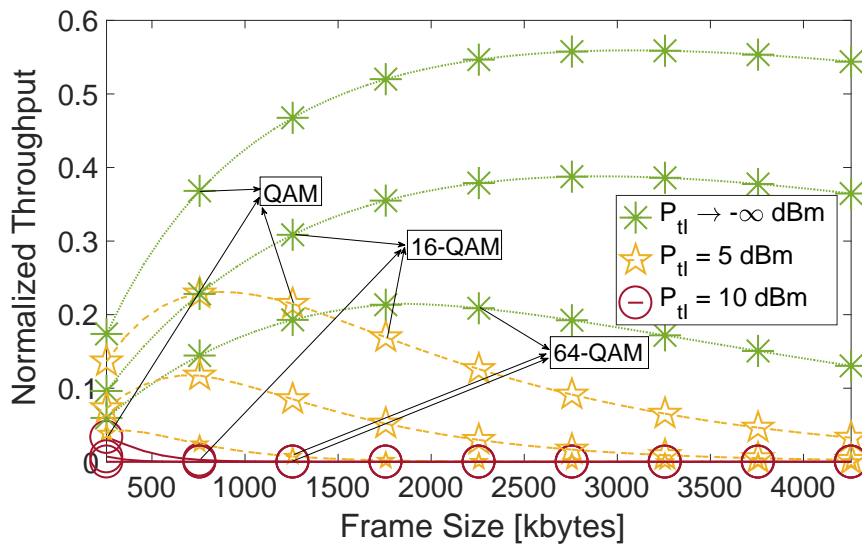
$$\varepsilon_{\text{rS}} = \frac{P_{\text{ts}}/N_0}{N_{\text{F}} \cdot L_0} \times \frac{1}{f_s^{(\text{wifi})}}, \quad \varepsilon_{\text{rI}} = \frac{P_{\text{fl}}/N_0}{N_{\text{F}} \cdot L_0} \times \frac{1}{f_s^{(\text{wifi})}},$$

where  $L_0$  is the free space path-loss at 1 meter,  $N_0 = -174$  dBm/Hz and  $N_{\text{F}} = 10$  dB is the noise figure.

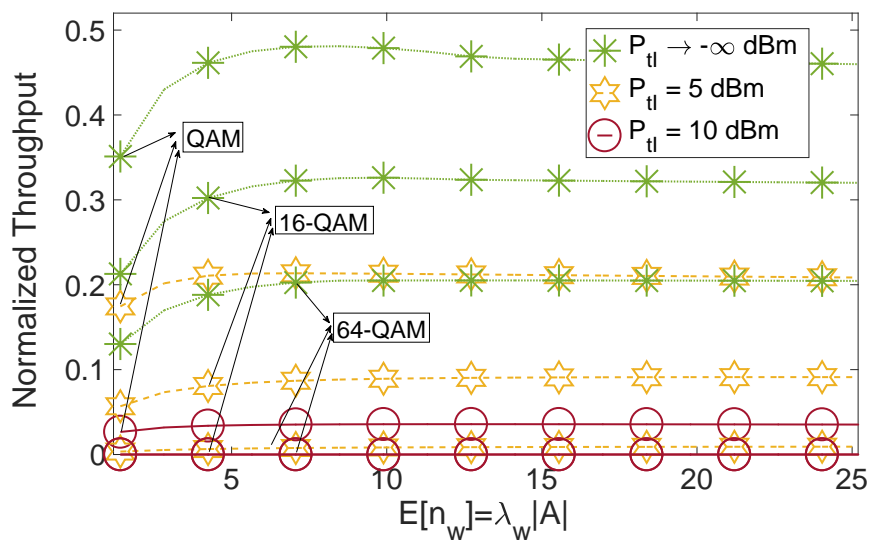
Figures 3.13(a), 3.13(b), and 3.13(c) respectively illustrate the normalized WiFi throughput varying  $P_b$ ,  $\ell_f$  and  $\bar{n}_w$ . To show the results for QAM, 16-QAM and 64-QAM, we consider the bit rates of the IEEE 802.11ac in SISO mode: 19.5, 39 and 78 Mbps. We notice that the additional presence of inter-network interference power (i.e.  $P_{\text{fl}}$ ) has high impact on the throughput compared to the case with intra-network interference, path-loss and fading only (green curves). Moreover, upon comparing the curves in figures 3.13(a) and 3.13(c), we notice that the system throughput will remain almost the same after a certain point (i.e.  $P_b \approx 0.05$  and  $\bar{n}_w \approx 5$ ), whereas depending on the interference power, the WiFi throughput can have a maximal point as a function of  $\ell_f$  as shown in Figure 3.13(b). As anticipated, our analytical tool can help to predict and optimize the WiFi network throughput in realistic inter-/intra-network spatial interference distribution.



(a)  $\ell_f = 1280$  bytes,  $\bar{n}_w = 5$



(b)  $P_b = 0.1$ ,  $\bar{n}_w = 5$



(c)  $\ell_f = 1280$  bytes,  $P_b = 0.1$

FIGURE 3.13: Normalized WiFi throughput, SNR  $\approx 30$  dB,  $\Lambda = -62$  dBm

TABLE 3.2: Parameters to evaluate Unsaturated numerical results

Param.	Description	Value
$R$	Radius of the area $A$	30 m
$r_u$	Useful link distance	$0 \leq r_u \leq R$
$f_s^{(wifi)}$	WiFi sampling frequency	20 MHz
$T_{mac}$	MAC header time	$224\text{bits}/R_{bs}$
$T_{phy}$	Physical header time	$20 \mu\text{s}$
DIFS	DCF Inter-frame space	$34 \mu\text{s}$
SIFS	Short Inter-frame Space	$16 \mu\text{s}$
$W_0$	Initial CW size	16
$T_{Ack}$	Ack Delay	$300 \mu\text{s}$
$T_{Delay}$	Propagation delay	$1 \mu\text{s}$
$M_b$	Max. packet retries	7
$m_b$	Max. backoff stage	6

### 3.5 Conclusion of the Chapter

In this chapter, we developed an analytical method to evaluate the effect of LTE transmissions that overlay with WiFi in the 5 GHz unlicensed band studying two main aspects: WiFi clear channel assessment at the physical layer and the MAC layer throughput in saturation condition of the network. Although mechanisms already exist (e.g. LTE-u and LTELAA) to avoid simultaneous transmission of LTE with WiFi, we noticed that even these methods may not solve completely the challenge of co-existence specially in indoors environments. To quantify the impact of LTE transmissions on the WiFi clear channel assessment, we modeled the effect of LTE as a random interfering process resorting to the characteristic function approach for the energy detector receiver. This has allowed us to identify different thresholds for the energy detection to maintain the false alarm probability constant. Moreover, we have modeled the WiFi throughput resorting to a one-dimensional Markov chain model. The combination of the two approaches led to obtain the WiFi network throughput in realistic propagation conditions that are typical of an indoor environment, modeling at the same time several WiFi network constraints. From our results, we noticed that the values of the LTE transmitted power and the number of active transmitters affect the most the WiFi throughput. This allows us to conclude that the control of both is crucial to let LTE transmit in the same band of WiFi. We also discussed that a centralized approach like in software-defined radio access networks can further improve the coexistence.

## Chapter 4

# Centralized Coordination of Unlicensed-LTE/WiFi

The actual assessment of the effects of Unlicensed-LTE (u-LTE) transmissions on WiFi performance is carried out in this chapter in an indoor office environment that is also published in [7]. First, we experimentally measure the WiFi throughput in the worst case of a continuous LTE transmission. Second, we compare the results with the baseline situation where there is no active u-LTE interfering transmitter. Third, the controllability level is achieved exploiting the new concept of Software-Defined Radio Access Network (SD-RAN). Therefore, a centralized SD-RAN controller that can control both WiFi Access Points (AP) and LTE-eNB is used. The controller monitors the network continuously and is able to reconfigure it when both technologies are in operation. Therefore, the research contribution of the work presented in this chapter is twofold: (i) we carry out measurements in a realistic office environment when the reception of WiFi station is affected by u-LTE and (ii) we use the results of the measurements to leverage the functionality of the SD-RAN controller.

### 4.1 LTE/WiFi Test-bed Implementation

In this work, we consider having one u-LTE eNB connected to the 4G Evolved Packet Core (EPC) and one active LTE User Equipment (UE) attached to the eNB. Since the goal of the work is to evaluate the effects of LTE transmissions on WiFi throughput, the LTE eNB transmits continuously. In other words, neither duty cycling (i.e. LTE-U) nor LBT (i.e. LAA) is enabled in the LTE equipment. Specifically, we consider u-LTE/WiFi coexistence on the 5 GHz unlicensed band. The choice of this set-up results in a heterogeneous radio network in which the shared communication channel is accessed in an aloha-like access scheme for both systems. This configuration allows us to completely evaluate the benefits of the SD-RAN controller. LTE transmissions are scheduled over the unlicensed band in the downlink, while all the uplink traffic is transmitted on the licensed LTE carrier.

Figure 4.1 shows the typical hidden node problem where there are both WiFi and LTE signals on the same frequency band. The scenario allows us to compare the WiFi throughput in an environment without LTE interference

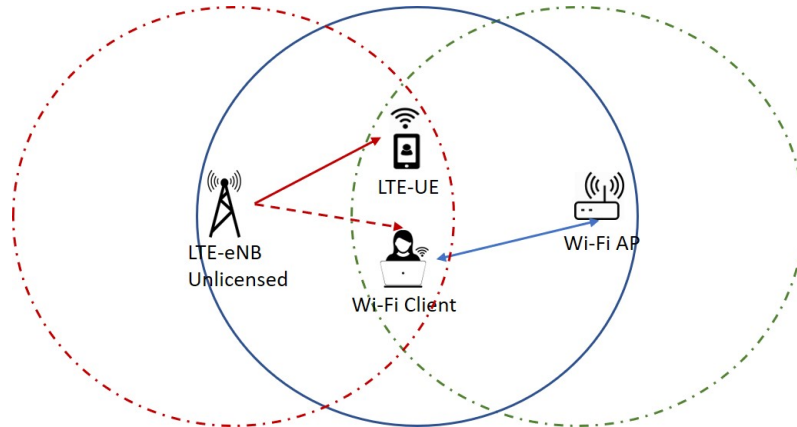


FIGURE 4.1: Conceptual representation of hidden node problem in u-LTE/WiFi coexistence

with the one with LTE. The number of active LTE networks is purposely limited to one considering that, as previously discussed, different channel access mechanisms have been developed to reduce the likelihood of a situation in which the WiFi network is overwhelmed by u-LTE transmissions. In this context, we measure the WiFi throughput when various LTE parameters such as transmit power, modulation and coding scheme (MCS) and bandwidth are changed.

#### 4.1.1 Test-Bed Components

**srsLTE:** Software Radio Systems LTE (srsLTE) is a high-performance LTE library for software-defined radio applications [86]. Supporting EPC, eNodeB and UE in different modules, the library has minimal inter-module dependencies, which makes it simple to use for developers. From the hardware perspective, the library deals with buffers of samples in the system memory, which enables the connection with any RF front-end. Its current version provides an interface to the Universal Hardware Driver (UHD), which is supported by the Ettus USRP family of devices [6]. Specifically, our test-bed relies on the Ettus B210 radio boards.

- I **srsEPC:** A light weight LTE core network implementation with Mobility Management Entity (MME), Home Subscriber Server (HSS) and (Serving/ PDN-Gateway) S/P-GW. The core network of srsLTE has all the 3GPP interfaces among the various parts of a standard 4G EPC. In the HSS database, we are able to define the information of the UE to pass the 4G authorization and authentication procedure in order to attach UEs to the network.
- II **srsENB:** A complete software package of a 4G eNB programmed in C++ and built upon the srsLTE library. Running on a computer, srsENB supports full uplink and downlink data rates using various standard LTE bandwidths from 1.4 MHz to 20 MHz. There are some templates in the open source library for instance for the physical downlink shared channel of the eNB (Pdsch-enodeb). The purpose of the template is to inject

information of an LTE radio frame into a file. This provides a very good approach for understanding the overall process of generating various downlink signals in LTE (e.g. primary/secondary reference signals) as well as physical channels (physical broadcast channel, physical downlink control channel, physical downlink shared channel, etc.) and combining all those signals and channels into a radio frame in any supported frequency region.

- III **srsUE**: A software package of an LTE UE programmed in C++ and built upon the srsLTE library. With an SISO configuration and running on an Intel Core i7-4790, srsUE can achieve up to 60 Mbps in downlink with a 20 MHz bandwidth. The same template approach as for the eNB holds also in the srsUE case, which is called Pdsch-ue. The purpose of the template is to enable reading OFDMA data from a file or RF board and decode the Physical Downlink Shared Channel (PDSCH).

Relying on the Pdsch-enodeb and Pdsch-ue templates, we are able to deploy an LTE small cell where the UE can attach to the eNB, and the eNB can perform downlink data transmissions to the UE. We make use of the template file to configure the measurement environment with LTE interference that overlaps in time and frequency with the WiFi network communications. Moreover, manipulating the source code in the template, we are able to tweak the transmit power of the eNB, as well as the modulation and coding scheme and the LTE downlink bandwidth during runtime of the measurements.

**OpenWRT**: The OpenWrt project is a Linux operating system targeting at embedded devices. Instead of trying to create a single, static firmware, OpenWrt provides a fully writable file system with packages management. This frees the users from the application selection and configuration provided by a vendor and allows to customize the device through the use of packages that can suit any application. For developers, OpenWrt is a framework to build an application without having to build a complete firmware around it; for users this means the ability for full customization [87]. In our testbed, the WiFi AP is built upon the PCEngines ALIX 2D board (x86 architecture based), to which a WiFi card based on the Atheros AR9220 chipset is connected. The WiFi AP we use in our test-bed is based on the OpenWRT Operating System 15.05.01 version, and is configured to deploy an IEEE 802.11n network with 5.18 GHz carrier frequency in channel 36. Furthermore, the WiFi AP is configured to use one spatial stream, which determines the UDP data rate up to 28 Mbps.

**Spectrum Analyzer**: We use two different spectrum analyzers in our testbed: the VNA Master MS2036A to measure the exact transmitted power of the USRP-B210 with various LTE frequencies and bandwidths, and the osmocom-fft to observe and analyze the received signal power at the WiFi client side. osmocom-fft is a spectrum analyzer tool that is implemented on top of the GNU Radio framework. It includes a visualization panel with tuning and gain controls at the User Interface (UI). It is worth mentioning that the power value in the USRP radio boards is encoded through the gain set in the transmitting chain. Anyway, there is no straightforward method to

compute the power radiated starting from the gain. The easiest approach is indeed that of carrying out measurements.

**SD-RAN Controller:** As already anticipated, our work relies on the SD-RAN controller 5G-EmPOWER [88]. 5G-EmPOWER is an open platform for agile 5G network services development. The goal of 5G-EmPOWER is to provide an open ecosystem where new services can be tested in realistic conditions. 5G-EmPOWER builds upon a set of high-level programming abstractions providing developers with full visibility of the network state and allowing them to dynamically deploy and orchestrate network services. We will discuss more in detail 5G-EmPOWER in Section 4.3.

### 4.1.2 Measurement Environment

Figure 4.3 sketches the implementation of the test-bed put in place to do the interference measurements. The LTE-eNB, the WiFi AP, and the LTE-EPC are connected to the network switch NETGEAR GS 108E and the switch is connected to a network router and thus to the Internet through a LAN cable. The LTE setting for LTE-UE, LTE-eNB and LTE-EPC includes three laptops in which Linux operating system is installed, specifically the Ubuntu distribution version 18.04.1 as shown in Figure 4.2. The eNB transmits to the UE a stream of bits generated at random in continuous mode in order to create a controllable interference environment on WiFi. As a remark, the downlink data is transmitted in the Physical Downlink Shared CHannel (PDSCH) through Transport Blocks (TBs) whose size depends on the modulation and coding scheme used for UE transmissions by the eNB. The MCS directly reflects the quality of the channel conditions experienced by the UE. Thus, TBs are passed from the MAC to the physical layer in every one-millisecond Transmission Time Interval (TTI). The WiFi AP is connected to a laptop with a LAN cable; therefore, we are able to control different parameters of AP through its operating system (OpenWRT). Further, we use another laptop as the WiFi client, where the spectrum analyzer on the same device shows us the received power at the client side.

Referring to Figure 4.3, measurements are carried out in an open office environment with desks and walls. The WiFi client is located 4m away from the WiFi AP and with the same distance from the LTE eNB. Since in a realistic indoor environment u-LTE and WiFi systems might co-exist in a relatively close proximity, we consider the case of interference in which the two transmitters, WiFi AP and LTE-eNB, are quite close to each other. Following this approach, the LTE transmitter, the WiFi AP and the WiFi client form a perfect triangle. In this work, the LTE performance is not studied and we rather focus on measuring the WiFi throughput in various interference environments, assuming that this is the incumbent system to protect.

The WiFi throughput is measured in the downlink and the system bandwidth is 20 MHz. The transmitted power of the WiFi AP is fixed to the maximum value of 20 dBm (i.e. 100 mW). LTE also transmits in the down-link in the same band of WiFi at the 5.18 GHz carrier frequency. For the LTE system we vary the transmit power, the bandwidth (BW) and the MCS index.



FIGURE 4.2: srsLTE test-bed configuration

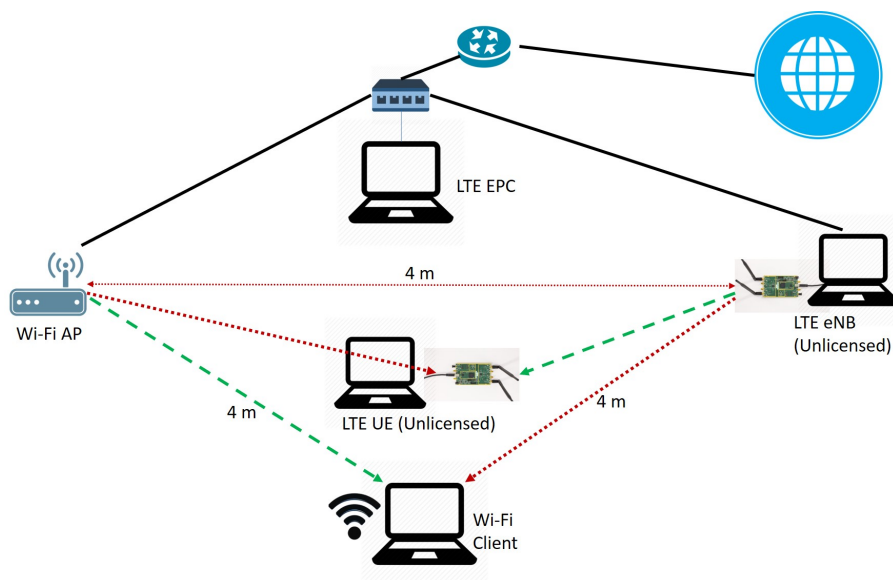


FIGURE 4.3: u-LTE/WiFi test-bed implementation

Moreover, as per the 3GPP standards, the LTE transmitted power can vary between -40 dBm and 23 dBm. To measure the WiFi throughput, we use the measurement tool iperf when we send application data over the User Datagram Protocol (UDP) for 2 minutes, and we record the average data rate as well as the packet loss and received signal power at the client side.

## 4.2 Coexistence Experiments of Unlicensed LTE and WiFi

### 4.2.1 Evaluation Methodology

In this section, we describe the experimental methodology used to carry out the coexistence study between u-LTE and WiFi. The challenge of any experimental set-up is to be able to reproduce realistic conditions that can take place in an actual deployment, while putting in place a controllable experimental environment. The obvious advantage is to obtain realistic measurement results. Since we target an indoor office environment propagation effects of the radio signals such as path-loss and fading are included in the measurement results.

### 4.2.2 Impacts of the LTE Transmitted Power

In the first set of experiments we vary the transmitted power of the LTE eNB for downlink transmissions. Since the uplink traffic is transmitted over the licensed LTE carrier, we do not need to evaluate the effect of the LTE UE transmitted power. The parameters defined in the srsLTE eNB open library to modify the power are *TX-gain* and *RF-amplitude*. The conversion of the TX-gain parameter to the actual power value in dBm is not straightforward since it depends on the carrier frequency and bandwidth selected. For fine tuning of the transmitted power in dBm, we connect the output of the USRP-B210 board to the MS2036A-VNA spectrum analyzer [89] to validate the exact value of the power over different bandwidths. In order to realize the exact value of the cable loss we used also the calibrated signal generator USB-TG124A [90], with which a signal at 5.18 GHz is generated. We report that the loss measured for the cable is approximately 1.5 dB.

**Impacts on WiFi Throughput:** Figure 4.4 shows the measured WiFi throughput behavior with the relative dispersion interval for different values of the LTE transmitted power. The number of resource blocks in the LTE downlink transmission is set to 100 while the modulation and coding scheme index is fixed to 10 for the sake of showing numerical results. As a result, we have an LTE bandwidth of 20 MHz, modulation 16-QAM and TB size of 17568 bits (see Table 4.1). The leftmost result in the figure stands for the case without LTE downlink interference. As expected, we can observe that increasing the value of the LTE transmitted power will degrade the WiFi performance. The results show the average WiFi throughput within 100 sec time window of the experiment. We measured the throughput every one second and, to

avoid the effect of some scattered samples, we show them in a box & whisker plot. Analyzing the results, for LTE signal with transmitted power of 10 dBm the WiFi throughput mostly fluctuates between 3-4 Mbps, whereas for a LTE transmitted power of -7.5 dBm it will vary between 23-25 Mbps, which is approximately the same WiFi throughput measured without LTE interference.

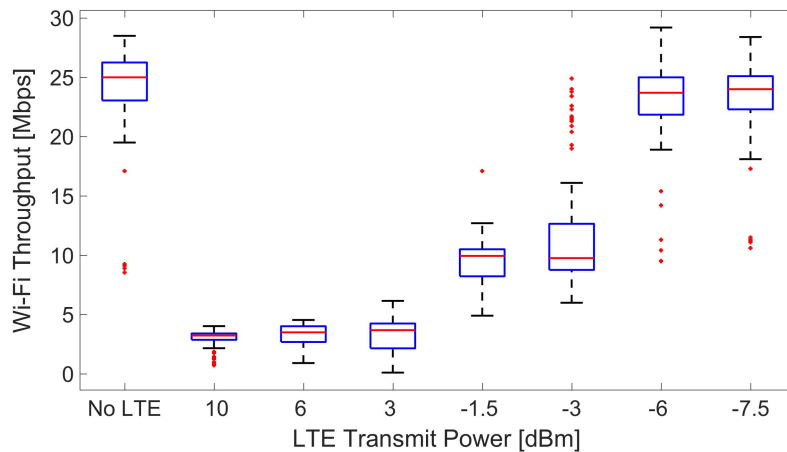


FIGURE 4.4: Impact of LTE transmitted power on WiFi throughput

**Impacts on WiFi Packet Loss:** Figure 4.5 depicts the measured packet loss at the WiFi client for different values of the LTE transmitted power. Obviously, we can realize from this figure that the packet loss and throughput behavior are opposite. While the packet loss in the case without interference is almost 0%, it will move up to 90% when we increase the LTE transmitted power to 10 dBm. Moreover, we can notice from the figure that the WiFi packet loss lays within an acceptable range of values only if the LTE-eNB transmitted power is below -6 dBm.

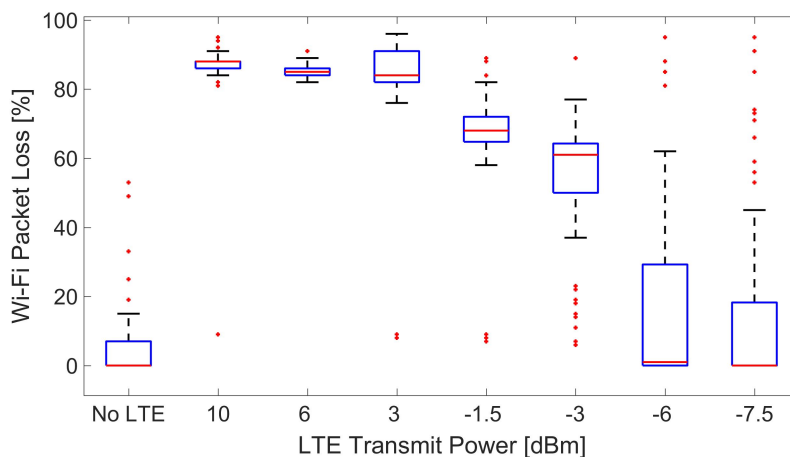


FIGURE 4.5: Impact of LTE transmitted power on WiFi packet loss

### 4.2.3 Impacts of MCS-index

The next set of measurements is used to evaluate the effects of different LTE modulation and coding schemes on the WiFi throughput. In this part, we fix the LTE transmitted power to -1.5 dBm while setting its bandwidth to 20 MHz. We use selected values for the MCS-index ( $I_{MCS}$ ) as shown in Table 4.1 in which the TB size is mapped for each  $I_{MCS}$  in order to measure the effects of this LTE parameter on the WiFi performance. Figure 4.6 shows the results of the measurements. As we can realize from the figure, changes in the LTE modulation and coding scheme will not have dramatic effect on the WiFi throughput performance.

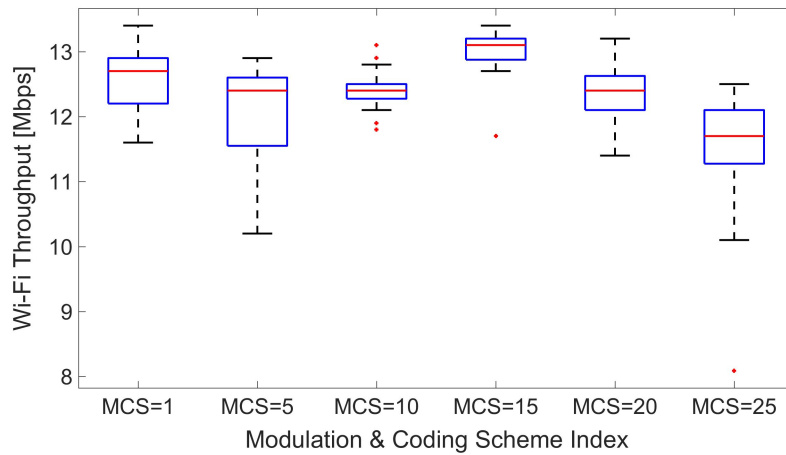


FIGURE 4.6: Impact of LTE MSC on WiFi throughput

TABLE 4.1: Transmitted block sizes with respect to MCS-index

$I_{MCS}$	Modulation	TX block size (bits)
1	QPSK	3624
5	QPSK	8760
10	16-QAM	15840
15	16-QAM	28336
20	64-QAM	39232
25	64-QAM	57336

### 4.2.4 Impacts of Number of LTE Resource Blocks

The last set of measurements relates to quantifying the effect of the number of resource blocks used in the LTE eNB downlink transmission or in other words the effect of the LTE bandwidth. For the measurements, we set the parameters of the eNB to constant values in such a way that the LTE transmitted power corresponds to -1.5 dBm when the LTE bandwidth is equal to 20 MHz. Changing the number of resource blocks in LTE, the transmitted power over the whole bandwidth is automatically scaled in the eNB while

the power per resource block remains nearly constant. Further, in order to show the numerical results and be harmonized with the previous subsections, the MCS-index in these measurements is yet set to 10. Consequently, the modulation of LTE is 16-QAM, whereas the transmitted TB size varies by changing the LTE bandwidth or number of physical resource blocks, as shown in Table 4.2. Figure 4.7 shows the WiFi throughput for different values of the LTE bandwidth in which the number of physical resource blocks varies from 15 to 100. The behavior shown by the figure highlights that decreasing the LTE bandwidth the WiFi throughput decreases as well. Although for a larger bandwidth the LTE transmitted power is higher, it will affect less the WiFi throughput performance. As a matter of fact, looking at Table 4.2, we may notice that the LTE link spectral efficiency is lower with a larger bandwidth and this reduces the negative effects on the WiFi throughput.

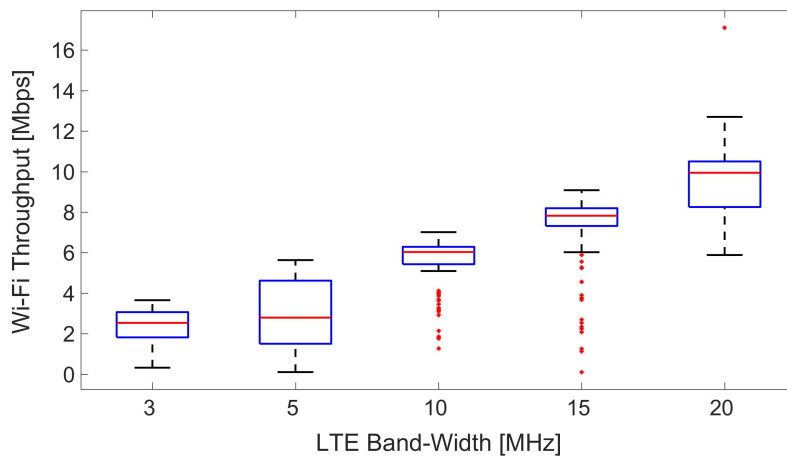


FIGURE 4.7: Impact of LTE Bandwidth on WiFi throughput

TABLE 4.2: Parameters to evaluate effects of LTE-BW

Bandwidth	Bit Rate (Mbs)	(dBm)/PRB	(bit/sec)/Hz	TX block size (bits)
3 MHz	12.5	$\simeq -20$	4.1	2344
5 MHz	14.5	$\simeq -20$	2.9	4008
10 MHz	24	$\simeq -20$	2.4	7992
15 MHz	26	$\simeq -20$	1.7	11832
20 MHz	26.5	$\simeq -20$	1.3	15840

### 4.3 Dynamic Interference Coordination Through SD-RAN Control

Referring to the measurements shown in Section 4.2, we observe that the modification of different parameters of the LTE transmission can have different effect on the WiFi performance. Also, we may infer that without an intelligent entity that can analyze the key performance indicators of both technologies, fair coexistence between the two networks is not straightforward

to achieve. In this section, we introduce the centralized SD-RAN controller concept and we discuss how this can be the tool to enable fair coexistence between u-LTE and WiFi since the controller can give priority to either of the technologies dynamically. To demonstrate the performance improvements introduced by the new centralized entity in an actual environment, we will define different scenarios for u-LTE and WiFi coexistence in which we insert the new dimension of the controller in the measurements. At first, we describe in detail the architecture and the different components of the 5G-EmPOWER controller. Afterward, we apply the controller to the u-LTE and WiFi co-existence problem, while comparing the throughput performance of WiFi with the case in which the central action of coordination provided by 5G-EmPOWER is absent.

### 4.3.1 5G-EmPOWER Controller

5G-EmPOWER is a multi-access software-defined RAN controller which supports heterogeneous access technologies such as LTE and WiFi as shown in Figure 4.8. The 5G-EmPOWER protocol allows remote management of various RAN elements, as well as network service programmability through an intent-driven application framework. Compliantly with the philosophy of Software-Defined Networking, the control plane is separated and taken care of by the controller itself, whereas the WiFi AP and the LTE-eNB are the Network Elements (NEs) which are controlled by 5G-EmPOWER. The identity (i.e. MAC address) of each entity connected to 5G-EmPOWER can be defined in the controller and whenever a WiFi AP or an LTE-eNB is activated the controller receives a notification showing whether they are available to provide service or not. This is, in fact, the network monitoring aspect that is done inside the controller. Furthermore, 5G-EmPOWER provides developers with full visibility of the network state while allowing them to dynamically orchestrate network services. Centralized mobility management of WiFi and LTE networks, custom resource allocation, and lightweight virtual network functions are some of the features already available on top of the 5G-EmPOWER framework [91], [88].

**5G-EmPOWER Agent:** The 5G-EmPOWER Agent, hereinafter referred to as Agent for simplicity, handles incoming messages inside the eNB protocol stack. The main purpose of the Agent is to create various interfaces with distinct layers of the eNB protocol stack in order to set/get specific parameters to/from the controller.

**5G-EmPOWER Protocol:** Referring to Figure 4.10, the 5G-EmPOWER protocol, hereinafter referred to as Proto, is an interface between the controller and the Agent to enable the communication between the two entities whenever required. Figure 4.9 shows the general structure of a request/reply message using the Proto interface. The *Header* contains the general information that has to be carried out by any exchanged message (cell ID, message length and so on). The *Event Header* embeds the information related to the type of events that are discussed below. *Action* specifies the operation that has to be executed by the Agent and the field *Data*, which is appended at the

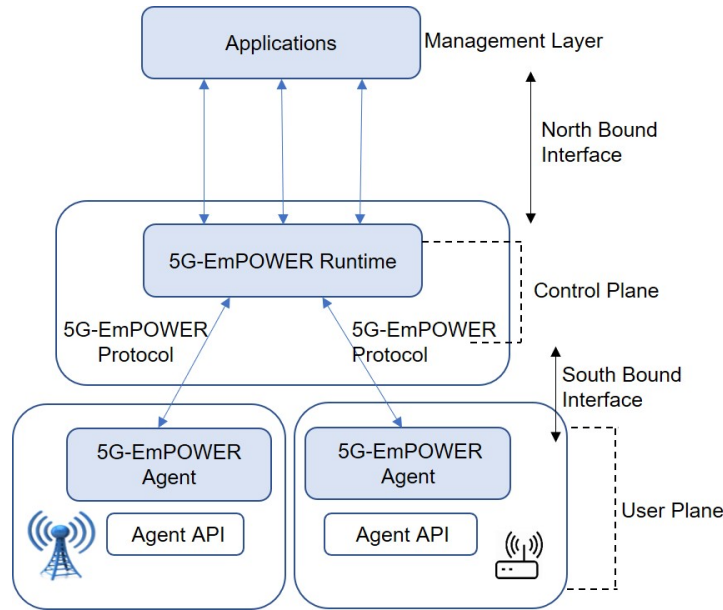


FIGURE 4.8: 5G-EmPOWER Operating System Architecture

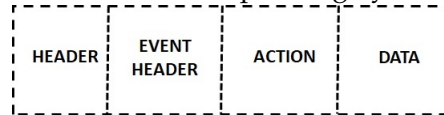


FIGURE 4.9: 5G-EmPOWER messaging structure

end of the message, can be used to exchange any information that is needed between 5G-EmPOWER controller and Agent. Referring to the Event Header field, there can be three major events around this protocol which are classified as below:

**Single Events:** these events occur only once and are generated by either the controller or the Agent and the reply will be sent back immediately by the other entity (i.e. Agent or controller) after receiving the request,

**Scheduled Events:** these events can take place once or repeatedly, but the reply will be reported at each scheduled interval,

**Triggered Events:** as it can be inferred from the name, these events are mainly used to enable or disable a functionality in the Agent based on the occurrence of a particular situation.

### 4.3.2 SD-RAN Enabled Test-Bed Architecture

Figure 4.10 sketches the general architecture of the proposed u-LTE/WiFi coordination approach that is implemented through the 5G-EmPOWER controller, as well as the terminology used throughout the rest of the paper. The controller is able to control both WiFi AP and LTE-eNB access nodes. The 5G-EmPOWER architecture consists of three layers: *infrastructure*, *control*, and *service*. The infrastructure layer where the data plane network elements are located consists of one LTE-eNB and one WiFi AP, whilst the 5G-EmPOWER runtime is located at the control layer [88]. The role of the runtime is to convert the service layer policies (e.g. u-LTE/WiFi interference management)

to the commands for the infrastructure elements. Figure 4.10(b) illustrates in detail how each eNB can communicate with the 5G-EmPOWER controller through the Proto interface.

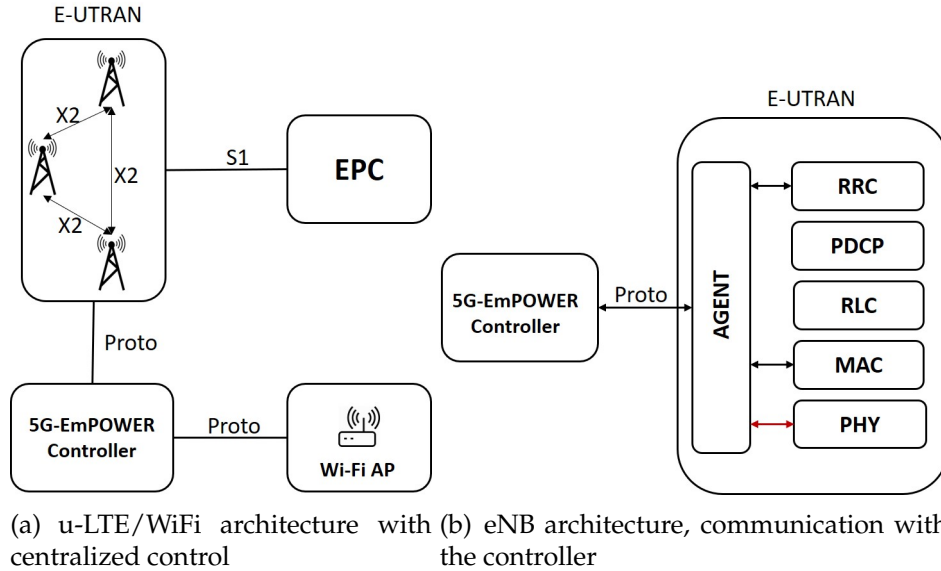


FIGURE 4.10: Centralized coordination of WiFi/LTE

Reconnecting to the set of measurements detailed in Section 4.2, the parameters of the LTE-eNB like transmitted power, bandwidth and the MCS-index are defined in the physical layer of the srsLTE-eNB. By developing an interface between the Agent and the physical layer, we are able to modify these parameters at runtime. The loop is closed considering that the Agent can communicate with the 5G-EmPOWER controller through the Proto interface. As illustrated by Algorithm 1, in the first place the controller sends an initialization request to the Agent to receive information regarding the parameters already set inside the eNB physical layer. The Agent will reply with a scheduled message the requested parameters within a predefined time interval. The parameters include the transmitted power currently used, bandwidth and MCS-index used by the eNB for downlink transmissions. As soon as the controller receives the information that the WiFi AP has activated a downlink transmission, it will command the eNB to lower the transmit power and increase the transmission bandwidth, while it will leave the MCS-index unmodified, as demonstrated in Section 4.2, in order to preserve the WiFi throughput.

Figure 4.11 shows the sequence diagram for the procedure that we have developed to improve the coexistence between u-LTE and WiFi networks through the use of the 5G-EmPOWER controller. As soon as the LTE-eNB begins a downlink transmission, it will communicate the physical layer parameters that are currently used to the controller through the Agent using the Proto interface. The controller can control the WiFi AP and it is aware of whether it is transmitting in the same band of LTE or not. Whenever the WiFi AP starts transmitting in downlink in the same band of LTE, the controller

```

Initialization: Send schedule msg;
while LTE-eNB connected do
  GET the PHY parameters reports;
  if WiFi AP is transmitting then
    if PHY param acceptable then
      Do nothing
    else
      Minimize the eNB transmit power;
      Maximize the eNB Bandwidth ;
    end
  else
    SET Max transmit power of eNB;
  end
end
end

```

**Algorithm 1:** u-LTE/WiFi algorithm application

will decide a new set of parameters for the eNB and will enforce them in the eNB physical layer again by means of the Agent. Finally, the new values of eNB physical layer are reported back to the controller until a new decision stage is performed.

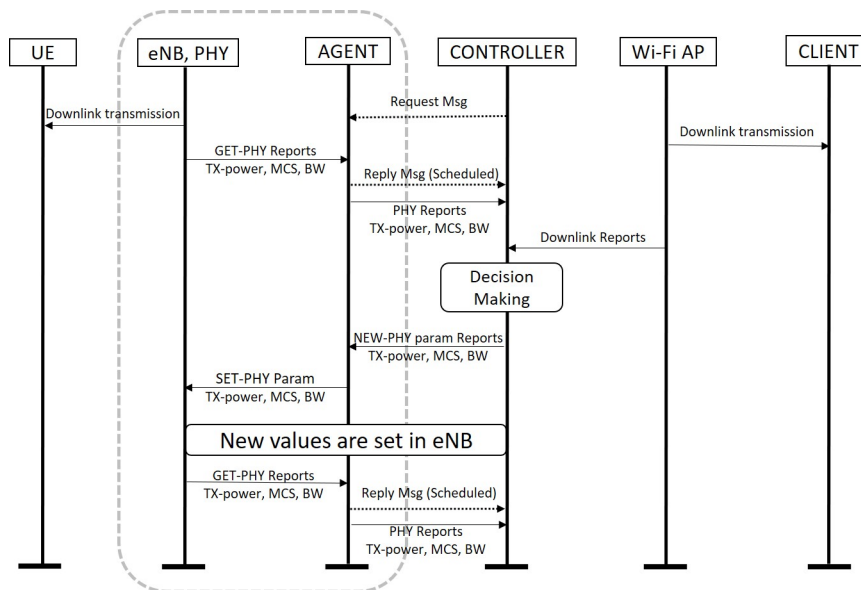


FIGURE 4.11: Sequence diagram showing the proposed approach to control eNB physical layer parameters

### 4.3.3 Measurement Results

Relying on the lessons learned from the first set of measurements shown in Section 4.2, we provide the results of another set of experiments in which we measured the throughput that can be achieved by the WiFi network when the 5G-EmPOWER controller is added to measurements to perform adaptation of u-LTE transmission parameters when the WiFi downlink transmission is

activated. For the purpose, we initially configure the LTE-eNB physical layer parameters with  $-1.5$  dBm transmitted power and 20 MHz of bandwidth. These parameters are reported to the controller within the message linked to a scheduled event. When the WiFi AP starts transmitting, the controller can adjust the LTE-eNB power to  $-6.2$  dBm, while the bandwidth is unmodified since it is already set to the maximum. To understand the benefits of the centralized control action, we define two different scenarios as shown in Figure 4.12. Similar to the measurements shown in Section 4.1.2, the distance between the WiFi AP and the LTE-eNB is fixed to 4m. In the first scenario shown in Figure 4.12(a), the WiFi client is moved away from the LTE-eNB, whereas in the second scenario shown in Figure 4.12(b) the WiFi client is moved in the direction of the LTE-eNB. The choice for the measurement set-up is motivated by thinking to scenarios of indoor mobility in which the client moves in proximity of the WiFi AP following a simplified linear motion. The two scenarios motivates two distinct sets of measurements in which the performance are aggregated using the measurement tool iperf when data traffic is sent over the UDP transport protocol. Unlike to the previous set of measurements, we record also the important parameter provided by the WiFi Received Signal Strength Indicator (RSSI). For the scenario in which the WiFi

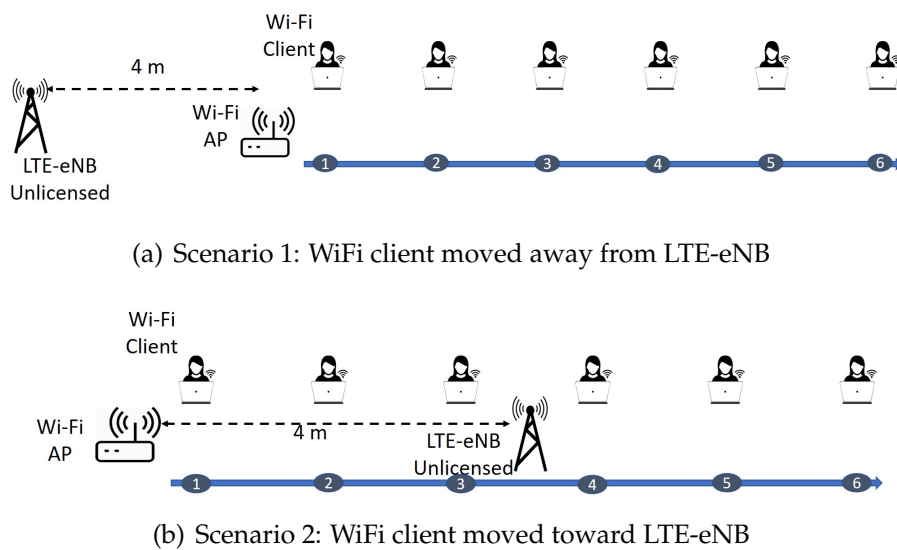


FIGURE 4.12: 5G-EmPOWER controller measurements environment

client is moved away from the LTE-eNB, Figure 4.13 compares the measurement results obtained in the situation of uncoordinated (i.e. 5G-EmPOWER does perform any control action) LTE transmissions with static transmitted power to the situation in which LTE-eNB transmission parameters are adjusted by the 5G-EmPOWER controller for different values of the RSSI measured at the WiFi client side. The measurement results for the scenario in which the WiFi client is moved toward the LTE-eNB are shown in Figure 4.14. As mentioned, the RSSI values are measured moving the WiFi client at various distances following a linear motion. We consider both Line-of-Sight and

Non-Line-of-Sight conditions when changing the WiFi client position with respect to the AP. Both figures prove the clear throughput performance improvement that arises from the centralized coordination action performed by the centralized SD-RAN controller. Even the simple action of dynamically adapting the LTE-eNB transmitted power can yield WiFi throughput improvements. Comparing Figure 4.13 to Figure 4.14, we may also notice that the 5G-EmPOWER control action is more effective when the WiFi client is moved away from the LTE-eNB. The explanation is quite intuitive since the channel propagation affects in a non-linear manner the radio signals. Increasing the distance separation between the interfering eNB and the WiFi client, the control action performed by 5G-EmPOWER has a non-linear effect on both LTE-eNB and WiFi AP transmitted signals until reaching a certain distance at which the radio signal of the WiFi AP becomes too low. For the sake of completeness, we may notice that the control action of 5G-EmPOWER is less effective when the WiFi client is moved toward the LTE-eNB simply because the interference power is remarkably higher than that received from the WiFi AP. Based on the new set of measurements in which 5G-EmPOWER can coordinate both LTE and WiFi technologies, we can learn the lesson that, to cope with the variety of situations that may arise in an indoor environment, though the action of the centralized SD-RAN controller is evidently positive, even more sophisticated techniques beyond transmitted power adaptation are needed on top of the controller. This aspect is further discussed as part of the future work activities that we plan to carry out to extend the present work.

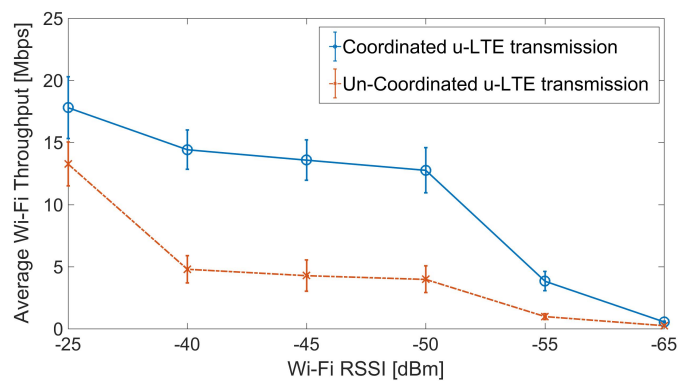


FIGURE 4.13: WiFi client moves away from LTE-eNB

## 4.4 Conclusion of the Chapter

This Chapter presented measurements results that quantify the effects of LTE transmissions in the unlicensed 5 GHz band on the Wi-Fi throughput performance in an actual office environment. In our test-bed we have used the open

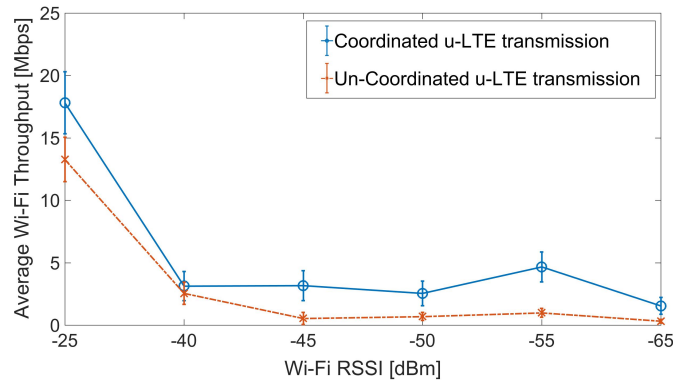


FIGURE 4.14: WiFi client moves towards LTE-eNB

source srsLTE libraries and the OpenWRT operating system. Our methodology is based on adopting a new degree of controllability added by the 5G-EmPOWER SD-RAN controller to coordinate the transmissions of both technologies, thus leveraging on the network programmability paradigm. First, we have presented an experimental set of results for the Wi-Fi network throughput affected by LTE transmissions showing the sensitivity of Wi-Fi with respect to LTE parameters such as transmitted power and system bandwidth. We measured the Wi-Fi throughput by modifying the eNB transmission parameters as the source of interference to Wi-Fi and compared the results with the case in which LTE interference is not present. In addition, we have developed an approach to improve coexistence by means of the 5G-EmPOWER controller, which we illustrated through a sequence diagram in order to enable modification of the LTE-eNB parameters based on network conditions to preserve the Wi-Fi down-link throughput. Measurement results demonstrate the viability of our approach and the improvement that can arise from controlling the LTE transmission parameters.

## Chapter 5

# Decentralized Coordination of Small Cells in Roaming

The distributed nature imposes novel challenges on service provision and raises consistency, completeness, and privacy concerns. Leveraging on the distributed nature, the Blockchain and Distributed Ledger Technologies (DLT) emerge as revolutionary approaches to decentralization with distributed consensus. We expected that the Blockchain-based approaches can play a disruptive role in the design of the next generations of cellular networks, [92]–[94]. Especially Fraud reduction is also gaining gradually more importance among MNOs. Although the estimated \$29.2 Billion in 2017 contains various types like Identity/Account theft, network hacking and bypassing laws and contracts (i.e. SIM boxing, femto cell abuse, roaming reselling), it remains a threat to the confidence in telecommunication means and the international security. Blockchain technology can help MNOs to enforce identity management, roaming partner agreements, and Call Detail Record (CDR) verification much more effectively because they support consensus, provenance, immutability, and finality [68]. In this chapter, we discuss how Blockchain technology can merge with the 5G networks to boost their performance. More specifically, we represent a new network architecture for the roaming scenario in 5G networks based on a Blockchain Network. Further, we show how different Mobile Network Operators (MNOs) can overcome the lacks of current roaming architecture by making a permissioned (consortium) Blockchain. The proof of concept using hyperledger fabric framework represents the components and the mechanism of the network.

## 5.1 Roaming in 5G Networks

Roaming is a service that allows a mobile user of one MNO to use the services of another MNO when inside the latter's coverage area [95]. Operators can ensure interoperability across network generations, network technologies and roaming partners. It will be important to have Voice over LTE (VoLTE) deployed for a seamless voice experience between 5G and 4G. Operators can also maximize their interconnection footprint to break down barriers between geographies. Many 5G use cases will be global in nature, so businesses will need to ensure seamless quality of service once their users, devices, and things begin roaming from their home 5G network.

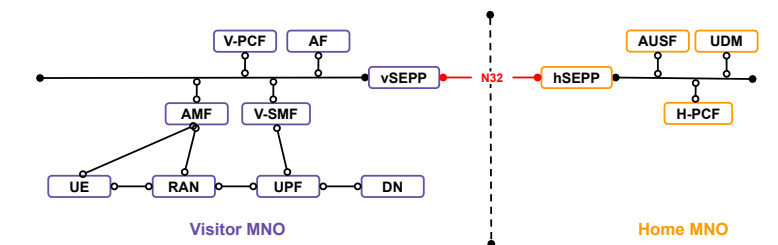
The legal roaming business aspects contracted among the roaming partners for charging of the services used are specified in so-called roaming agreements. The GSM association describes the content of such roaming agreements in a regulated form for all its members [96]. Moreover, for the contractual aspects of authentication, authorization, and charging of the visiting user, the roaming agreements should comprise of a minimum safety standards (e.g., billing procedures, location update procedures, warranty procedures).

### 5.1.1 Roaming Architecture

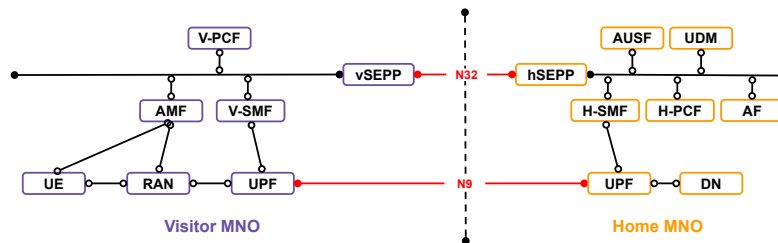
Regardless of the various interfaces between home and visited MNOs, according to the 3GPP standard, National and International roaming services use the same network architecture. As briefly stated in Section 1.2.2, the 3GPP standards support two roaming models, as described below:

*Local breakout roaming.* The data traffic of the roaming user is served directly by the visited MNO allowing for more efficient routing in terms of latency and bandwidth as shown in Figure 5.1(a). In this model, the home operator loses the control over their subscriber. In theory, it is considered as the best architecture for the roaming Quality of Service.

*Home-routed roaming.* The data traffic of the roaming user is always served by the home MNO giving more control over the user's traffic (Figure 5.1(b)). Albeit higher latency, the model is recommended when the relationship between two operators is not totally trustfully.



(a) Local-breakout Roaming architecture



(b) Home-routed Roaming architecture

FIGURE 5.1: Roaming in 5G Network

### 5.1.2 Challenges and Requirements

- **Billing settlement:** In the Local Breakout roaming for charging, roaming information must be associated with charging accounts. The problem with this configuration is the visited network does not have subscriber charging information whereas the home network also does not have the subscriber roaming information. This means that the MNOs need to manage multiple relationships, interconnect globally, and handle complicated financial relationships [15]. To this extent, two possible relationship scenarios between operators are establishing either direct relationship or un-direct through intermediaries. In the former scenario, although MNOs do have a choice to connect directly to all the other MNOs, it is obvious that a point-to-point relationship with each roaming partner is not feasible and is cost-prohibitive because each MNO needs to maintain hundreds of such agreements to share resources efficiently for having universal roaming service. Whereas in the latter scenario, a 3<sup>rd</sup> operator or a clearinghouse is used to connect the two operators as shown in Figure 5.2. Although this kind of roaming is working in current Lte network by establishing settlement relationships with all relevant operators, it still has many drawbacks. First of all, the presence of an intermediate entity applies many extra expenses to the network; more importantly, it raises the concept of security and trust by introducing a 3<sup>rd</sup> party.
- **Scalability:** The existing peer-to-peer roaming agreements between MNOs is quite inefficient and impractical because each MNO needs to maintain hundreds of such agreements to share resources efficiently for having universal roaming service.
- **Security and Trust:** The roaming user before gaining access to the visited MNO must be authenticated through the home MNO. There exists a number of user authentications and key exchange protocols that are proposed in the literature for roaming. However, each of them concentrates solely on the mutual authentication between the user and the visited MNO. Moreover, The roaming user may have accepted to different policies in the home MNO regarding the access to user information (user protection act) than that in the visited MNO. Therefore, it requires re-accepting the roaming privacy terms before providing any services.

## 5.2 Blockchain-based Roaming in 5G Networks

In this section we explain how a Blockchain platform can be deployed in a roaming scenario to handle billing settlements among different operators. We later describe in detail the proof of concept using Hyperledger Operating System for deploying a permissioned Blockchain for the roaming usecase.

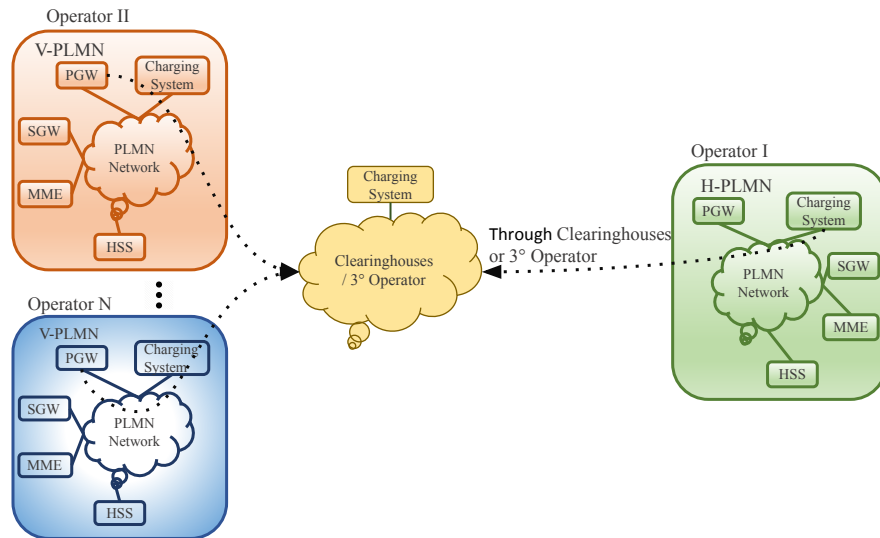


FIGURE 5.2: Roaming with a third party clearing house.

### 5.2.1 Blockchain Topology

Looking from the system design, four implementation layers can be abstracted for a Blockchain network [97]. As shown in part of Figure 5.4, starting from bottom to top, the first layer, data and network organization, provides the approaches to form cryptographic data and organize blocks of data in chronological order to establish a chain of blocks. The cryptographic representation of data provides security and privacy for the Blockchain network. The consensus layer, however, guarantee reliable data synchronization (e.g. transactions) in a peer to peer connections. In a permissioned Blockchain, the participants can benefit from information sharing and peer-to-peer transactions among inter-authorized organizations by forming a consortium chain. Moreover, the consensus mechanisms are semi-centralized which can provide high transaction processing throughput. The smart contracts are deployed on a distributed virtual system in the third layer. This is a user-defined business logic aims to automatically execute its content (e.g. the costs of roaming users) across inter-authorized organizations. The contents of smart contract are agreed by all the organizations of a permissioned Blockchain. Upon agreement, the smart contract will be applied on the Blockchain and its self-executable nature makes it apply a transaction once a new data is uploaded on the Distributed Ledger. The transactions which is done by smart contract and confirmed through consensus mechanisms will be added to the chain of blocks. Finally, the application layer on top defines a user interface and programming language implementation for smart contracts as well as the sand-boxed runtime environments (e.g. Hyperledger Fabric, Ethereum Virtual Machine).

### 5.2.2 Role of Blockchain in Roaming

- **Discovery** When a roaming user attempts to associate to the visited MNOs network, the visited MNO discovers that the user is a visitor

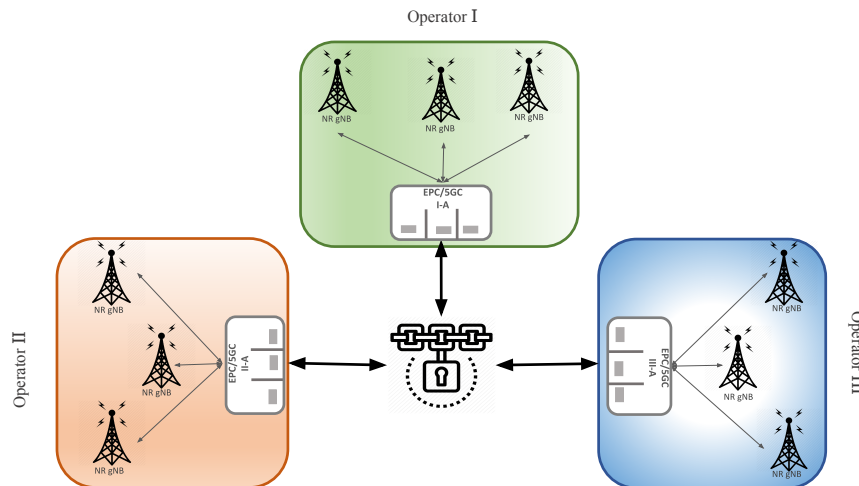


FIGURE 5.3: Blockchain-based Roaming.

from the home MNO. This exchange of user information between home and visited MNOs takes place on the Blockchain network by generating a new block. The added block include the updated location, the home operator, the visited operator, and the time of discovery.

- **Identity management** After the discovery, its time to identify the user and register as a roaming user. Based on the rules defined in the smart contract, the user is either authenticated or declined by the visited MNO. Upon completed registration, the user can start a call or use data.
- **Billing settlements** When a roaming user begins a voice call on the visited MNO, this event is recorded on the Blockchain network. Once the call is terminated, the duration of the call is also recorded. Based on the charging rules defined in the smart contract, the payment is initiated from the home MNO to the visited MNO based on the consensus mechanism used in the Blockchain network. Therefore, by avoiding a third party or a clearinghouse (e.g. instead of Figure 5.2), the issue of disagreements amongst the involved parties can be completely avoided using Blockchain and DLT as shown in Figure 5.3.

### 5.2.3 Roaming Charging with Blockchain

The message flow of UE attach procedure initiated by a roaming user towards the MME of the visited operator is the same as in the current roaming architecture which consists of UE ID acquisition, authentication, NAS security setup, location update, and finally session establishment. It is to be noted that the HSS of the home operator executes the authentication procedure. After that, the visited operator starts offering the demanded services to the roaming user through the established Packet Data Network (PDN) sessions. Figure 5.4 shows the Non-Stand Alone (NSA) architecture where the control plane traffic is through X2 interface between gNB and eNB, using the

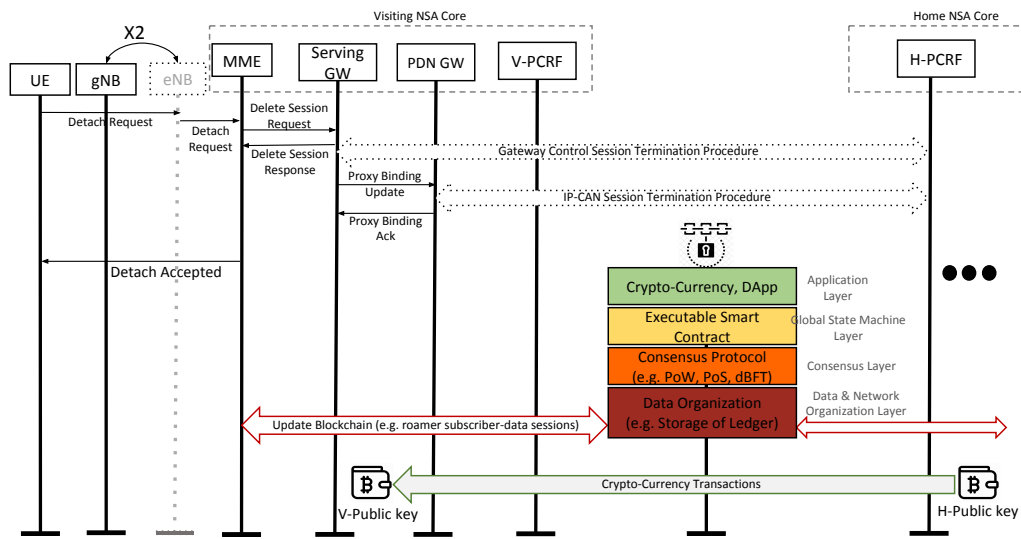


FIGURE 5.4: Blockchain enabled billing settlement for roaming in NSA core

Evolved Packet Core (EPC). As illustrated in the figure, once the UE initiates UE Detach Procedure, the established PDN sessions are deleted, and the detach accept message is sent to the UE. Then, the EPC of the visited operator pushes the session activities of the roaming user onto the distributed ledger where a smart contract with a predefined set of rules can be executed based on the obtained information. The contents of the smart contract can be defined in advance by the participant MNOs which gives the possibility of token/cryptocurrency transaction among different MNOs. Each transaction in the network is validated and confirmed by other nodes (EPCs) of the Blockchain through a consensus mechanism. All these procedures will be explained in details in the next section.

### 5.3 Proof of Concept

As mentioned in the previous sections, we need to have a permissioned Blockchain for our roaming scenario. This Blockchain is consist of different MNOs who act as the organizations of the network. Each organization is responsible to identify the participant nodes of the Blockchain which are the 5G-core networks. All the core networks have a copy of the distributed ledger and they are able to read and update the ledger through an application on top of them. Moreover, the consortium of the MNOs will define the rules and the content of the smart contract.

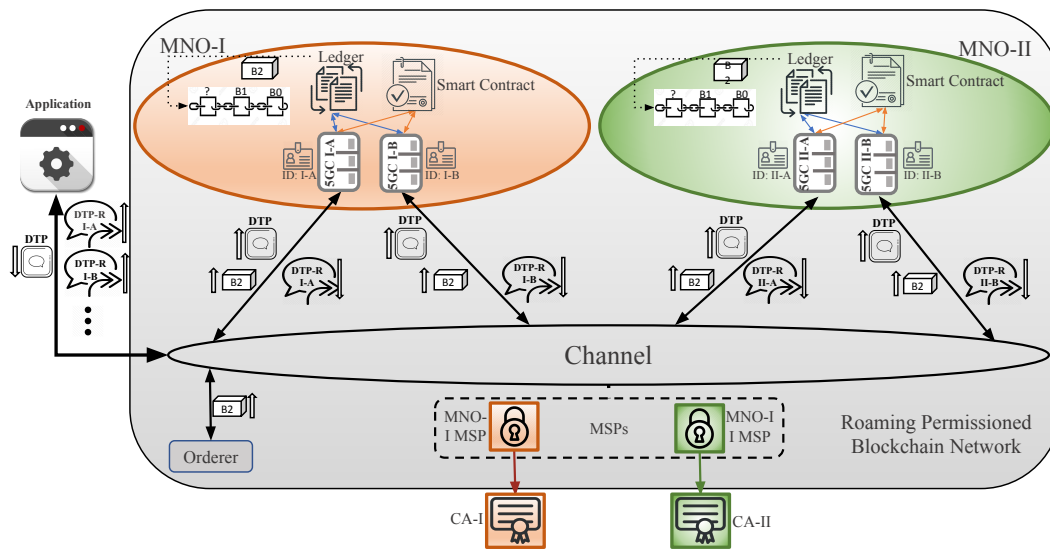


FIGURE 5.5: Configuration of Roaming Blockchain

### 5.3.1 Components

To define our network, we are using Hyperledger Fabric which is a permissioned Blockchain framework implementation that leverages container technology to host smart contracts [98]. Its abilities allow entities to conduct confidential transactions without passing through a central authority. Figure 5.5 shows the general architecture of proof of concept. The 5G-core networks (shown as 5GC in the figure) are the fundamental elements of the network and they host copies of the ledger while using the smart contract(s) to access to their instance of the distributed ledger. Each of the 5G-cores has a smart contract installed on them which make it possible to query, read, or update the ledger instances. There can be also application(s) that connect to 5G-cores when they need to access to the ledger as well as the smart contract. The main rule of the application is to connect to 5G-cores, invoke smart contracts to generate required transactions, submit transactions to the distributed ledger, and receive events. Then there is a private channel that allows a specific set of 5G-cores and applications to communicate with each other within a Blockchain network. The channel allows different actors of the network privately agree on the terms of their interaction in a trust-less environment. Each of the participant nodes (5G-core) are identified by a unique digital certificate assigned by an administrator who is their owning MNOs through a particular Certificate Authority (CA). For example in Figure 5.5, 5GC I-A and 5GC I-B have identities issued by CA-I. As soon as a new 5G-core connects to a channel, its digital certificate identifies its owning MNO via a channel Membership Service Provider (MSP). After defining all components of our Blockchain network, we will see how transactions can be initiated, blocks are generated, and the consensus is achieved.

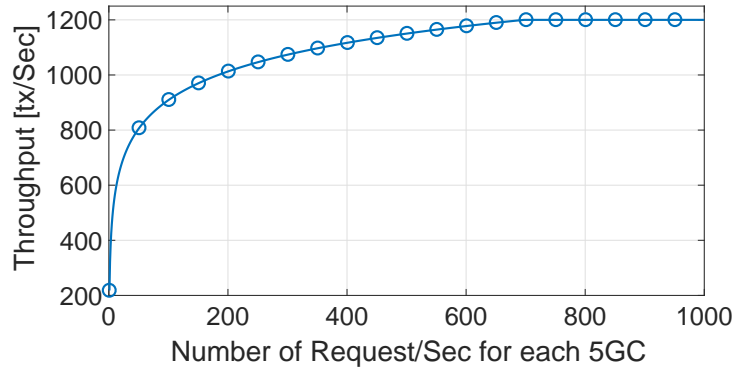
### 5.3.2 Transactions and Consensus

In this section, we only speak about billing settlement after a roaming user detach successfully from visiting operator. When the detach is complete, in the first step the application generates a transaction proposal and will push it to the set of 5G-cores using the channel. We call it Detach-Transaction Proposal (DTP) as shown in Figure 5.5. The DTP includes the identity of the visited MNO (which is recognized based on the visited 5G-core ID), the identity of the home MNO (which is recognized during authentication management), the duration of the calls or data usage, the location and time of the provided service, and the value of the roamer consumption. Second, the 5G-cores who receive the DTP independently execute the smart contract to produce proper response. Once the cores check the values with the smart contract, they produce a unique and independent response (we call it DTP-R) by adding their digital signature and signing the entire payload using their private key and finally, send it back to the application. This procedure is called endorsement and can be subsequently used to prove that each MNOs' 5G-Cores generated a particular response. The set of 5G-cores to get the DTP depends on the pre-defined policy which defines the set of MNOs that need to endorse a proposed ledger change before it can be accepted by the network. For this scenario, selecting the two visiting and home MNOs are enough to validate a transaction proposal and achieve consensus. Upon achieving consensus, application triggers a token/Cryptocurrency transaction from the wallet address of home operator to the wallet address of visited operator. Finally, the orderer receives transactions from the application, packages them into a block, and distribute to all the 5G-cores where they are added to the ledger.

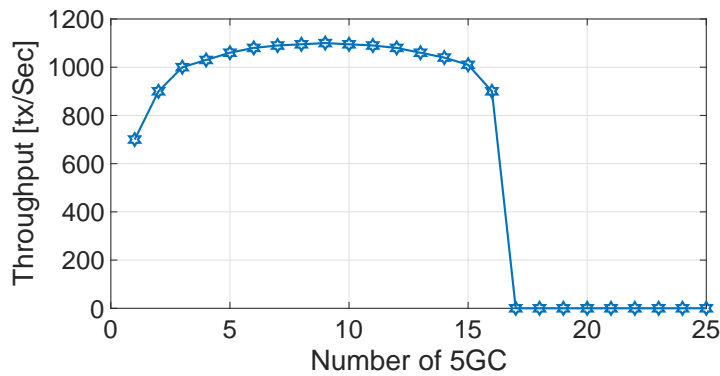
### 5.3.3 Evaluation

Since the transactions among operators will settle after the roaming user is detached from the network, they do not need to be real time. Hence, the network latency is not so important for the network operators. However, it is very important to evaluate the scalability of the permissioned blockchain based on Hyperledger Fabric. Figure 5.6(a) shows the network throughput with respect to the number of requests per second that each 5G-core produces. The throughput shown in the figure is the number of successful transactions per second in the Hyperledger Fabric permissioned Blockchain. We can conclude from the figure that while initially the whole network throughput increase with higher requests rate, it will go to a saturation condition after a certain number of request per second ( $\simeq 600$ ). Further, relying of the works in [99] and as shown in Figure 5.6(b), we can see the Hyperledger fail to scale when the number of 5G-cores go beyond 16 in the network. The main reason is that with the higher number of participant nodes, the network will fail to reach the consensus. To solve the scalability issue, the network need to have different channels in such a way that a cluster of 5G-cores (less than 16), each capable of serving as an endorser for the channels, communicate with the application through separate channels. Generally, Channels are important aspect of Hyperledger to slip a bigger blockchain into many

smaller blockchain which allows not only data isolation and confidentiality, but also use for scalability. Combine the DLTs with channels we can a scalable network, where any 5G-core only need to communicate with other participants in the same channel. We plan to evaluate the performance of roaming blockchain with multiple channel in the future works.



(a) Throughput Vs Request Rate



(b) Throughput Vs #5GC

FIGURE 5.6: Roaming Blockchain Scalability

## 5.4 Conclusion of the Chapter

In this chapter we first discussed despite the Local BreakOut roaming has many advantages to be use in the roaming, most MNOs still prefer to use the Home-routed architecture in order to have full control of their users even out of their geographical coverage. Due to the technical potentials of the Local BreaOut approach in roaming, we propose a permissioned and smart contract-based blockchain to remove the problem of missing trust among operators. With this approach, the billing settlement can be performed automatically with the help of the smart contract deployed on the blockchain. Further, as a result of the transparent nature of blockchain, MNOs can ensure the accuracy of charging system.



## Chapter 6

# Conclusions and Future Works

This chapter summarizes the contributions of the research presented in this dissertation and provides concluding remarks. We also suggest some promising research directions for future work.

Fifth generation of the mobile network (5G) are currently under the spotlight and are expected to create new market opportunities for small and large enterprises alike. The heterogeneous networks is called as one the most important features of the 5G systems. Having densified and diverse networks (e.g. Heterogeneous Wireless Networks), the need of system analysis and novel controlling methods has never been higher.

In this Ph.D. dissertation, while we first analyze completely a specific heterogeneous wireless networks (LTE/WiFi coexistence in unlicensed bands), we introduced a new paradigm of central controllability for it. Moreover, we propose a distributed controlling system for another dense network with heterogeneous participants (roaming in 5G networks) to facilitate interaction among different mobile network operators in an autonomous manner.

At first, in chapter 3, we developed an analytical method to evaluate the effect of LTE transmissions that overlay with WiFi in the 5 GHz unlicensed band studying two main aspects: WiFi clear channel assessment at the physical layer and the MAC layer throughput in saturation condition of the network. Although mechanisms already exist (e.g. LTE-u and LTE LAA) to avoid simultaneous transmission of LTE with WiFi, we noticed that even these methods may not solve completely the challenge of co-existence in indoors. To quantify the impact of LTE transmissions on the WiFi clear channel assessment, we modeled the effect of LTE as a random interfering process resorting to the characteristic function approach for the energy detector receiver. This has allowed us to identify different thresholds for the energy detection to maintain the false alarm probability constant. Moreover, we have modeled the WiFi throughput resorting to a one dimensional Markov chain model. The combination of the two approaches led to obtain the WiFi network throughput in realistic propagation conditions that are typical of an indoor environment, modeling at the same time several WiFi network constraints. Further, we extent the work for the unsaturated conditions generalizing the interference to any OFDM-based systems in Section 3.4. we developed an analytical model to evaluate the 802.11 unsaturated throughput in a Poisson field of interference. We modeled both the presence of interference inside the WiFi network (i.e. intra-network) and due to OFDM-based

transmitters other than WiFi (i.e. inter-network) whereby again stochastic geometry. As before, with the characteristic function, we evaluated the ED-CCA based of the new general conditions, while the Markov chain models CSMA/CA in non-saturation conditions accurately. Hence, we used a cross-layer method that combines both physical layer and MAC layer analysis. Our method generalizes existing techniques to evaluate the performance of WiFi in heterogeneous network conditions. Parameters such as transmitted power, nodes density, frame size and detection threshold can be varied to assess the WiFi network behavior.

In Chapter 4, by using some testbeds we presented measurements results that quantify the effects of LTE transmissions in the unlicensed 5 GHz band on the WiFi throughput performance in an actual open office environment. In our testbed we have used the open source srsLTE libraries for srsEPC, srseNB, srsUE and the OpenWRT operating system. Our methodology is based on adopting a new degree of controllability added by an SD-RAN controller to coordinate the transmissions of both technologies, thus leveraging on the network programmability paradigm. In this chapter, we first presented an experimental set of results for the WiFi network throughput affected by LTE transmissions showing the sensitivity of WiFi with respect to LTE parameters such as transmitted power, system bandwidth and modulation and coding scheme. We measured the WiFi throughput by modifying the eNB transmission parameters as the source of interference to WiFi and we compared the results with the case in which LTE interference is not present. In addition, we have developed an approach to improve coexistence by means of the 5G-EmPOWER controller, which we illustrated through a sequence diagram in order to enable modification of the LTE-eNB parameters based on network conditions to preserve the WiFi downlink throughput. Measurement results demonstrate the viability of our approach and the improvement that can arise from the central controlling of the LTE transmission parameters at runtime.

Finally, in Chapter 5 we demonstrated a novel network architecture based on the distributed ledger technology for handling transaction in roaming. Our proposed architecture is based on a permissioned blockchain with smart contracts (Hyperledger Fabric) which allowed to have only authorized participants as the network's nodes. By delegating the authorization and charging tasks to the blockchain, the roaming billing settlement can be performed without the need of any third-party trusted clearinghouses. In this chapter, at first, we noticed even though Local BreakOut roaming has many advantages, most MNOs still prefer to use the Home-routed architecture to have full control of their users even out of their geographical coverage. Due to the technical potentials of the Local BreakOut approach in roaming, and to make possible the use of Local BreakOut, our propose permissioned and smart contract-based blockchain can remove the problem of missing trust among operators. Different mobile network operators who are willing to join to the distributed ledger will play the role of the blockchain organizations. They are responsible to certify the participant nodes that are the 5G cores. Each 5G core, as fundamental elements of the network, host copies of the ledger while

using the smart contract(s) to access their instance of the distributed ledger and to reach to the consensus. With this approach, the billing settlement can be performed automatically with the help of the smart contract deployed on the blockchain. Further, as a result of the transparent nature of blockchain, MNOs can ensure the accuracy of charging.

Inspired by the works done in this dissertation on both centralized and decentralized coordination of heterogeneous networks, we have outlined the following research directions in order to delve deeper into the self-x features in heterogeneous and densified networks.

- Wireless networks are becoming more cognitive and possibly cope with more complex situations than in the past. Therefore, self-organization and self-optimizations are key features more than ever. Our framework introduced in Chapter 3 sheds light onto the implications of tuning many parameters in both LTE eNB and WiFi AP and ultimately can provide a tool for automating the network planning. In the future, WiFi 802.11ax mode has Basic Service Set (BSS) coloring which dynamically changes the ED threshold. Moreover, to the best of our knowledge, 802.11ax can use adjustable preamble detection threshold depending on the source of interference, whether it is inter-BSS or intra-BSS frame transmission. For the sake of the CSMA/CA mechanism, in the case of inter-BSS transmission, a station detect the medium busy only for the time required to determine that the color bit is different. In our approach, we target the Energy Detection (ED) mechanism rather than Preamble Detection (PD) as we assume that LTE transmission stand as an unknown signal to a WiFi node doing CCA. However, our framework is general so that it can be tailored also to model the 802.11ax with due modifications in the analysis of the CCA targeting PD and in the Markov-chain model of the binary exponential backoff as needed. This new work requires some more investigations and can be done as future activity.
- The Software Defined Radio Access Control (SD-RAN) platforms can introduce a new level of central controlling over different technologies operating in the same band. The extension of the works in chapter 4 can go to the direction of putting the heterogeneous LTE/WiFi two-tier network under a programmable Software-Defined controlled RAN (as shown in Fig. 6.1) and defining new network applications on top of the SD-RAN platform to apply:
  - Fully reconfigurable LTE and WiFi parameters at runtime depending on the network priorities.
  - Central coordination of LTE activation in unlicensed bands.
  - Using machine learning algorithms to optimize automatically the radio and network environment through network applications.

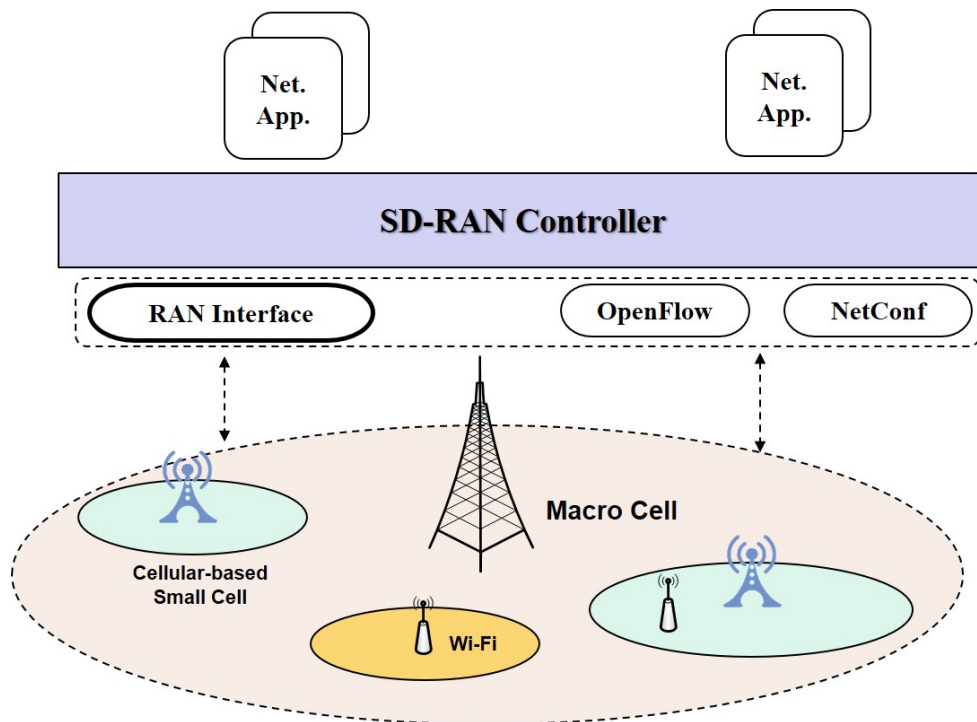


FIGURE 6.1: Conceptual representation of SD-RAN based Multi-tier network control

- The concepts revealed by recent applications of Distributed Ledger Technologies (DLT) permit further applications beyond roaming: the network services rendered by MNOs can be aligned and synchronized, an approach already in discussion in the area of network slicing. Different MNOs must guarantee a distinct network quality and service level agreement which again are of crucial importance for users who continuously move from coverage area of one operator to others such as autonomous vehicles crossing national borders. DLT can be used as slice broker, for cross-charging, as service management tool and is thus the currently missing trust link between Mobile Network Operators (MNOs).

# Appendix A

## Proofs

### A.1 Derivation of Theorem 2

*Proof.* In hypothesis  $\mathcal{H}_0^{(B)}$ , relying on the general expression of the CF of the Chi-Square distributed d.v.  $Y$ , we can rewrite it, conditioning upon the fading and distance distributions.

$$\Psi_0^{(B)}(v | g, r) = \frac{1}{(1 - j2v)Q} e^{\frac{jv}{1-2jv} g c \frac{\epsilon_I}{N_0} r^{-\alpha}}.$$

To obtain the unconditional expression of the CF it suffices to compute  $\Psi_0^{(B)}(v) = \mathbb{E}_g \mathbb{E}_r \Psi_0^{(B)}(v | g, r)$ . We remove first the conditioning on  $g$  by means of the CF of an exponentially distributed r.v. as in Theorem 1. After doing a sign change we obtain:

$$\Psi_0^{(B)}(v | r) = \frac{1}{(1 - 2jv)Q} \times \frac{1}{1 + \frac{jv}{-1+j2v} c \frac{\epsilon_I}{N_0} r^{-\alpha}},$$

where the above expression was obtained computing equation (3.11) in  $c \times (\epsilon_I/N_0)r^{-\alpha}$ . Moreover, we rely also on the following result.

$$\int_0^R \frac{1}{1 + Gr^{-\alpha}} \frac{2r}{R^2} dr = \frac{2R^\alpha {}_2F_1(1, \frac{2+\alpha}{\alpha}; 2 + \frac{2}{\alpha}; -\frac{R^\alpha}{G})}{G(2 + \alpha)}, \quad (\text{A.1})$$

for any complex constant  $G \in \mathbb{C}$ , any real valued  $\alpha > 2$  and  $R > 0$ . This result comes from the tool of Mathematica.

Assuming that  $G = \frac{jv}{-1+j2v} c \times (\frac{\epsilon_I}{N_0})$  and using the result above, we obtain the unconditional  $\Psi_0^{(B)}(v)$ .

To compute the CF of  $Y$  under hypothesis  $\mathcal{H}_1$ , it suffices to replace the non-centrality parameter with  $\mu_1$  provided in the second of equation (3.10). We remove the dependence upon the statistically independent fading coefficients and the random distance:  $\Psi_1(v) = \mathbb{E}_{g_s} \mathbb{E}_g \mathbb{E}_r \Psi(v | g_s, g, r)$ . Repeating similar steps, we can demonstrate equation (3.13). □

## A.2 Derivation of Lemma 2

*Proof.* First of all, by some manipulations, we can write the left hand side of (3.14) as follow:

$$\frac{2s}{R^2} \int_0^\infty \frac{r}{s + r^\alpha} dr. \quad (\text{A.2})$$

Using [100, eq. 3.241/4], we can see

$$\int_0^\infty \frac{x^{u-1}}{(p + qy^\nu)^{k+1}} dx = \frac{1}{\nu p^{k+1}} \left(\frac{p}{q}\right)^{u/\nu} \frac{\Gamma(u/\nu)\Gamma(1+k-u/\nu)}{\Gamma(1+k)}$$

Replacing  $u = 2$ ,  $\nu = \alpha$ ,  $p = s$ ,  $q = 1$ ,  $k = 0$  and  $y = r$  we are able to perform the integration in equation (A.2).

$$\int_0^\infty \frac{r}{(s + r^\alpha)} dr = \frac{1}{\alpha s} s^{(2/\alpha)} \left( \frac{\Gamma(\frac{2}{\alpha})\Gamma(1 - \frac{2}{\alpha})}{\Gamma(1)} \right). \quad (\text{A.3})$$

By means of the Euler's reflection formula,  $\Gamma(\frac{2}{\alpha})\Gamma(1 - \frac{2}{\alpha}) = \pi \csc(\pi \frac{2}{\alpha})$ , equation (A.3) can be rewritten as

$$\int_0^\infty \frac{r}{(s + r^\alpha)} dr = \frac{1}{\alpha s} s^{(\frac{2}{\alpha})} \pi \csc\left(\frac{2\pi}{\alpha}\right).$$

Replacing the result above in (A.2), the proof is complete.  $\square$

## A.3 Derivation of Theorem 3

*Proof.* Conditioning upon exactly  $K$  independent LTE active transmitters  $I_K(t) = \sum_{k=0}^K \xi_k(t)$ . Similar to the single interferer case, the received energy from the  $k$ -th transmitter is written as  $\varepsilon_{rIk} = c_k \times g_{Ik} \varepsilon_{I_k} r_k^{-\alpha}$ , where  $g_{Ik}$  are the i.i.d. channel power fading coefficients, and  $r_k$  the random distance of the  $k$ th interferer from the CCA station in the 2-dimensional plane. Conditioning upon the aggregate interference distribution, under the statistical hypothesis  $\mathcal{H}_0^{(B)}$ , the distribution of the d.v.  $Y$  is non-central Chi-Square distributed with a non-centrality parameter:  $\mu_0^{(B)} = \frac{1}{2\sigma^2} \sum_{k=0}^K c_k g_{Ik} \varepsilon_{I_k} r_k^{-\alpha}$ . This is plugged in the CF of the non-Central Chi-Square distributed d.v. as follows

$$\frac{1}{(1 - j2v)^Q} \exp\left(\frac{jv}{1 - j2v} \frac{1}{2\sigma^2} \sum_{k=0}^K c_k g_{Ik} \varepsilon_{I_k} r_k^{-\alpha}\right).$$

The previous expression can be rewritten as

$$\Psi_{0|K}^{(B)}(v | g_{1k}, r_k) = \frac{1}{(1 - j2v)^{\mathcal{Q}}} \prod_{k=1}^K \exp(-a_k g_{1k} r_k^{-\alpha}),$$

where  $a_k = a = \frac{jv}{-1+j2v} \frac{c \times \varepsilon_1}{2\sigma^2}$ ,  $\forall k$  since the energy of each signal and the scaling factor  $c$  are the same for each interferer. Since the CF is conditioned upon the specific realization of fading and distances  $g_{1k}$  and  $r_k$ , we can remove the conditioning as  $\Psi_{0|K}^{(B)}(v) = \mathbb{E}_{g_{1k}} \mathbb{E}_{r_k} \Psi_{0|K}^{(B)}(v | g_{1k}, r_k)$ . Relying on the assumption of exponential fading with  $\mathbb{E}\{g\} = 1$ , we obtain  $\Psi_{0|K}^{(B)}(v | r_k) = \frac{1}{(1-j2v)^{\mathcal{Q}}} \prod_{k=1}^K (1 + s r_k^{-\alpha})^{-1}$ , where the last expression is computed in  $s = a$ . Dropping the index  $k$  in the distance we are able to rewrite:  $\Psi_{0|K}^{(B)}(v | r) = \frac{1}{(1-j2v)^{\mathcal{Q}}} \times \left(\frac{1}{1+s r^{-\alpha}}\right)^K$ .

Since the r.v.  $K$  is Poisson distributed, we can use equation (3.1) to remove the dependence on it. For a real-valued measurable function  $f$  that takes values on the point process  $\Phi$ , it holds that  $\prod_{x \in \Phi} f(x) = \exp\left(-\lambda_s \int_{\mathbb{R}^2} (1 - f(x)) dx\right)$ , which yields:

$$\begin{aligned} \Psi_0^{(B)}(v) &= \frac{1}{(1 - j2v)^{\mathcal{Q}}} \exp\left(-\lambda_s \int_{\mathbb{R}^2} \left(1 - \frac{1}{1 + s r^{-\alpha}}\right) dr\right) \\ &= \frac{1}{(1 - j2v)^{\mathcal{Q}}} \exp\left(-\lambda_s \int_{\mathbb{R}^2} \left(\frac{1}{1 + s^{-1} r^{\alpha}}\right) dr\right). \end{aligned}$$

The last part of the proof consists of using the result in Lemma 2 for  $s = \frac{jv}{-1+j2v} \frac{c \times \varepsilon_1}{2\sigma^2}$ , which proves equation (3.15).

In statistical hypothesis  $\mathcal{H}_1$ , the conditional CF of the d.v.  $Y$  is  $\Psi_1(v | g_s, g_{1k}, r_k) = \frac{1}{(1-j2v)^{\mathcal{Q}}} e^{\frac{jv}{1-2jv} \mu_1}$ . The non-centrality parameter  $\mu_1$  was provided in the second of (3.10) but using the received interference energy of the aggregate process  $I_K(t)$  when exactly  $K$  interfering LTE transmitters are active. We remove the conditioning upon the fading of both useful signal and interference, as well as the conditioning on the random distance separating the  $k$ -th interferer from the CCA station as done above:  $\Psi_1(v) = \mathbb{E}_{g_s} \mathbb{E}_{g_{1k}} \mathbb{E}_{r_k} \Psi_1(v | g_s, g_{1k}, r_k)$ . To remove the conditioning on fading, we use that all the power fading coefficients are i.i.d. exponential r.v.s. and the CF is computed in  $\frac{jv}{1-j2v} \frac{\varepsilon_s}{N_0 r^{-\alpha}}$  for the useful signal and in  $\frac{jv}{1-j2v} \frac{c \times \varepsilon_1}{N_0 r^{-\alpha}}$  for the interference. Removing all conditionings and using Lemma 2 the theorem is proved.  $\square$

## A.4 Derivation of equation (3.22)

*Proof.* When a single LTE transmitted signal interferes with the reception of the test Wi-Fi receiver, we write  $V$  in equation (3.19) as follows:

$$V = \frac{2 \varepsilon_{\text{bI}}}{3 N_0} \times \frac{e^{2\sigma_1}}{r_1^\alpha}.$$

Hence, the received SINR can be expressed as

$$\eta_{\text{one}}(r_1) = \frac{e^{2\sigma_s} \log_2 M \times \frac{\varepsilon_{\text{bs}} r_s^{-\alpha}}{N_0}}{\frac{2}{3} \log_2 M' \times \frac{\varepsilon_{\text{bI}} r_1^{-\alpha}}{N_0} e^{2\sigma_1} + 1}. \quad (\text{A.4})$$

We remove the dependence of  $\eta_{\text{one}}^{\text{LTE}}(r_1)$  upon the position of the interferer over the space by means of the 2-dimensional uniform distribution with probability  $2r/R^2 dr$  for the distance  $r_1$  inside a disk of radius  $R$  wherein the single LTE transmitter is located.

$$\eta_{\text{one}} = \int_0^R \eta_{\text{one}}(r_1) \frac{2r_1}{R^2} dr_1,$$

using the result of equation (A.1), the derivation of equation (3.22), the SINR with only one LTE interferer, is complete.  $\square$

## A.5 Derivation of equation (3.27)

*Proof.* We remove the dependence of  $\omega$  and  $\varrho$  in equation (3.26) from the exact value of  $n_w$  as follows

$$\bar{\omega} = \mathbb{E} \left\{ P_e^{(\text{sys})} \times \left( 1 - P_d^{n_w-1} \right) \right\} = P_e^{(\text{sys})} \times \left( 1 - \mathbb{E} \{ P_d^{n_w-1} \} \right)$$

We use the PPP assumption for  $n_w$  through the probability  $\frac{\lambda_w |A|^{n_w}}{n!} e^{-\lambda_w |A|}$ . Therefore, we can write

$$\begin{aligned} \mathbb{E} \{ P_d^{n_w-1} \} &= \sum_{n_w=0}^{\infty} P_d^{n_w-1} \times \frac{(\lambda_w |A|)^{n_w}}{n_w!} e^{-\lambda_w |A|} \\ &= e^{-\lambda_w |A|} P_d^{-1} \sum_{n_w=0}^{\infty} \frac{(P_d \lambda_w |A|)^{n_w}}{n_w!}. \end{aligned}$$

Using an exponential series expansion for the summation, we can derive  $\mathbb{E} \{ P_d^{n_w-1} \}$  as

$$\mathbb{E} \{ P_d^{n_w-1} \} = e^{-\lambda_w |A|} P_d^{-1} \times e^{P_d \lambda_w |A|} = P_d^{-1} e^{-\lambda_w |A| (1-P_d)} = P_d^{-1} e^{-\bar{n}_w (1-P_d)}.$$

Substituting this last finding in equation (3.26), (3.27) is derived.  $\square$

# Bibliography

- [1] 3rd Generation Partnership Project, "Study on Licensed-Assisted Access to Unlicensed Spectrum," Technical Specification group Radio Access Network, Tech. Rep., 2016.
- [2] L. Simić, A. M. Voicu, P. Mähönen, M. Petrova, and J. P. De Vries, "LTE in Unlicensed Bands is Neither Friend Nor Foe to Wi-Fi," *IEEE Access*, vol. 4, pp. 6416–6426, 2016.
- [3] V. Sathya, M. Mehrnoush, M. Ghosh, and S. Roy, "Association Fairness in Wi-Fi and LTE-U Coexistence," in *Proc. of WCNC, Barcelona, Spain*, IEEE, 2018.
- [4] (). Qualcomm Research, LTE in Unlicensed Spectrum: Harmonious Coexistence with Wi-Fi. Access on February, 2019, [Online]. Available: <https://www.qualcomm.com/media/documents/files/lte-unlicensed-coexistence-whitepaper.pdf>.
- [5] M. Mehrnoush, V. Sathya, S. Roy, and M. Ghosh, "Analytical Modeling of Wi-Fi and LTE-LAA Coexistence: Throughput and Impact of Energy Detection Threshold," *arXiv preprint arXiv:1803.02444*, 2018.
- [6] I. Gomez-Miguel, A. Garcia-Saavedra, P. D. Sutton, P. Serrano, C. Cano, and D. J. Leith, "SrsLTE: An Open-Source Platform for LTE Evolution and Experimentation," in *Proc. of WiNTECH, New York City, US*, ACM, 2016.
- [7] B Mafakheri, L Goratti, R Abbas, S Reisenfeld, and R Riggio, "LTE/Wi-Fi Coordination in Unlicensed Bands: An SD-RAN Approach," in *Proc. of the NETSOFT, Paris, France*, IEEE, 2019.
- [8] N. Bitar, M. O. Al Kalaa, S. J. Seidman, and H. H. Refai, "On the Coexistence of LTE-LAA in the Unlicensed Band: Modeling and Performance Analysis," *IEEE Access*, vol. 6, pp. 52 668–52 681, 2018.
- [9] E. Pei, D. Meng, L. Li, and P. Zhang, "Performance Analysis of Listen Before Talk Based Coexistence Scheme Over the Unlicensed Spectrum in the Scenario With Multiple LTE Small Bases," *IEEE Access*, vol. 5, pp. 10 364–10 368, 2017.
- [10] (May 2017). Response to IEEE LS to 3GPP RAN/RAN1/RAN4 Related to PD and ED Issues, [Online]. Available: <https://mentor.ieee.org/802.11/dcn/17/11-17-0867-00-0000-liaison-statement-from-3gpp-ran1-ran4-on-pded.doc>.
- [11] B. Bojović, L. Giupponi, Z. Ali, and M. Miozzo, "Evaluating Unlicensed LTE Technologies: LAA vs LTE-U," *IEEE Access*, vol. 7, pp. 89 714–89 751, 2019.

- [12] "3GPP TR 36.889 V13.0.0, Study on Licensed-Assisted Access to Unlicensed Spectrum," June, 2015.
- [13] (May 2018). Agenda for IEEE 802.11 Coexistence SC meeting in Warsaw in May 2018, [Online]. Available: <https://mentor.ieee.org/802.11/dcn/18/11-18-0659-03-coex-agenda-for-may-2018-in-warsaw.pptx>.
- [14] M. Iqbal, C. Rochman, V. Sathya, and M. Ghosh, "Impact of Changing Energy Detection Thresholds on Fair Coexistence of Wi-Fi and LTE in the Unlicensed Spectrum," in *Proc. of WTS, Chicago, USA*, IEEE, 2017.
- [15] (). LTE International Roaming Whitepaper. Access on August, 2019, [Online]. Available: <http://carrier.huawei.com/en/technical-topics/core-network/lte-roaming-whitepaper>.
- [16] B. Xie, *Heterogeneous Wireless Networks: Networking Protocol to Security*. AV Akademikerverlag, 2012.
- [17] H. Hu, J. Zhang, X. Zheng, Y. Yang, and P. Wu, "Self-configuration and Self-optimization for LTE Networks," *IEEE Communications Magazine*, vol. 48, no. 2, pp. 94–100, 2010.
- [18] O. Narmanlioglu and E. Zeydan, "Mobility-aware Cell Clustering Mechanism for Self-Organizing Networks," *IEEE Access*, vol. 6, pp. 65 405–65 417, 2018.
- [19] C. Hoymann, D. Astely, M. Stattin, G. Wikstrom, J.-F. Cheng, A. Høglund, M. Frenne, R. Blasco, J. Huschke, and F. Gunnarsson, "LTE Release 14 Outlook," *IEEE Communications Magazine*, vol. 54, no. 6, pp. 44–49, 2016.
- [20] S. Zinno, G. Di Stasi, S. Avallone, and G. Ventre, "On a Fair Coexistence of LTE and Wi-Fi in the Unlicensed Spectrum: A Survey," *Computer Communications*, vol. 115, pp. 35–50, 2018.
- [21] Y. Zeng, T. Zhou, H. Hu, Y. Yang, J. Tian, and Z. Li, "Weight Based Channel Selection Towards 5G in the Unlicensed Spectrum," *China Communications*, vol. 15, no. 8, pp. 54–66, 2018.
- [22] X. Lu, E. Sopin, V. Petrov, O. Galinina, D. Moltchanov, K. Ageev, S. Andreev, Y. Koucheryavy, K. Samouylov, and M. Dohler, "Integrated Use of Licensed-and Unlicensed-Band mmwave Radio Rechnology in 5G and Beyond," *IEEE Access*, vol. 7, pp. 24 376–24 391, 2019.
- [23] H. Song, Q. Cui, Y. Gu, G. L. Stüber, Y. Li, Z. Fei, and C. Guo, "Cooperative LBT Design and Effective Capacity Analysis for 5G NR Ultra Dense Networks in Unlicensed Spectrum," *IEEE Access*, vol. 7, pp. 50 265–50 279, 2019.
- [24] D. Laselva, D. Lopez-Perez, M. Rinne, and T. Henttonen, "3GPP LTE-WLAN Aggregation Technologies: Functionalities and Performance Comparison," *IEEE Communications Magazine*, vol. 56, no. 3, pp. 195–203, 2018.

- [25] P. Nuggehalli, "LTE-WLAN Aggregation [Industry Perspectives]," *IEEE Wireless Communications*, vol. 23, no. 4, pp. 4–6, 2016.
- [26] M.-Y. Cheng, Y.-S. Chen, C.-M. Chou, P. S. K. Nuggehalli, and C.-C. Hsu, *Rate Adaptation for LTE-WLAN Aggregation*, US Patent 9,918,252, 2018.
- [27] H.-J. Kwon, J. Jeon, A. Bhorkar, Q. Ye, H. Harada, Y. Jiang, L. Liu, S. Nagata, B. L. Ng, T. Novlan, *et al.*, "Licensed-Assisted Access to Unlicensed Spectrum in LTE Release 13," *IEEE communications magazine*, vol. 55, no. 2, pp. 201–207, 2016.
- [28] M. Labib, V. Marojevic, J. H. Reed, and A. I. Zaghloul, "Extending LTE into the Unlicensed Spectrum: Technical Analysis of the Proposed Variants," *IEEE Communications Standards Magazine*, vol. 1, no. 4, pp. 31–39, 2017.
- [29] R. Zhang, M. Wang, L. X. Cai, Z. Zheng, X. Shen, and L.-L. Xie, "LTE-Unlicensed: The Future of Spectrum Aggregation for Cellular Networks," *IEEE Wireless Communications*, vol. 22, no. 3, pp. 150–159, 2015.
- [30] L. Giupponi, T. Henderson, B. Bojovic, and M. Miozzo, "Simulating LTE and Wi-Fi Coexistence in Unlicensed Spectrum with NS-3," *arXiv preprint arXiv:1604.06826*, 2016.
- [31] B. Chen, J. Chen, Y. Gai, and J. Zhang, "Coexistence of LTE-LAA and Wi-Fi on 5 GHz With Corresponding Deployment Scenarios: A Survey," *IEEE Communications Surveys & Tutorials*, vol. 19, no. 1, pp. 7–32, 2017.
- [32] X. Wang, T. Q. S. Quek, M. Sheng, and J. Li, "Throughput and Fairness Analysis of Wi-Fi and LTE-U in Ulicensed Band," *IEEE Journal on Selected Areas in Communications*, vol. 35, no. 1, pp. 63–78, 2016.
- [33] Y. Li, T. Zhou, Y. Yang, H. Hu, and M. Hamalainen, "Fair Downlink Traffic Management for Hybrid LAA-LTE/Wi-Fi Networks," *IEEE Access*, vol. 5, pp. 7031–7041, 2016.
- [34] L. Li, J. P. Seymour, L. J. Cimini, and C.-C. Shen, "Coexistence of Wi-Fi and LAA Networks With Adaptive Energy Detection," *IEEE Transactions on Vehicular Technology*, vol. 66, no. 11, pp. 10 384–10 393, 2017.
- [35] S. Xu, Y. Li, Y. Gao, Y. Liu, and H. Gačanin, "Opportunistic Coexistence of LTE and WiFi for Future 5G system: Experimental Performance Evaluation and Analysis," *IEEE Access*, vol. 6, pp. 8725–8741, 2017.
- [36] M. Alliance, "Multefire Release 1.0 Technical Paper: A New Way to Wireless," *white paper*, JAN, 2017.
- [37] F. Baccelli, B. Błaszczyszyn, *et al.*, "Stochastic Geometry and Wireless Networks: Volume ii Applications," *Foundations and Trends® in Networking*, vol. 4, no. 1–2, pp. 1–312, 2010.
- [38] U. Schilcher, S. Toumpis, M. Haenggi, A. Crismani, G. Brandner, and C. Bettstetter, "Interference Functionals in Poisson Networks," *IEEE Transactions on Information Theory*, vol. 62, no. 1, pp. 370–383, 2016.

- [39] T. D. Novlan, R. K. Ganti, A. Ghosh, and J. G. Andrews, "Analytical Evaluation of Fractional Frequency Reuse for OFDMA Cellular Networks," *IEEE Transactions on Wireless Communications*, vol. 10, no. 12, pp. 4294–4305, 2011.
- [40] M. Z. Win, P. C. Pinto, and L. A. Shepp, "A Mathematical Theory of Network Interference and Its Applications," *Proceedings of the IEEE*, vol. 97, no. 2, pp. 205–230, 2009.
- [41] Y. Li, F. Baccelli, J. G. Andrews, T. D. Novlan, and J. C. Zhang, "Modeling and Analyzing the Coexistence of Wi-Fi and LTE in Unlicensed Spectrum," *IEEE Transactions on Wireless Communications*, vol. 15, no. 9, pp. 6310–6326, 2016.
- [42] J. G. Andrews, F. Baccelli, and R. K. Ganti, "A Tractable Approach to Coverage and Rate in Cellular Networks," *IEEE Transactions on Communications*, vol. 59, no. 11, pp. 3122–3134, 2011.
- [43] P. C. Pinto and M. Z. Win, "Communication in a Poisson Field of Interferers—Part I: Interference Distribution and Error Probability," *IEEE Transactions on Wireless Communications*, vol. 9, no. 7, pp. 2176–2186, 2010.
- [44] H. ElSawy, A. Sultan-Salem, M.-S. Alouini, and M. Z. Win, "Modeling and Analysis of Cellular Networks Using Stochastic Geometry: A Tutorial," *IEEE Communications Surveys & Tutorials*, vol. 19, no. 1, pp. 167–203, 2017.
- [45] V. Gatteschi, F. Lamberti, C. Demartini, C. Pranteda, and V. Santamaría, "To Blockchain or Not to Blockchain: That is the Question," *IT Professional*, vol. 20, no. 2, pp. 62–74, 2018.
- [46] S. Nakamoto *et al.*, "Bitcoin: A Peer-to-Peer Electronic Cash System," 2008.
- [47] A.-J. Jameela and M. Nader, "Blockchain in Industries: A Survey," *IEEE Access*, vol. 7, pp. 22 328–22 370, 2019.
- [48] A. Gervais, G. O. Karame, K. Wüst, V. Glykantzis, H. Ritzdorf, and S. Capkun, "On the Security and Performance of Proof of Work Wlockchains," in *Proceedings of the 2016 ACM SIGSAC Conference on Computer and Communications Security*, ACM, 2016, pp. 3–16.
- [49] C. T. Nguyen, D. T. Hoang, D. N. Nguyen, D. Niyato, H. T. Nguyen, and E. Dutkiewicz, "Proof-of-Stake Consensus Mechanisms for Future Blockchain Networks: Fundamentals, Applications and Opportunities," *IEEE Access*, vol. 7, pp. 85 727–85 745, 2019.
- [50] (). *Permissioned Blockchains*. Access on August, 2019, [Online]. Available: <https://www.investopedia.com/terms/p/permissioned-blockchains.asp>.
- [51] D. Ongaro and J. Ousterhout, "In Search of an Understandable Consensus Algorithm," in *2014 {USENIX} Annual Technical Conference ({USENIX}{ATC} 14)*, 2014, pp. 305–319.

- [52] H. Lu, K. Huang, M. Azimi, and L. Guo, "Blockchain Technology in the Oil and Gas Industry: A Review of Applications, Opportunities, Challenges, and Risks," *IEEE Access*, 2019.
- [53] A. Dorri, M. Steger, S. S. Kanhere, and R. Jurdak, "Blockchain: A Distributed Solution to Automotive Security and Privacy," *IEEE Communications Magazine*, vol. 55, no. 12, pp. 119–125, 2017.
- [54] V. Ortega, F. Bouchmal, and J. F. Monserrat, "Trusted 5G Vehicular Networks: Blockchains and Content-Centric Networking," *IEEE Vehicular Technology Magazine*, vol. 13, no. 2, pp. 121–127, 2018.
- [55] G. Dittmann and J. Jelitto, "A Blockchain Proxy for Lightweight IoT Devices," in *2019 Crypto Valley Conference on Blockchain Technology (CVCBT)*, IEEE, 2019, pp. 82–85.
- [56] J. Fiaidhi, S. Mohammed, and S. Mohammed, "EDI with Blockchain as an Enabler for Extreme Automation," *IT Professional*, vol. 20, no. 4, pp. 66–72, 2018.
- [57] H.-T. Wu and C.-W. Tsai, "Toward Blockchains for Health-Care Systems: Applying the Bilinear Pairing Technology to Ensure Privacy Protection and Accuracy in Data Sharing," *IEEE Consumer Electronics Magazine*, vol. 7, no. 4, pp. 65–71, 2018.
- [58] C. Song, S. Wu, S. Liu, R. Fang, and Q.-L. Li. (). ANKR — Build a Faster, Cheaper, Securer Cloud Using Idle Processing Power in Data Centers and Edge Devices, [Online]. Available: <https://www.ankr.network>.
- [59] K. Kotobi and S. G. Bilén, "Blockchain-Enabled Spectrum Access in Cognitive Radio Networks," in *Wireless Telecommunications Symposium (WTS), 2017*, IEEE, 2017, pp. 1–6.
- [60] R. B. Uriarte and R. De Nicola, "Blockchain-Based Decentralized Cloud/Fog Solutions: Challenges, Opportunities, and Standards," *IEEE Communications Standards Magazine*, vol. 2, no. 3, pp. 22–28, 2018.
- [61] A. L. Susan Zhou. (). Qlink White Paper, [Online]. Available: <https://qlink.mobi/qlink2/res/WhitePaper.pdf>.
- [62] E. Langberg. (). Blockchain in Mobile Networks, [Online]. Available: [http://e.huawei.com/us/publications/global/ict/\\_insights/201703141505/core-competency/201703150928](http://e.huawei.com/us/publications/global/ict/_insights/201703141505/core-competency/201703150928).
- [63] T. Sanda and H. Inaba, "Proposal of New Authentication Method in Wi-Fi Access Using bitcoin 2.0," in *Consumer Electronics, 2016 IEEE 5th Global Conference on*, IEEE, 2016, pp. 1–5.
- [64] Z. Xiong, Y. Zhang, D. Niyato, P. Wang, and Z. Han, "When Mobile Blockchain Meets Edge Computing: Challenges and Applications," *arXiv preprint arXiv:1711.05938*, 2017.
- [65] L. Xie, Y. Ding, H. Yang, and X. Wang, "Blockchain-Based Secure and Trustworthy Internet of Things in SDN-Enabled 5G-VANETs," *IEEE Access*, vol. 7, pp. 56 656–56 666, 2019.

- [66] L. Zhou, L. Wang, Y. Sun, and P. Lv, "Beekeeper: A Blockchain-Based IoT System With Secure Storage and Homomorphic Computation," *IEEE Access*, vol. 6, pp. 43 472–43 488, 2018.
- [67] M. S. Ali, M. Vecchio, M. Pincheira, K. Dolui, F. Antonelli, and M. H. Rehmani, "Applications of Blockchains in the Internet of Things: A Comprehensive Survey," *IEEE Communications Surveys & Tutorials*, vol. 21, no. 2, pp. 1676–1717, 2018.
- [68] B. Mafakheri, T. Subramanya, L. Goratti, and R. Riggio, "Blockchain-based Infrastructure Sharing in 5G Small Cell Networks," in *Proc. IEEE CNSM, Rome, Italy*, 2018.
- [69] (). Blockchain @ Telco. How Blockchain Can Impact the Telecommunications Industry and its Relevance to the C-Suite. Access on August, 2019, [Online]. Available: [https://www2.deloitte.com/content/dam/Deloitte/za/Documents/technology-media-telecommunications/za\\_TMT\\_Blockchain\\_TelCo.pdf](https://www2.deloitte.com/content/dam/Deloitte/za/Documents/technology-media-telecommunications/za_TMT_Blockchain_TelCo.pdf).
- [70] "Generic Network Slice Template. GSMA, Version 1.0," Tech. Rep., 2019.
- [71] B. Nour, A. Ksentini, N. Herbaut, P. A. Frangoudis, and H. Moun gla, "A Blockchain-Based Network Slice Broker for 5G Services," *IEEE Networking Letters*, 2019.
- [72] J. Backman, S. Yrjölä, K. Valtanen, and O. Mämmelä, "Blockchain Network Slice Broker in 5G: Slice Leasing in Factory of the Future Use Case," in *2017 Internet of Things Business Models, Users, and Networks*, IEEE, 2017, pp. 1–8.
- [73] K. Valtanen, J. Backman, and S. Yrjölä, "Creating Value Through Blockchain Powered Resource Configurations: Analysis of 5G Network Slice Brokering Case," in *2018 IEEE Wireless Communications and Networking Conference Workshops (WCNCW)*, IEEE, 2018, pp. 185–190.
- [74] R. B. Davies, "Numerical Inversion of a Characteristic Function," *Biometrika*, vol. 60, no. 2, pp. 415–417, 1973.
- [75] B. Mafakheri, L. Goratti, R. Riggio, C. Buratti, and S. Reisenfeld, "LTE Transmission in Unlicensed Bands: Evaluating The Impact Over Clear Channel Assessment," IEEE, 2018.
- [76] A. Rabbachin, T. Q. Quek, P. C. Pinto, I. Oppermann, and M. Z. Win, "UWB Energy Detection in the Presence of Multiple Narrowband Interferers," in *Proc. of ICUWB, Singapore*, IEEE, 2007, pp. 857–862.
- [77] F. F. Digham, M.-S. Alouini, and M. K. Simon, "On the Energy Detection of Unknown Signals Over Fading Channels," *IEEE Transactions on Communications*, vol. 55, no. 1, pp. 21–24, 2007.
- [78] M. Z. Win, P. C. Pinto, and L. A. Shepp, "A Mathematical Theory of Network Interference and its Applications," *Proceedings of the IEEE*, vol. 97, no. 2, pp. 205–230, 2009.

- [79] R. Fedrizzi, L. Goratti, K. Gomez, and T. Rasheed, "On the Feasibility of Handover Over WiFi Backhaul in LTE-based Aerial-Terrestrial Networks," in *Proc. of WCNC, Istanbul, Turkey*, IEEE, 2014.
- [80] Q. Ni, *Design and Analysis of MAC Protocol for IEEE 802.11n*, 2005.
- [81] R. Karmakar, S. Chattopadhyay, and S. Chakraborty, "Impact of IEEE 802.11 n/ac PHY/MAC High Throughput Enhancements on Transport and Application Protocols, a Survey," *IEEE Communications Surveys & Tutorials*, vol. 19, no. 4, pp. 2050–2091, 2017.
- [82] S. Sesia, M. Baker, and I. Toufik, *LTE-the UMTS Long Term Evolution: from Theory to Practice*. John Wiley & Sons, 2011.
- [83] M. Gast, *802.11 Wireless Networks: the Definitive Guide*. "O'Reilly Media, Inc.", 2005.
- [84] R. P. F. Hoefel, "IEEE WLANs: 802.11, 802.11e MAC and 802.11a, 802.11b, 802.11g PHY Cross Layer Link Budget Model for Cell Coverage Estimation," in *Proc. of CCECE, Ontario, Canada*, IEEE, 2008.
- [85] G. Bianchi, "Performance Analysis of the IEEE 802.11 Distributed Coordination Function," *IEEE Journal on Selected Areas in Communications*, vol. 18, no. 3, pp. 535–547, 2000.
- [86] (). SrsLTE, Software Radio Systems LTE. Access on December, 2018, [Online]. Available: <https://github.com/srsLTE/srsLTE>.
- [87] (). OpenWrt, Wireless Freedom. Access on December, 2018, [Online]. Available: <https://openwrt.org/about>.
- [88] R. Riggio, "Demo: The Empower Mobile Network Operating System," in *Proc. International Workshop on Wireless Network Testbeds, Experimental Evaluation, and Characterization, WiNTECH*, ACM, 2016.
- [89] (). Anritus-MS2036A. Access on December, 2018, [Online]. Available: <https://www.anritsu.com/en-gb/test-measurement/products/ms2036a>.
- [90] (). USB-TG124A Tracking Generator User Manual. Access on December, 2018, [Online]. Available: <https://signalhound.com/sigdownloads/TG124A/TG124A-User-Manual.pdf>.
- [91] (July 2017). The 5G-Empower Wiki, [Online]. Available: <https://github.com/5g-empower/5g-empower.github.io/wiki>.
- [92] Z. Chen, S. Chen, H. Xu, and B. Hu, "A Security Authentication Scheme of 5G Ultra-Dense Network Based on Block chain," *IEEE Access*, vol. 6, pp. 55 372–55 379, 2018.
- [93] V. Sharma, I. You, F. Palmieri, D. N. K. Jayakody, and J. Li, "Secure and Energy-Efficient Handover in Fog Networks Using Blockchain-based DMM," *IEEE Communications Magazine*, vol. 56, no. 5, pp. 22–31, 2018.
- [94] P. A. Vanleeuwen and D. van de Ruit, "Blockchain – Operator Opportunities. version1.0," Tech. Rep., 2018.

- [95] R. Noldus and L. Norell, "Roaming Unbundling Challenges and Opportunities," in *Proc. of ICIN. Venice, Italy*, IEEE, 2013, pp. 118–125.
- [96] "GSM Association Roaming Database, Structure and Updating Procedures. Version 9.1," Tech. Rep., 2013.
- [97] W. Wang, D. T. Hoang, P. Hu, Z. Xiong, D. Niyato, P. Wang, Y. Wen, and D. I. Kim, "A Survey on Consensus Mechanisms and Mining Strategy Management in Blockchain Networks," *IEEE Access*, vol. 7, pp. 22 328–22 370, 2019.
- [98] Y. Manevich, A. Barger, and Y. Tock, "Endorsement in Hyperledger Fabric via Service Discovery," *IBM Journal of Research and Development*, 2019.
- [99] T. T. A. Dinh, J. Wang, G. Chen, R. Liu, B. C. Ooi, and K.-L. Tan, "Block-bench: A Framework for Analyzing Private Blockchains," in *Proc. of the 2017 ACM International Conference on Management of Data*, ACM, 2017.
- [100] I. Gradshteyn and I. Ryzhik, "Table of Intergrals, Series, and Products, vol. 7th," *Academic PressSan Diego*, 2007.